

University of Windsor

Scholarship at UWindor

Electronic Theses and Dissertations

Theses, Dissertations, and Major Papers

1-1-1968

Curvature effects on a turbulent jet flow over a wall.

Peter Kuo-Chih Tu
University of Windsor

Follow this and additional works at: <https://scholar.uwindsor.ca/etd>

Recommended Citation

Tu, Peter Kuo-Chih, "Curvature effects on a turbulent jet flow over a wall." (1968). *Electronic Theses and Dissertations*. 6063.

<https://scholar.uwindsor.ca/etd/6063>

This online database contains the full-text of PhD dissertations and Masters' theses of University of Windsor students from 1954 forward. These documents are made available for personal study and research purposes only, in accordance with the Canadian Copyright Act and the Creative Commons license—CC BY-NC-ND (Attribution, Non-Commercial, No Derivative Works). Under this license, works must always be attributed to the copyright holder (original author), cannot be used for any commercial purposes, and may not be altered. Any other use would require the permission of the copyright holder. Students may inquire about withdrawing their dissertation and/or thesis from this database. For additional inquiries, please contact the repository administrator via email (scholarship@uwindsor.ca) or by telephone at 519-253-3000ext. 3208.

CURVATURE EFFECTS ON A TURBULENT
JET FLOW OVER A WALL

A Thesis

Submitted to the Faculty of Graduate Studies Through
the Department of Mechanical Engineering in Partial
Fulfillment of the Requirements for the Degree of
Doctor of Philosophy at the
University of Windsor

by

Peter Kuo-Chih Tu

B.S.Eng., The National Taiwan University, Taiwan, China, 1959

M.A.Sc., The University of Windsor, Windsor, Ontario, Canada, 1965

Windsor, Ontario, Canada

1968

UMI Number:DC52629

UMI[®]

UMI Microform DC52629
Copyright 2007 by ProQuest Information and Learning Company.
All rights reserved. This microform edition is protected against
unauthorized copying under Title 17, United States Code.

ProQuest Information and Learning Company
789 East Eisenhower Parkway
P.O. Box 1346
Ann Arbor, MI 48106-1346

ABX 6581

APPROVED BY:

S. L. Man

A. B. Smith

W. J. Colborne

S. P. Blee

H. J. Tucker

L. W. M. Donald

217496

SUMMARY

Streamwise curvature effects on a two-dimensional turbulent incompressible jet flow of air over a surface were investigated. Experiments were carried out on a plane wall and on semicircular convex and concave surfaces of different radii.

The entrainment velocity (rate of entrainment) induced by the jet and the rate of jet growth were found to increase with curvature. There were no appreciable curvature effects on the mean velocity profiles and the potential core length.

It was found that in the inner layer of the curved wall jets the region, where u/u_m varied approximately as $(y/y_m/2)^{1/N}$, was rather limited. Further, the value of N increased with R for the convex surfaces and remained constant for the concave surfaces.

An analysis based on the line sink and its image system was developed to predict the entrainment velocity of a plane wall jet and curved wall jets with convex curvature. Agreement between the analysis and experiment was found to be satisfactory. The sink strength coefficient K was found to increase linearly with curvature.

ACKNOWLEDGEMENTS

The author is grateful to Professor W.G. Colborne, Head of the Department of Mechanical Engineering, for his interest and continuous support.

The author wishes to express his gratitude to Dr. K. Sridhar for his supervision, generous aid and encouragement throughout this work.

Thanks are also due to Professors A. C. Smith and T. W. McDonald for their most helpful advice and their efforts towards the writer's better understanding of the problem.

The technical assistance given by Messrs. O. Brudy, D. K. Liebsch and R. Myers in constructing the apparatus is gratefully acknowledged.

The author wishes to thank his wife, Dinea, for her help in preparation of this thesis.

The work was financially supported by the Grant (No. A-2190) and Studentship of the National Research Council of Canada.

TABLE OF CONTENTS

	Page
NOTATION	vii
LIST OF FIGURES	xi
LIST OF TABLES	xv
CHAPTER	
I INTRODUCTION	1
II LITERATURE SURVEY	4
2.1 FREE JET	4
2.2 WALL JETS	6
III LINE SINK ANALYSIS	12
3.1 INTRODUCTION	12
3.2 PLANE WALL JET	12
3.3 CURVED WALL JET	17
3.3.1 CONTRIBUTION FROM THE LINE SINK AND ITS IMAGE SYSTEM IN REGIONS I AND II ...	20
3.3.2 CONTRIBUTION FROM THE LINE SINK AND ITS IMAGE SYSTEM IN REGION III	23
3.3.3 ENTRAINMENT VELOCITY	25
IV TEST FACILITIES	28
4.1 AIR SUPPLY AND FLOW-CALIBRATION PIPE	28
4.2 PLENUM CHAMBER AND NOZZLE	29
4.3 END-PLATES AND SUPPORTING TABLE	29
4.4 SURFACES AND TRAVERSING MECHANISM	29
4.4.1 PLANE SURFACE	29

TABLE OF CONTENTS (CONTINUED)

	Page
4.4.2 CONVEX SURFACE	30
4.4.3 CONCAVE SURFACE	30
4.5 PROBING EQUIPMENT	31
V EXPERIMENTS	32
5.1 CALIBRATION	32
5.2 EXPERIMENTAL PROGRAMME	34
5.2.1 PLANE WALL JET	34
5.2.2. CONVEX SURFACE	34
5.2.3 CONCAVE SURFACE	35
VI EXPERIMENTAL RESULTS	36
6.1 DATA REDUCTION	36
6.2 PRESENTATION AND DISCUSSION OF RESULTS	36
6.2.1 ENTRAINMENT FLOW	36
6.2.2 JET GROWTH AND MAXIMUM VELOCITY DECAY ..	42
6.2.3 POTENTIAL CORE LENGTH	44
6.2.4 NON-DIMENSIONAL VELOCITY PROFILE	45
6.2.5 INNER LAYER VELOCITY POWER LAW	46
6.3 COMPARISION BETWEEN ANALYSIS AND EXPERIMENTS ..	47
6.4 SOME SUGGESTIONS FOR FUTURE WORK	50
VII CONCLUSIONS	51
REFERENCES	52
FIGURES	56
TABLES	96
VITA AUCTORIS	99

NOTATION

a, b	constants in table I
a_1, b_1	constants in Eq. (6.16)
A	constant in Eq. (3.9), (L)
B	constant in Eq. (3.9)
c, d & e	constants in Eq. (2.7)
E	entrainment ratio defined by Eq. (6.10)
J	jet momentum at the nozzle exit per unit span, (MT^{-1})
K	empirical sink strength coefficient in Eq. (6.15)
l	transverse movement of the eddy in straight flow, (L)
$(1+\epsilon)l$	transverse movement of the eddy in curved flow, (L)
M	two dimensional sink strength, (L^2T^{-1})
m, m_1, m_2 & m_3	two dimensional sink strength per unit distance of the jet axis, (LT^{-1})
N	exponent defined by Eq. (6.14), describing the inner layer velocity power law
P_0	total pressure at the nozzle exit, ($ML^{-1}T^{-2}$)
P_∞	ambient pressure, ($ML^{-1}T^{-2}$)
Q	flow rate per unit span, (L^2T^{-1})
Q_0	flow rate per unit span at the nozzle exit, (L^2T^{-1})

Q_{en}	$Q - Q_0, (L^2T^{-1})$
\bar{Q}	non-dimensional flow rate i.e., Q/Q_0
$\bar{Q}_{P.W.}$	\bar{Q} for plane wall jet
R_e	Reynolds number, $R_e = u_0 t / \nu$ for free jet and plane wall jet and $R_e = \left[(P_0 - P_\infty)(Rt) / (\rho \nu^2) \right]^{1/2}$ for curved wall jets
R	radius of surface, (L)
R_s	radius of curved line sink defined in Fig. 5, (L)
R_i	radius of curved line sink image defined in Fig. 5, (L)
r	radial distance defining the position of point P in polar coordinates, (L)
S	slope given by Eq. (6.6)
t	width of the nozzle exit, (L)
u	velocity component in the x - direction, (LT^{-1})
u_m	maximum velocity along the jet, (LT^{-1})
u_0	average jet velocity at the nozzle exit, (LT^{-1})
$v_{R'}, v_r$ & v_y	component of velocity induced by the line sink in the R' , r & y - direction respectively, (LT^{-1})
v_{en}	component of the entrainment velocity normal to the surface, (LT^{-1})
\bar{v}_{en}	non-dimensional entrainment velocity, i.e., v_{en}/u_0
$(\bar{v}_{en})_{P.W.}$	\bar{v}_{en} for plane wall jet

x	coordinate along the jet from the nozzle exit, (L)
x_0	value of x where maximum velocity begins to decay, (L)
\bar{x}	non-dimensional distance, i.e., x/t or $R\theta/t$
x_p	x - coordinate of point P, (L)
x'	x - coordinate defined in Fig. 5, (L)
X	x - coordinate of point P on approximate jet boundary, (L)
y	coordinate normal to the centre line of a free jet or normal to the surface of a wall jet, (L)
y_m	value of y at the maximum velocity point, (L)
$y_{m/2}$	larger value of y for which $u = u_m/2$, (L)
y_p	y - coordinate of point P, (L)
Y	value of y where the jet velocity is equal to 10% of the local maximum velocity, (L)
OB,OA	distance defined by the relation $OB = R^2/OA$; (L)
ρ	air density, (ML^{-3})
ν	kinematic viscosity, (L^2T^{-1})
α	angular position of point P
θ	angle measured from the nozzle exit
θ_h	angle between the nozzle exit and the hypothe- tical origin
β	constant defined by $\theta_h = \beta t/R$

δ constant related to the growth of jet used
in Eq. (2.1)

ψ stream function, (L^2T^{-1})

Surface Designation: Examples $(9)_{+c}$, $(9)_{-c}$ & $(\infty)_{oc}$.

Number inside the brackets refers to the radius of curvature in inches. Subscript $+c$ indicates convex curvature, $-c$ indicates concave curvature and oc indicates zero curvature.

LIST OF FIGURES

		Page
FIG. 1	CONTINUOUS LINE SINK	13
FIG. 2	LINE SINK FOR A FREE JET	15
FIG. 3	LINE SINK AND ITS IMAGE SYSTEM FOR A PLANE WALL JET	15
FIG. 4	CURVED WALL JET WITH CONVEX CURVATURE	18
FIG. 5	LINE SINK AND ITS IMAGE SYSTEM FOR A CURVED WALL JET WITH CONVEX CURVATURE	19
FIG. 5(a)	LINE SINK OUTSIDE OF THE CYLINDER IN REGIONS I AND II	21
FIG. 5(b)	SINK IMAGE SYSTEM IN REGIONS I AND II	22
FIG. 5(c)	LINE SINK IN REGION III	23
FIG. 5(d)	SINK IMAGE SYSTEM IN REGION III	24
FIG. 6	CONTROL VOLUME IN A PLANE WALL JET	37
FIG. 7(a)	SCHEMATIC DIAGRAM OF THE TEST FACILITIES ..	56
FIG. 7(b)	SCHEMATIC DIAGRAM OF THE TEST REGIONS	57
FIG. 8(a)	TEST REGION AND PRESSURE PROBES FOR CONVEX SURFACE	58
FIG. 8(b)	TRAVERSING MECHANISM AND PRESSURE PROBES FOR CONCAVE SURFACE	58
FIG. 9	STATIC AND TOTAL PRESSURE PROBE	59
FIG. 10	FREE JET NOMENCLATURE	60
FIG. 11	WALL JET NOMENCLATURE	61

LIST OF FIGURES (CONTINUED)

		Page
FIG. 12	NOMENCLATURE OF CURVED WALL JET WITH CONVEX CURVATURE	62
FIG. 13	NOMENCLATURE OF CURVED WALL JET WITH CONCAVE CURVATURE	63
FIG. 14	SKETCH OF THE INSTRUMENT FOR DRAWING TANGENT TO A CURVE	64
FIG. 15	VARIATION OF FLOW RATE ALONG THE JET	65
FIG. 16	VARIATION OF ENTRAINMENT VELOCITY ALONG THE JET	66
FIG. 17	VARIATION OF THE FLOW RATE DIFFERENCE BETWEEN THE CURVED WALL JETS AND PLANE WALL JET ALONG THE SURFACE	67
FIG. 18	PLOT OF SLOPE S vs CURVATURE	68
FIG. 19	PLOT FOR JET GROWTH LAW	69
FIG. 20	JET GROWTH FOR PLANE AND CONVEX SURFACES	70
FIG. 21	JET GROWTH FOR CONCAVE SURFACE	71
FIG. 22	PLOT FOR JET GROWTH LAW	72
FIG. 23	VARIATION OF c, d AND e WITH CURVATURE	73
FIG. 24	VARIATION OF c, d AND e WITH CURVATURE	74
FIG. 25	APPROXIMATE JET BOUNDARY OF THE PLANE WALL JET	75
FIG. 26	MAXIMUM VELOCITY DECAY.....	76

LIST OF FIGURES (CONTINUED)

		Page
FIG. 27	POTENTIAL CORE BOUNDARIES FOR CURVED WALL JETS WITH CONVEX CURVATURE	77
FIG. 28	POTENTIAL CORE BOUNDARIES FOR CURVED WALL JETS WITH CONCAVE CURVATURE	78
FIG. 29	NON-DIMENSIONAL VELOCITY PROFILES FOR (9) _{+c} SURFACE	79
FIG. 30	NON-DIMENSIONAL VELOCITY PROFILES FOR (6) _{+c} SURFACE	80
FIG. 31	NON-DIMENSIONAL VELOCITY PROFILES FOR (3) _{+c} SURFACE	81
FIG. 32	NON-DIMENSIONAL VELOCITY PROFILES FOR (9) _{-c} SURFACE	82
FIG. 33	NON-DIMENSIONAL VELOCITY PROFILES FOR (6) _{-c} SURFACE	83
FIG. 34	NON-DIMENSIONAL VELOCITY PROFILES FOR (3) _{-c} SURFACE	84
FIG. 35	MEAN NON-DIMENSIONAL VELOCITY PROFILES FOR DIFFERENT RADII OF CURVATURE	85
FIG. 36	NON-DIMENSIONAL INNER LAYER VELOCITY PROFILES FOR (9) _{+c} SURFACE	86
FIG. 37	NON-DIMENSIONAL INNER LAYER VELOCITY PROFILES FOR (6) _{+c} SURFACE	87

LIST OF FIGURES (CONTINUED)

	Page
FIG. 38	NON-DIMENSIONAL INNER LAYER VELOCITY PROFILES FOR (3) _{+c} SURFACE 88
FIG. 39	NON-DIMENSIONAL INNER LAYER VELOCITY PROFILES FOR (9) _{-c} SURFACE 89
FIG. 40	NON-DIMENSIONAL INNER LAYER VELOCITY PROFILES FOR (6) _{-c} SURFACE 90
FIG. 41	NON-DIMENSIONAL INNER LAYER VELOCITY PROFILES FOR (3) _{-c} SURFACE 91
FIG. 42	VARIATION OF POWER LAW EXPONENT WITH CURVATURE 92
FIG. 43	ANALYTICAL (CONSTANT m_1) AND EXPERIMENTAL VARIATION OF ENTRAINMENT VELOCITY ALONG THE JET 93
FIG. 44	ANALYTICAL (m_1 VARIED WITH x) AND EXPERIMENTAL VARIATION OF ENTRAINMENT VELOCITY ALONG THE JET 94
FIG. 45	VARIATION OF a_1 , b_1 & K WITH CURVATURE 95

LIST OF TABLES

	Page
TABLE I CONSTANT a AND b IN $u_m \propto x^a$ AND $y_m/2 \propto x^b$...	96
TABLE II INDEX OF THE POWER LAW MEASURED BY EXPERIMENTS	97
TABLE III COEFFICIENTS OF EQUATION (6.13)	43
TABLE IV TEST CONDITIONS	98
TABLE V EMPIRICAL COEFFICIENTS IN EQUATIONS (6.15) & (6.16)	48

CHAPTER I

INTRODUCTION

The phenomena of the so-called free jet (Refs. 1 to 4), defined as a two dimensional flow emerging from a nozzle and spreading into still air; the plane wall jet (Refs. 4 to 13), where the jet flows over a straight surface; and the curved wall jet (also Coanda Effect) (Refs. 15 to 19), where the flow surface is curved; have drawn intensive interests of many research workers in the past.

The investigations done in this field could be listed under the following headings:

1. Surrounding medium (Refs. 10 to 14)
 - a. still air
 - b. moving stream
2. Jet - surface geometry (Refs. 14 to 21 and 24 to 26)
 - a. plane deflecting surface
 - b. plane surface without deflection
 - c. circular convex and concave surfaces
 - d. logarithmic spiral surface
 - e. without surface (jet deflection by pressure difference or by an external stream)
 - f. surface with an initial gap

3. Jet fluid (Refs. 22 and 23)

- a. cold air jet
- b. hot air or gas jet

Force and sound measurements were also made and reported in many papers (Refs. 22, 27, 28 and 35).

The purpose of conducting these investigations was to provide basic information on the jet flow and its applications. Among the applications the following examples were often cited by leading researchers:

1. High lift devices such as the blown flap (Ref. 28)
2. Thrust augmentation (Ref. 31)
3. Jet deflection (Ref. 31)
4. Fluidic devices (Ref. 31)

In spite of these studies, a reasonably complete understanding has not yet been achieved particularly as regards the effect of curvature on a turbulent jet flow over a wall (Ref. 31). This investigation was, therefore, intended to serve as a complementary study of curvature effects. Experiments were performed with a two dimensional turbulent jet flow over a plane surface and over circular convex and concave surfaces of various radii in still air. The study was limited to the mean properties of the flow and was not primarily concerned with the turbulence mechanism or momentum loss on the surface.

The analytical part of the investigation was concerned with the entrainment induced by the jet flow over a plane wall and convex surfaces of different radii by the application of line sink and its image system. Mathematical models were constructed to replace the actual jet flows.

CHAPTER II

LITERATURE SURVEY

The material covered in this section summarizes briefly the existing literature and is included in the report for the sake of completeness and ease of reference. The following survey consists of the theoretical and experimental investigations of free jets and wall jets with plane and curved surfaces.

2.1 FREE JET

When a jet discharges into a region of quiescent air, the surrounding air is induced into the jet and thus the mass flow in the jet increases in the downstream direction while its momentum is very nearly conserved. This mixing process causes the potential core region (or central core) of uniform velocity to diminish gradually downstream from the nozzle exit. The jet width increases and after the potential core region the maximum velocity along the centre line of the jet decreases.

Prandtl (Ref. 1) found from dimensional considerations that (a) the velocity at the centre of the jet was proportional to $(1/x)^{1/2}$, (b) the jet width was proportional to x and (c) the mean velocity profiles were similar.

Gortler (Ref. 2) used Prandtl's mixing length theory (Ref. 2) and developed the theoretical velocity distribution as follows:

$$u = \left(\frac{3}{4} \frac{J\delta}{\rho x} \right)^{1/2} \operatorname{sech}^2 \frac{\delta y}{x} \quad (2.1)$$

where δ is a constant determined by experiment.

Reichardt (Ref. 3) and Forthmann (Ref. 4) found from their measurements that $\delta = 7.67$ for large values of x . Borque (Ref. 3) found from his measurements that $\delta = 12$ near the nozzle exit and $\delta = 7.5$ for large values of x .

In order to determine the amount of flow induced in the surrounding air, Taylor (Ref. 33) obtained the streamline pattern of the entrainment flow for various forced and thermal turbulent jets by replacing the jets with continuous distributions of sinks (line sink). He assumed the sink strength to be $m = (1/x)^{1/2}$ and obtained the stream function:

$$\psi = r^{1/2} \cos\left(\frac{\theta}{2}\right) \quad (2.2)$$

for the two-dimensional free jet emerging from a slot into an unbounded space.

Wyganski in his two separate papers (Refs. 34 and 35) and one joint paper with Newman (Ref. 28) extended the application of the line sink of variable strength and its image system technique to predict the entrainment velocity,

the loss of thrust, lift and moment for jet-flap aerofoils. In his analysis, the jet was divided into two regions: Region I, which was near the exit of the jet (about 6 slot widths), consisted of a core of uniform velocity (potential core) and two mixing layers which spread linearly in the downstream direction. In region II the mixing layers had joined and the mixing took place across the entire jet (see Fig. 10).

According to the results by Tollmien (Ref. 36) and Liepman and Laufer (Ref. 37), the inflow velocity at the outer edge of region I was $0.032u_0$. Wygnanski determined the associated sink strength per unit span length and per unit distance of the jet axis to be $m_1 = 0.064u_0$. For region II, the sink strength was determined as $m_2 = \left(\frac{3}{4} \frac{t}{6x}\right)^{1/2} u_0$ based on Gortler's velocity equation (Ref. 2).

Wygnanski's main purpose was to analyze the jet drag for the jet flap aerofoils and lift and moment for a thin aerofoil with blowing by using a line sink and its image system. He developed the equation for entrainment velocity close to the plane surface normal to the jet nozzle. However, other complex jet patterns such as the wall jet were not considered.

2.2 WALL JETS

Although a great number of papers concerning various aspects of wall jets have been written, only those dealing with the following aspects will be considered: Jet growth,

velocity decay, potential core, inner layer velocity profile and entrainment flow.

A plane wall jet is defined as a jet flowing over a plane surface (see Fig. 11). Glauert (Ref. 5) in 1956 presented a theoretical analysis of the plane wall jet. By using Prandtl's hypothesis (Ref. 2) for the outer layer (see Fig. 11) and Blasius shear stress formula (Ref. 2) in the inner layer, he determined that $u_m \propto x^a$ and $y_m/2 \propto x^b$, where a and b were constants determined by experiments. For turbulent flow values of a and b were found to be approximately -0.5 and 1 respectively (see Table I).

The Blasius shear stress formula (Ref. 2) used by Glauert's theoretical analysis (Ref. 5) is based on a $1/7^{\text{th}}$ power law for the velocity distribution in the inner layer of the wall jet. However, this was found to be incorrect by experimental measurement. The exponent of the power law was found to be in the neighbourhood of $1/12$ (see Table II).

A curved wall jet is a jet flowing over a curved surface. Fekete (Ref. 18), Nakaguchi (Ref. 17) and Newman (Ref. 15) made comprehensive analyses both in theory and experiments on the curved jet over circular convex surfaces.

Newman (Ref. 15) made a dimensional study of this type of flow. $(P_0 - P_\infty)$, t , R , ρ , γ and θ were the parameters used to define the incompressible jet flow. Pressure difference across the jet sheet and angular position of jet separation were determined as functions of these parameters. The static pressure distribution on the surface and the jet

growth were also investigated by Newman (Ref. 15). His jet growth equation was as follows:

$$\frac{y_m/2}{R\theta} = 0.11 + 1.65 \frac{y_m/2}{R} \quad (2.3)$$

A non-dimensional variable $\frac{\rho u_m^2 R \theta}{(P_0 - P_\infty) t}$ was used to describe the maximum velocity decay. Newman found theoretically that the above dimensionless group decreased linearly with θ and that the agreement between the measured and theoretical values was satisfactory.

A relationship for the jet growth which deviated rapidly from that given by Newman for θ values larger than about 160° was developed theoretically by Nakaguchi (Ref. 17):

$$\frac{y_m/2}{R} = 0.086 \theta + 0.04 (\theta)^2 \quad (2.4)$$

He also gave the following formula for the local maximum jet velocity:

$$\frac{u_m}{(u_m)_c} = \left[\frac{y_m/2}{(y_m/2)_c} \right]^n \quad (2.5)$$

Where subscript c expressed the values at some arbitrarily chosen point in the fully developed flow. The value of n was approximately -0.5.

Fekete gave a method for finding the growth law constants and for finding a relation for the position of the hypothetical origin. The constants for his growth law equation:

$$\frac{y_m/2}{R(\theta + \beta \frac{t}{R})} = c + d \frac{y_m/2}{R} \quad (2.6)$$

obtained by hot wire measurements, were found to be equal to $\beta = 7.43$, $c = 0.073$ and $d = 0.233$.

The position of the hypothetical origin from the nozzle exit was defined as $\theta_h = \beta \frac{t}{R}$

Newman, Nakaguchi and Fekete all assumed similarity of the velocity profiles in their analyses. Guitton (Ref. 19) has pointed out that this assumption was an approximation only. He made investigations on the curved wall jet with concave surface. In his analysis he stated that, when the radius of the surface was a constant, the self-preservation solution was no longer possible and the shape of the jet velocity profile would vary downstream.

The concave wall jet grew less rapidly than the plane wall jet. A polynomial equation was used by Guitton in predicting the jet growth:

$$\frac{y_m/2}{|R|(\theta + \beta \frac{t}{|R|})} = c + d \left(\frac{y_m/2}{R}\right) + e \left(\frac{y_m/2}{R}\right)^2 \quad (2.7)$$

For the concave surface alone, the values of constants were

$$\beta = 16.86, c = 0.065, d = 0.32 \text{ and } e = 0.24.$$

Based on the results for both convex and concave surfaces,

$$\beta = 5.86, c = 0.069, d = 0.30 \text{ and } e = -0.08.$$

In these investigations (Refs. 18 and 19) the radius of curvature was not a variable. However, the effect of varying the radius was suggested for a future work.

The entrainment flow induced by the wall jets has also drawn the attention of several researchers. Eyles and Foster (Ref. 14) visualized the stream patterns induced in a low speed airstream by high pressure air ejected through a thin slot tangentially over a curved surface. Very clear pictures were taken by the techniques of liquid film, smoke and Schlieren. They indicated that an "overturning" effect occurred on the main airstream near the exit of the jet. Further, the air in this region was induced into the flow nearly perpendicular to the jet. Their experiments were performed with the use of a plane surface, plane deflecting surfaces (30° and 60°) and a circular convex surface. Unfortunately, only the flow visualization was their primary interest; therefore, no quantitative measurement on the entrainment flow was included.

Stratford et al (Ref. 32) approached this problem from the concept of mixing length. They related the increase in mixing length to the flow curvature by examining the transverse motion of turbulent eddies from a kinematic point

of view. They derived that the mixing length for a jet flowing over a convex cylindrical surface, as compared with that over a plane surface, was increased by a factor of

$$\frac{l + l\epsilon}{l} = \frac{1}{1 - \frac{2u}{R} / \left(-\frac{\partial u}{\partial y}\right)} \quad (2.8)$$

due to flow curvature in the outer part of the jet. By taking a mean value for $u/(\partial u/\partial y)$ over the outer velocity profile, it was found that this factor could be expressed as:

$$\frac{l + l\epsilon}{l} = 1 + \frac{2}{3} \frac{Y'}{R} + \frac{4}{9} \left(\frac{Y'}{R}\right)^2 + \dots \quad (2.9)$$

for a jet in still air, where Y' was the width of the mixing region. The width of the mixing region was defined as the distance between the point of maximum jet velocity and the outer edge of the jet. Since the edge of the jet was difficult to determine by experiments, errors in the value of $\frac{l + l\epsilon}{l}$ were to be expected. The range of radius of curvature covered by their experiments was rather limited ($R = 4$ in. and 6 in.) because they were primarily interested in a comparison between the plane wall jet and the curved wall jet. In order to obtain a better picture on how the entrainment velocity is affected by the curvature of the flow surface, the range of radius should be increased.

CHAPTER III

LINE SINK ANALYSIS

3.1 INTRODUCTION

When a two dimensional free jet spreads into still air, the mixing with the surrounding air governs the jet development. A study of the entrainment flow is necessary for understanding the jet mixing process. The entrainment velocity is defined as the velocity of the surrounding air when being entrained into the jet.

Among analyses of the entrainment problems, the method of using a line sink distribution (Ref. 33) has drawn the author's special interest. As already noted in Chapter 2, Taylor's theoretical analysis for a free jet (Ref. 33) well described the stream function of the entrained flow. Wagnanski (Ref. 35), by examining the actual jet, was able to obtain the sink strength more precisely as $m_1 = 0.064u_0$ and $m_2 = (3/4 \cdot t/5x)^{1/2}u_0$ for region I and II respectively (see Fig. 10).

In this Chapter it is shown that line sink distributions can be used to predict the entrainment flow of plane and curved wall jets.

3.2 PLANE WALL JET

For a single sink in two-dimensional incompressible flow the radial velocity, $v_{R'}$, at radius R' is given by:

$$v_{R'} = \frac{-M}{2\pi R'} \quad (3.1)$$

where M is the sink strength.

Consider a continuous line sink extending from the origin to infinity on the x -axis. The velocity at a point $P(x_p, y_p)$ in R' - direction for any line element of strength, mdx , is expressed as:

$$dv_{R'} = - \frac{mdx}{2\pi R'} \quad (3.2)$$

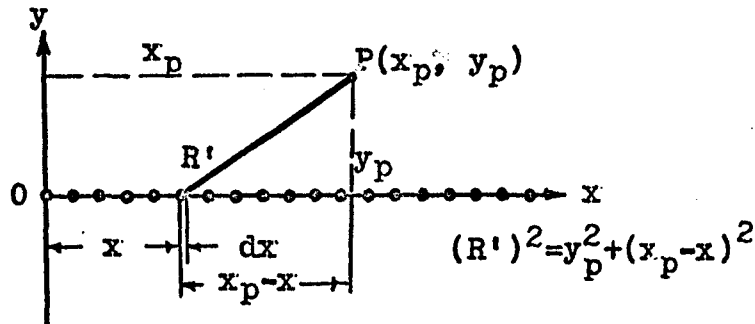


FIG. 1 CONTINUOUS LINE SINK

From Fig. 1 it is seen that the component in the y - direction, dv_y , is given by:

$$dv_y = (dv_{R'}) \cdot \frac{y_p}{R'} \quad (3.3)$$

From Eqs. (3.2) and (3.3) and by substituting $(R')^2 = y_p^2 + (x_p - x)^2$ for R'

$$dv_y = \frac{-my_p dx}{2\pi [y_p^2 + (x_p - x)^2]} \quad (3.4)$$

is obtained.

For the whole line sink, the value, v_y , is determined by the following integral:

$$v_y = - \int_0^{\infty} \frac{my_p dx}{2\pi [y_p^2 + (x_p - x)^2]} \quad (3.5)$$

If this continuous line sink is placed at the free jet axis and the sink strength is given by m_1 and m_2 in regions I and II respectively (see Fig. 2), the above integral becomes

$$v_y = - \int_0^{x_0} \frac{m_1 y_p dx}{2\pi [y_p^2 + (x_p - x)^2]} - \int_{x_0}^{\infty} \frac{m_2 y_p dx}{2\pi [y_p^2 + (x_p - x)^2]} \quad (3.6)$$

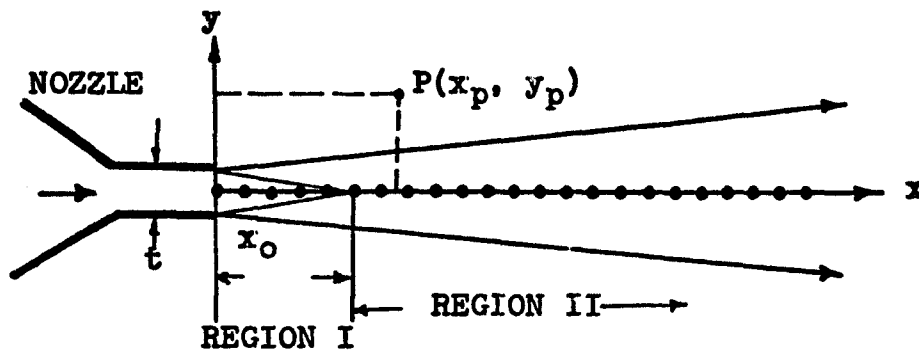


FIG. 2 LINE SINK FOR A FREE JET

In the case of a plane wall jet there exists a wall with zero component of velocity perpendicular to surface. In order to use the continuous line sink to predict the entrainment flow, the image of the line sink is added. The sinks are placed $t/2$ above the wall and their images are on the line $t/2$ below the wall. The theoretical wall created by the pairs of sinks, then, matches the actual surface of the plane wall jet (see Fig. 3).

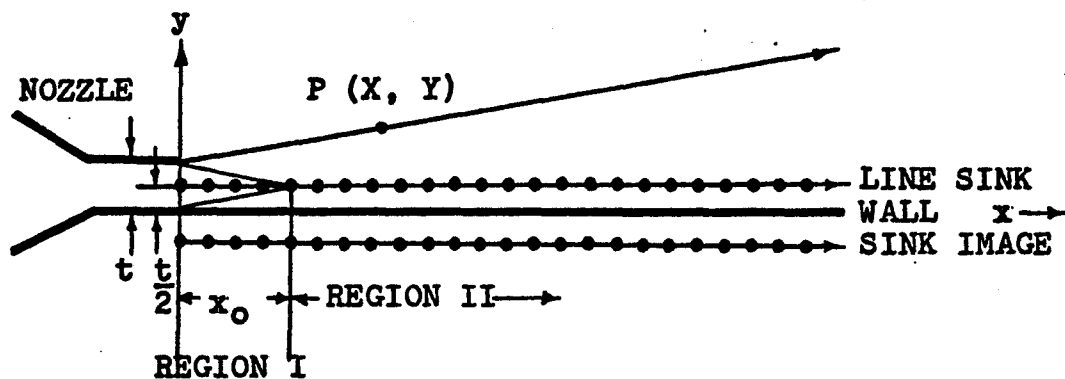


FIG. 3 LINE SINK AND ITS IMAGE SYSTEM FOR A PLANE WALL JET

Unlike the free jet, the line of sinks in this case does not quite coincide with the line of maximum velocity

along the jet. However, the difference would be small if a thin jet is assumed.

Then the velocity, v_y , at point P (x_p, y_p) is:

$$v_y = - \int_0^{x_0} \left\{ \frac{m_1(y_p - t/2)}{2\pi[(y_p - t/2)^2 + (x_p - x)^2]} + \frac{m_1(y_p + t/2)}{2\pi[(y_p + t/2)^2 + (x_p - x)^2]} \right\} dx$$

$$- \int_{x_0}^{\infty} \left\{ \frac{m_2(y_p - t/2)}{2\pi[(y_p - t/2)^2 + (x_p - x)^2]} + \frac{m_2(y_p + t/2)}{2\pi[(y_p + t/2)^2 + (x_p - x)^2]} \right\} dx \quad (3.7)$$

By knowing the jet boundary equation and placing the point P (X, Y) on the boundary, the entrainment velocity is determined by the following two equations:

$$v_{en} = - \int_0^{x_0} \left\{ \frac{m_1(Y - t/2)}{2\pi[(Y - t/2)^2 + (X - x)^2]} + \frac{m_1(Y + t/2)}{2\pi[(Y + t/2)^2 + (X - x)^2]} \right\} dx$$

$$- \int_{x_0}^{\infty} \left\{ \frac{m_2(Y - t/2)}{2\pi[(Y - t/2)^2 + (X - x)^2]} + \frac{m_2(Y + t/2)}{2\pi[(Y + t/2)^2 + (X - x)^2]} \right\} dx \quad (3.8)$$

$$Y = A + B \cdot X$$

(3.9)

where A and B are empirical constants. In order to have the same basis for comparison of plane and curved wall jets, this integral is evaluated numerically instead of solving analytically. The results are presented in Chapter 6.

3.3 CURVED WALL JET

Only the curved wall jet with a convex surface is analysed in this chapter because of the difficulty in forming the mathematical model.

Due to mixing with the surrounding medium the jet width increases and the maximum velocity of the jet decreases with increasing θ . The pressure at the surface which is initially lower than the pressure of the surrounding air because of the convex curvature tends to rise with distance downstream. When the pressure difference between the surface and the surrounding air reaches zero, the jet separates from the surface.

Although in the test programme the curved surface is formed by a half cylinder (θ from 0 to π) (see Fig. 12), a full cylinder is considered in the analysis (see Fig. 4).

The jet is assumed to separate from the surface at $\theta = \pi$ and become a fully developed free jet after the separation. Thus the jet flow consists of three regions: (I) Region I is the region of potential core extending from the nozzle exit to $x = 6t$, (2) Region II is the region of a fully

developed curved wall jet ($\theta = 6t/R$ to π) and (3) Region III is the region of a fully developed free jet (from $x' = 0$ at $\theta = \pi$ to $x' = \infty$) (see Fig. 4).

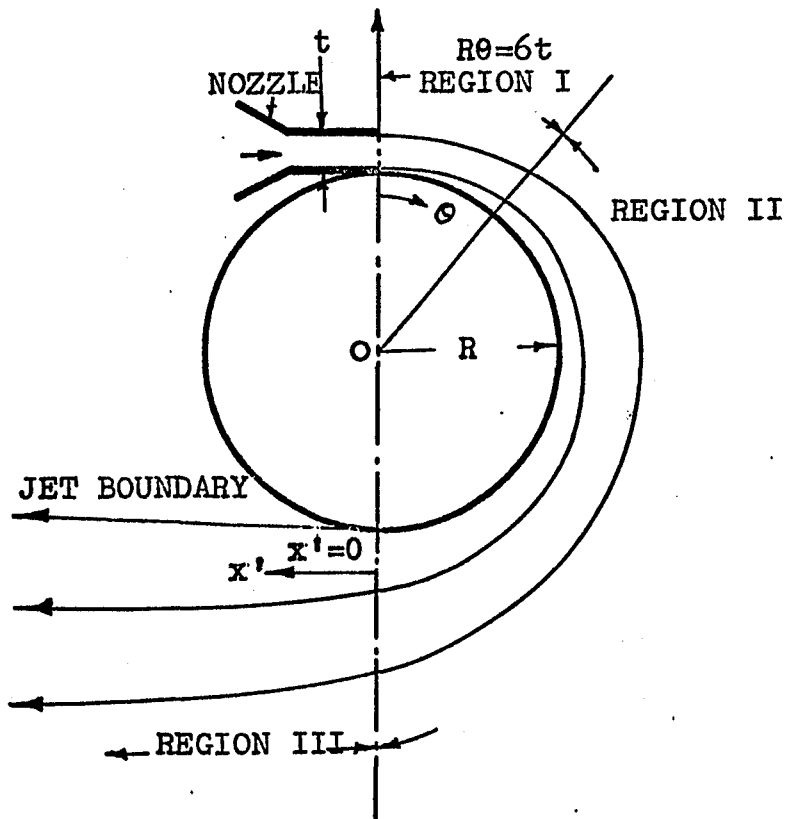


FIG. 4 CURVED WALL JET WITH CONVEX CURVATURE

In regions I and II of the mathematical model (see Fig. 5), a continuous line sink is placed on the circumference of the semicircle with radius $R_s = R + (t/2)$ and the centre coinciding with that of the convex surface. In region III, the line sink is placed on the tangent to the semicircle at $\theta = \pi$.

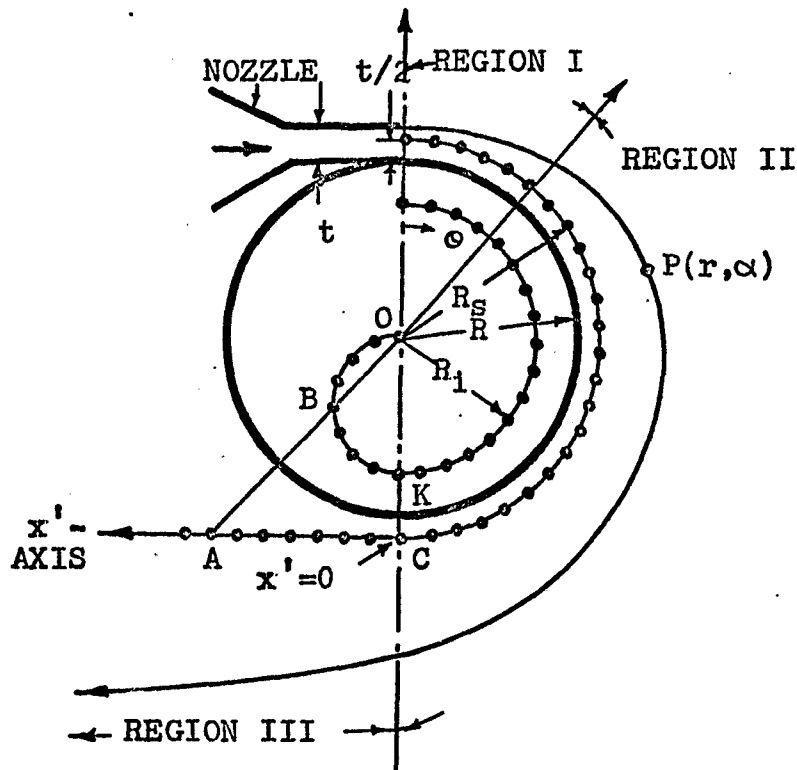


FIG. 5 LINE SINK AND ITS IMAGE SYSTEM FOR A CURVED WALL JET WITH CONVEX CURVATURE

In order to form a circle of radius R coinciding with the surface of the cylinder, an image of each sink is added at the inverse point and a source of the same strength is added at the centre of the circle (Ref. 29). In this case, in regions I and II the sinks and their images lie on the circumferences of concentric semicircles of radius R_s and R_i . These radii are related by $R^2 = R_s \cdot R_i$. In region III, the sinks are on the x' - axis from point C ($x' = 0$ at $\theta = \pi$) to infinity and their images are on the circle through O and K ($OK = \text{diameter}$) formed by the relation $OB = R^2/OA$ (see Fig. 5).

As mentioned in the previous case the difference between the line of maximum velocity and the line of sinks would be small if a thin jet is assumed.

The velocity induced by the line sink and its image system at any point P (x_p, y_p) is analysed by the following procedure:

- (1) The line sink and its image system in regions I and II are considered together. The analyses in these two regions are identical except that the sink strengths are different (m_1 & m_2).
- (2) The line sink and its image system in region III are considered.
- (3) The induced velocity at P (x_p, y_p) is obtained by adding the results of step (1) and (2).

3.3.1 CONTRIBUTION FROM THE LINE SINK AND ITS IMAGE SYSTEM IN REGIONS I AND II

In these two regions, the line sink outside of the cylinder is considered. The velocity caused by any line element of strength $mR_s d\theta$ at point P (r, α) [see Fig. 5(a)] is given as:

$$(dv_{R'}) \text{ Sink in Region I or II} = \frac{-mR_s d\theta}{2\pi R'} \quad (3.10)$$

where R' is the distance between the point and the element, θ and α are angular positions of the element and point P measured from the nozzle exit respectively.

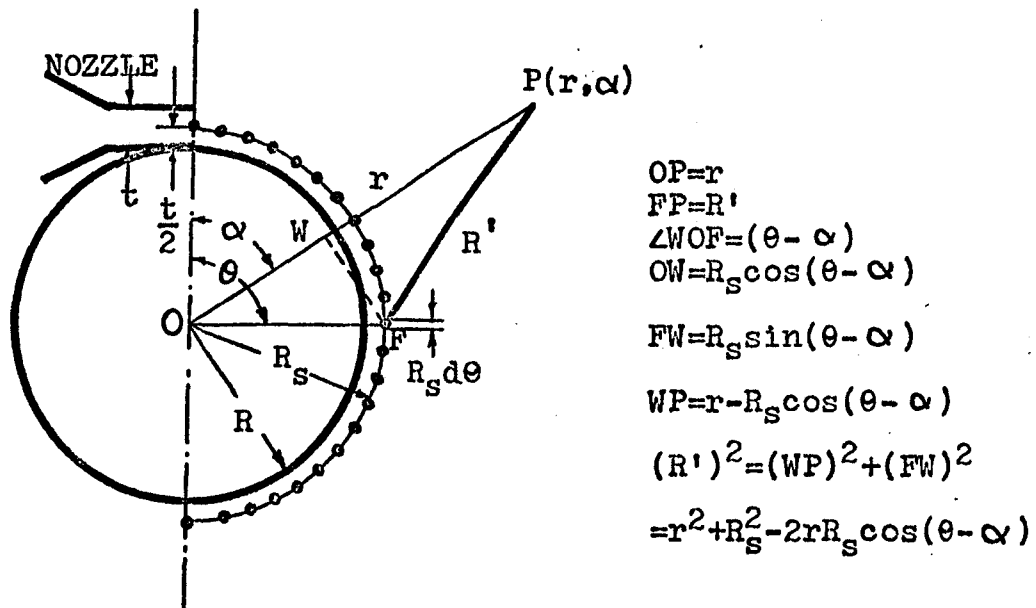


FIG. 5(a) LINE SINK OUTSIDE OF THE CYLINDER
IN REGIONS I AND II

From Fig. 5(a) it is seen that the component of $(dv_{R'})$ Sink in Region I or II in r - direction is:

(dv_r) Sink in Region I or II

$$= (dv_{R'}) \text{ Sink in Region I or II} \cdot \frac{r-R_s \cos(\theta-\alpha)}{R'}$$

(3.11)

Equations (3.10) & (3.11) yield after the substitution for R' :

The velocity induced by the source image of the line element of strength $mR_s d\theta$ located at the centre of the circle is given by:

$$\begin{aligned} & (dv_r) \text{ Source Image in Region I or II} \\ & = \frac{mR_s d\theta}{2\pi r} \end{aligned} \quad (3.14)$$

3.3.2 CONTRIBUTION FROM THE LINE SINK AND ITS IMAGE SYSTEM IN REGION III

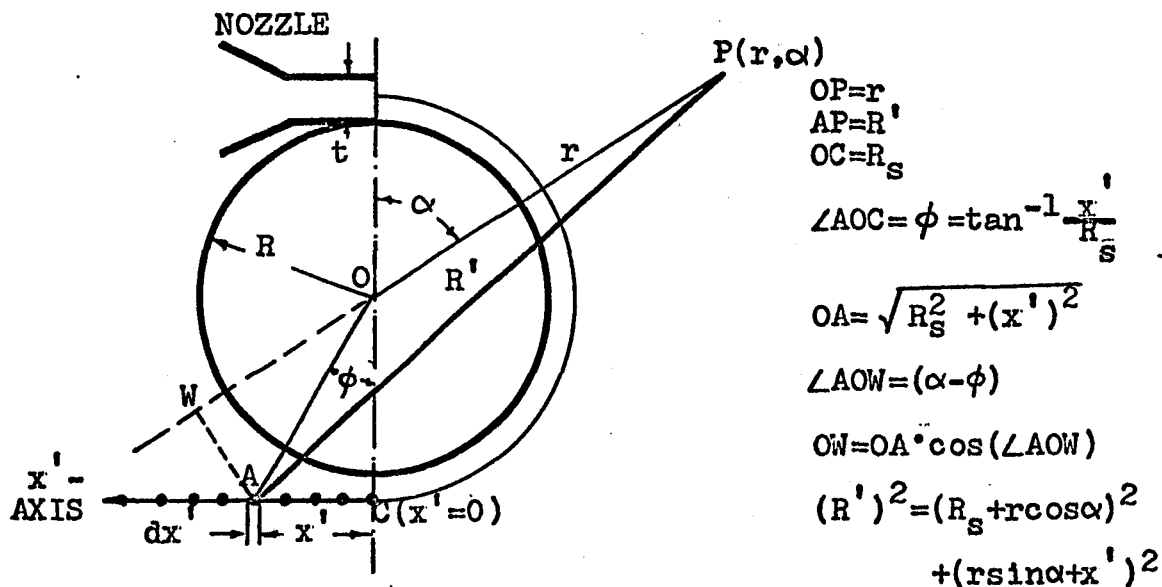


FIG. 5(c) LINE SINK IN REGION III

As shown in Fig. 5(c), the velocity caused by any line element dx' at the point $P(r, \alpha)$ is:

$$(dv_{R'}) \text{ Sink in Region III} = \frac{-m dx'}{2\pi R'} \quad (3.15)$$

The sink image in region III is on the circle through O and K (OK = diameter) formed by the relation $OB = R^2/OA$ [see Fig. 5(d)]. The following velocity is obtained by a method similar to that used for Eq. (3.17):

(dv_r) Sink Image in Region III

$$= - \frac{m \left[r + \frac{R^2}{\sqrt{R_s^2 + (x')^2}} \cdot \cos\left(\alpha - \tan^{-1} \frac{x'}{R_s}\right) \right] dx'}{2\pi \left[\left(r + \frac{R^2}{\sqrt{R_s^2 + (x')^2}} \cdot \cos\left(\alpha - \tan^{-1} \frac{x'}{R_s}\right) \right)^2 + \left(\frac{R^2}{\sqrt{R_s^2 + (x')^2}} \sin\left(\alpha - \tan^{-1} \frac{x'}{R_s}\right) \right)^2 \right]}$$

(3.18)

For the source image at the centre of the circle, the velocity is, then, given as:

(dv_r) Source Image in Region III

$$= \frac{m dx'}{2\pi r} \quad (3.19)$$

3.3.3 ENTRAINMENT VELOCITY

The velocity at P (r, α) induced by the elements of the line sink and its image system is given by the following summation:

21749C

$$\begin{aligned}
dv_r = & \left\{ (dv_r) \text{ Sink} + \text{Sink Image} + \text{Source Image} \right\} \text{Region I} \\
& + \left\{ (dv_r) \text{ Sink} + \text{Sink Image} + \text{Source Image} \right\} \text{Region II} \\
& + \left\{ (dv_r) \text{ Sink} + \text{Sink Image} + \text{Source Image} \right\} \text{Region III}
\end{aligned}
\tag{3.20}$$

Therefore, the component of the entrainment velocity in the radial direction at point P (r, α) located on the boundary of the jet is given by the following integral:

$$\begin{aligned}
v_r = & \left\{ \int_0^{\frac{6t}{R}} \frac{m_1 R_s [r - R_s \cos(\theta - \alpha)] d\theta}{2\pi [(r^2 + R_s^2) - 2rR_s \cos(\theta - \alpha)]} \right. \\
& + \int_0^{\frac{6t}{R}} \frac{m_1 R_s [r - R_1 \cos(\theta - \alpha)] d\theta}{2\pi [(r^2 + R_1^2) - 2rR_1 \cos(\theta - \alpha)]} \left. - \int_0^{\frac{6t}{R}} \frac{m_1 R_s d\theta}{2\pi r} \right\} \text{Region I} \\
& - \left\{ \int_{\frac{6t}{R}}^{\pi} \frac{m_2 R_s [r - R_s \cos(\theta - \alpha)] d\theta}{2\pi [(r^2 + R_s^2) - 2rR_s \cos(\theta - \alpha)]} \right. \\
& + \int_{\frac{6t}{R}}^{\pi} \frac{m_2 R_s [r - R_1 \cos(\theta - \alpha)] d\theta}{2\pi [(r^2 + R_1^2) - 2rR_1 \cos(\theta - \alpha)]} \left. - \int_{\frac{6t}{R}}^{\pi} \frac{m_2 R_s d\theta}{2\pi r} \right\} \text{Region II}
\end{aligned}$$

$$\begin{aligned}
& - \left\{ \int_0^{\infty} \frac{m_3 \left[r + (R_s^2 + x'^2)^{\frac{1}{2}} \cdot \cos\left(\alpha - \tan^{-1} \frac{x'}{R_s}\right) \right]}{2\pi \left[(R_s + r \cos\alpha)^2 + (r \sin\alpha + x')^2 \right]} dx' \right. \\
& + \int_0^{\infty} \frac{m_3 \left[r + \frac{R^2}{(R_s^2 + x'^2)^{\frac{1}{2}}} \cos\left(\alpha - \tan^{-1} \frac{x'}{R_s}\right) \right]}{2\pi \left[r + \frac{R^2}{(R_s^2 + x'^2)^{\frac{1}{2}}} \cos\left(\alpha - \tan^{-1} \frac{x'}{R_s}\right) \right]^2} dx' \\
& \left. - \int_0^{\infty} \frac{m_3 dx'}{2\pi r} \right\} \quad \text{Region III} \quad (3.21)
\end{aligned}$$

and

$$r = (A + B \cdot R\alpha) + R \quad (3.22)$$

Knowing the sink strengths m_1 , m_2 and m_3 , equation (3.21) may be integrated. The entrainment velocity v_r is obtained by a numerical method. The results and discussion are presented in Chapter 6.

CHAPTER IV

TEST FACILITIES

Test facilities and regions are shown in Figs. 7 and 8. References to the letter code used in Fig. 7(a) are made in the description of the test facilities.

4.1 AIR SUPPLY AND FLOW-CALIBRATION PIPE

Air was supplied by a type E, size 7 Canadian Buffalo blower (B) with a rating of 2,000 C.F.M., 56.1 inches of water S.P., 3,500 R.P.M. and 31.9 B.H.P.. This blower was driven by a 40 Hp., 550 volts and 3,500 R.P.M. General Electric induction motor. The air flow could be varied by a 10 inch blast gate (A) fitted at the intake of the blower.

A bleeding section (C) with constant opening was added to reduce air flow through the system while maintaining a considerably large intake flow to prevent generation of excess heat by the blower.

A 30 inch long cold rolled seamless steel pipe (D) with 5 in. O.D. was attached to the blower exit. This pipe served as a flow measuring section. A standard pitot-static probe mounted on a traversing mechanism (T) was able to traverse across the pipe and the air flow thus could be determined by knowing the velocity profiles inside the pipe.

4.2 PLENUM CHAMBER AND NOZZLE

The plenum chamber (F) was made of two identical wooden boxes with a dimension of 4 x 4 x 4 ft.. Two layers of 40 x 40 mesh screen were installed between the two wooden boxes. Because of the large volume of the plenum chamber the flow out of the chamber was fairly steady.

A converging nozzle (N) made of brass with a 0.500 x 9 in. exit was attached to the plenum chamber. By inserting a plastic plate of 0.375 x 9 x 5 in., the nozzle width was reduced from 0.500 to 0.125 in.. The contraction ratio for the nozzle was well above 100.

4.3 END-PLATES AND SUPPORTING TABLE

Two 36 in. radius, 1/4 in. thick semicircular plexiglass plates were used as the end-plates. One plate was placed horizontally on the top of a supporting table. The other plate was kept 9 in. above the bottom plate and supported by five 1 in. diameter and 9 in. long acrylic rods. The supporting table was provided with leveling screws to ensure correct alignment.

4.4 SURFACES AND TRAVERSING MECHANISM

4.4.1 PLANE SURFACE

A 34 x 9 x 1 in. acrylic plastic sheet was mounted vertically between the end-plates with the 9 in. direction being parallel to the spanwise (9 in. length) direction of the jet slot.

By using the traversing mechanism the pressure probe could be moved parallel and perpendicular to the surface at its mid-span position. The distance could be measured to an accuracy of 0.001 in. with a full range up to 8 in. in the perpendicular direction and of 0.020 in. with a full range up to 3/4 in. in the parallel direction.

4.4.2 CONVEX SURFACE

There were three convex surfaces, i.e., 9, 6 and 3 in. outside radius, made of 9 in. long plexiglass half cylinders. These surfaces were fitted in turn between the end-plates and aligned with the nozzle exit in a position that allowed the jet to flow tangentially onto the outside of the cylinder. These surfaces were designated as (9)_{+c}, (6)_{+c} and (3)_{+c} respectively.

The traversing mechanism with pressure probes was able to move along the circumference of the top semicircular end-plate with an accuracy of 1° and permitted the probes to traverse in the radial direction to an accuracy of 0.001 in.

4.4.3 CONCAVE SURFACE

Three concave surfaces were formed by keeping the same half cylinders aligned to the nozzle exit in such a way that the jet flowed around the inside of the cylinder. Because of the 1/4 in. wall thickness of the cylinder, the radii of curvature were reduced to 8.75, 5.75 and 2.75 in.. These surfaces were denoted as (9)_{-c}, (6)_{-c} and (3)_{-c} for simplicity in symboling.

The traversing mechanism consisted of a small turning device mounted at the centre of the cylinder. This mechanism positioned the pressure probes in the radial direction with an accuracy of 0.001 in. and in the circumferential direction (from 0° to 180°) with 1° accuracy.

4.5 PROBING EQUIPMENT

A flattened stainless steel hypodermic tube with an opening of 0.002 x 0.066 in. was used to measure the total pressure in the jet. The static pressure probe was made by a similar hypodermic tube of the same outer dimensions with thin slots on the narrow sides (see Fig. 9). The static and total pressure probes were placed at a distance of 0.5 in. above and below the centre line of the flow surface respectively.

A Lambrecht sloping micromanometer with a maximum accuracy of 0.001 in. of water was utilized in making all pressure measurements.

CHAPTER V

EXPERIMENTS

The experiments were conducted to determine the curvature effect on the entrainment flow of the surrounding still air into the jet as well as the non-dimensional velocity profile, the jet growth, the maximum velocity decay, the length of the potential core and the inner layer velocity power law.

Experimental measurements were carried out on three convex surfaces denoted by the symbols of $(3)_{+c}$, $(6)_{+c}$ and $(9)_{+c}$; three concave surfaces, $(3)_{-c}$, $(6)_{-c}$ and $(9)_{-c}$ respectively; and a 3/4 in. long flat surface, $(\infty)_{oc}$ (see Table IV).

Probing of the jet sheet at mid-span position and at various stations along its length were made for those surfaces mentioned. There were two nozzle widths, 1/2 and 1/8 in. and the jet velocity at the nozzle exit was kept constant during the test programme, except for the potential core measurements.

5.1 CALIBRATION

The flattened hypodermic probe used for measuring the total pressure was compared with a small Kiel probe under actual test conditions. The results indicated a very good

agreement with $\pm 0.1\%$ error. The static pressure probe, calibrated and used in an earlier experiment (Ref. 25), was utilized. Since the static pressure probe was used to get the surface pressure for present experiments, a pressure comparison between the readings from surface taps on the cylinder $(6)_{+c}$ and the static pressure probe was carried out by placing the probe on the surface under actual test conditions. A correction factor was obtained and, therefore, throughout the test programme all the static pressure readings on the surface were measured by the probe.

Velocity distributions across the width of the nozzle exit at different positions along the span of the nozzle were determined. The velocity distribution was found to be effectively uniform over 85% of the nozzle width and 99% of the nozzle span varying only $\pm 1\%$ from the central-core velocity.

The two dimensionality was checked by probing across the jet at various spanwise positions above and below the centre line (at $\theta = 100^\circ$ in the case of curved wall jets and $\bar{x} = 20$ for plane wall jet). The results were found to be satisfactory with a maximum difference of $\pm 1\%$ in the local velocity over a range of 2 in. above and below the centre line.

Frequent repeatability checks were also carried out throughout the experimentation.

5.2 EXPERIMENTAL PROGRAMME

5.2.1 PLANE WALL JET

The 34 in. long flat surface was installed between the two end-plates and the leading edge was sealed against the nozzle lip. The two-dimensional plane wall jet was then probed with the total pressure probe at stations with 1 in. intervals along the wall starting from the nozzle exit. In the inner layer (see Fig. 11) the probe was positioned across the jet in steps of 0.001 in. while in the outer layer the step distance was 0.005 in.. Correction for the effective centre (Ref. 38) was not applied to the readings taken close to the wall because of the very small opening of the probe.

The measurements were performed with both nozzles.

5.2.2 CONVEX SURFACE

The $(9)_{+c}$ surface was installed between the two end-plates and aligned with the nozzle exit such that the jet issued tangentially to the surface [see Fig. 7(b)]. The surface was sealed against the nozzle lip. The two-dimensional curved wall jet was then probed at mid-span and at different values of θ along the jet. The values of θ were so chosen that the interval of θ was 1° in the region covering the potential core ($0 \leq \bar{x} \leq 10$) and 10° for the rest of the jet flow.

By adopting the assumption (Ref. 15) that the static pressure across the jet varies linearly with the distance from the surface of the wall, the static pressure probe was used only to get the surface static pressure.

The radial distance between two consecutive measuring points was varied from 0.001 in. to 0.050 in. depending upon the local jet thickness and the proximity to the wall.

The above procedure was repeated for the other two convex surfaces, namely $(6)_{+c}$ and $(3)_{+c}$ surfaces.

5.2.3 CONCAVE SURFACE

The concave surfaces, i.e., $(9)_{-c}$, $(6)_{-c}$ and $(3)_{-c}$, were fitted in position [see Fig. 7(b)] to replace the convex surfaces. The jet velocity was measured by the same procedure as for the convex surfaces.

CHAPTER VI

EXPERIMENTAL RESULTS

6.1 DATA REDUCTION

With the help of an IBM 1620 computer and a CALCOMP 565 plotter the experimental data was reduced and plotted. Input data were fluid temperature, barometric pressure, surface pressure, nozzle width, radius of curvature, the probing locations, radial positions and pressure readings from jet probing.

The fluid was treated as incompressible because the maximum jet velocity was less than 250 ft./sec..

6.2 PRESENTATION AND DISCUSSION OF RESULTS

6.2.1 ENTRAINMENT FLOW

In order to find the entrainment flow of the surrounding still air into the jet, the method based upon the rate of increase of volume flow in the jet (Ref. 32) is used here. The volume flow rate, Q , per unit span length at any value of \bar{x} is defined as:

$$Q = \int_0^{\infty} u dy \quad (6.1)$$

and the entrainment flow rate per unit span, Q_{en} , is given by $Q_{en} = Q - Q_0$ where Q_0 is the value of Q at the nozzle exit.

When a control volume $lmnp$ is considered inside the jet flow (a typical sketch is shown in Fig. 6 for a plane wall jet), the volume flow rate per unit span across the line lm and pn are Q and $Q + \frac{dQ}{dx} \Delta x$ respectively.

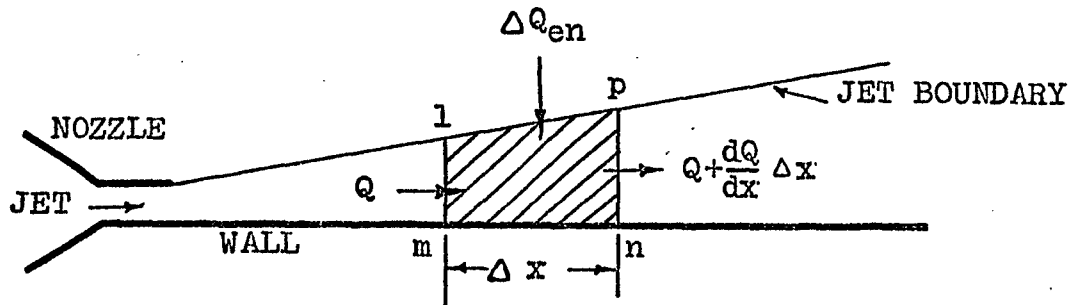


FIG. 6 CONTROL VOLUME IN A PLANE WALL JET

There is no flow across the line mn because of the wall and the entrainment flow rate per unit span, across lp is, therefore, equal to the difference between the flow rate across lm and pn , that is,

$$\Delta Q_{en} = (Q + \frac{dQ}{dx} \cdot \Delta x) - Q = \frac{dQ}{dx} \cdot \Delta x \quad (6.2)$$

Hence, the component of the entrainment velocity normal to the wall is obtained as:

$$v_{en} = \frac{\Delta Q_{en}}{\Delta x} = \frac{dQ}{dx} \quad (6.3)$$

When the volume flow rate per unit span is expressed in non-dimensional form $\bar{Q} = Q/Q_0$ and the distance as $\bar{x} = x/t$, the dimensionless entrainment velocity is given by:

$$\frac{d\bar{Q}}{d\bar{x}} = \frac{d(Q/Q_0)}{d(x/t)} = \frac{v_{en}}{u_0} = \bar{v}_{en} \quad (6.4)$$

where u_0 is the average velocity at the nozzle exit.

Because of the upper limit in equation (6.1), a practical way of determining Q is given as follows:

$$Q = \int_0^Y u dy \quad (6.5)$$

where Y is the value of y where $u=0.1u_m$ which is the smallest value that can be measured with confidence over the entire length of the jet probed.

The formation of the boundary layers on the end-plates would cause some errors in the measurements of the jet velocity at mid-span. However, the errors could be considered negligible because the aspect ratio, defined as the ratio of span to width at the nozzle exit, is fairly large (18 or more). Further, the results of the jet growth and maximum velocity decay obtained with this experimental facility for the free jet and the plane wall jet agree very well with others who have used nozzles with much higher aspect ratios.

By using a planimeter, the areas under the dimensional velocity profiles, obtained by experiments, in the region $0 \leq y \leq Y$ are determined. These values are also checked by numerical integration using the trapezoidal rule with the help of the computer.

The areas, each of which represents the volume flow rate per unit span length, Q , of the jet at station \bar{x} , are divided by Q_0 . Figure 15 shows the results of \bar{Q} vs \bar{x} for plane and curved wall jets.

The values of $d\bar{Q}/d\bar{x}$, i.e., \bar{v}_{en} or (v_{en}/u_0) , for plane and curved wall jets are then obtained by taking the slope of the curves in Fig. 15 and are plotted against \bar{x} in Fig. 16. An instrument for drawing the tangent to a curve (Fig. 14), provided by the Central Research Shop of the University has been employed. The instrument consists of two small $1/4$ in. diameter plastic rods of 1 in. length and a $6 \times 1-1/2 \times 1/8$ in. plastic plate. A $1/2 \times 3/4$ in. slot is cut in the plate. The rods are glued together and fitted in the slot with their longitudinal edges evenly aligned with one flat surface of the plate. The tangent (line AB in Fig. 14) to a curve can be drawn by placing this instrument on the curve and adjusting the angle of the plate until the two straight line elements of the curve appearing through the rods align together. This instrument was checked by using it on a known curved and the accuracy was found to be $\pm (1/2)^\circ$.

The clear and distinct patterns seen in Fig. 16 show that the distribution of \bar{v}_{en} has a flat portion at the peak. \bar{v}_{en} has a relatively low value at the nozzle exit. As \bar{x} increases \bar{v}_{en} increases sharply, reaching its maximum in the region of $6 \leq \bar{x} \leq 10$. After the maximum \bar{v}_{en} decreases gradually with \bar{x} . It is worth noting that the maximum occurs near the end of the potential core.

The maximum value of \bar{v}_{en} is seen to increase with decreasing radius of curvature.

In order to show more clearly the effects of curvature on entrainment, plots of $(\bar{Q} - \bar{Q}_{p.w.})$ vs \bar{x} for different surfaces are given by Fig. 17. For $\bar{x} \geq 4$, $(\bar{Q} - \bar{Q}_{p.w.})$ varies almost linearly with \bar{x} and the rate of variation depends on R. In other words, for $\bar{x} \geq 4$

$$\frac{d}{d\bar{x}} (\bar{Q} - \bar{Q}_{p.w.}) = S \quad (6.6)$$

where the slope S is a function of R as shown in Fig. 18. It is seen from Fig. 18 that a linear variation of S with curvature is a good approximation. The rates of increase for the convex and concave surfaces are different. The concave surfaces have a smaller rate than the convex surfaces. Expression for S in terms of $1/R$ are:

for convex surfaces,

$$S = 0.19/R \quad (6.7)$$

for concave surfaces,

$$S = 0.03/R \quad (6.8)$$

where R is measured in inches.

Equation (6.6) can be written as:

$$\bar{v}_{en} = (\bar{v}_{en})_{P.W.} + S \quad (6.9)$$

A new term, the entrainment ratio E, is defined as the ratio of \bar{v}_{en} of a curved wall jet to that of a plane wall jet:

$$E = \frac{\bar{v}_{en}}{(\bar{v}_{en})_{P.W.}} \quad (6.10)$$

Equation (6.10) can be expressed as:

for convex surfaces,

$$E = 1 + 0.19/R \cdot (\bar{v}_{en})_{P.W.} \quad (6.11)$$

for concave surfaces,

$$E = 1 + 0.03/R \cdot (\bar{v}_{en})_{P.W.} \quad (6.12)$$

By using the maximum value of $(\bar{v}_{en})_{P.W.}$ (Fig. 16) in Eq. (6.11) it can be shown that for convex surfaces the minimum increase of entrainment velocity compared with plane wall jet is not only of an order of 50% as stated in Ref. 32 but also of an order as high as 150% when the radius of curvature is very small ($R = 3$ in.). From Eqs. (6.11) & (6.12) it can be concluded that for a given \bar{x} , \bar{v}_{en} increases linearly with curvature.

In the case of the concave surfaces the entrainment velocity is less than that of the convex and plane surfaces. The rate of entrainment compared to the plane wall jet is found to decrease with increasing curvature.

6.2.2 JET GROWTH AND MAXIMUM VELOCITY DECAY

The polynomial equation for the jet growth given in Ref. 19,

$$\frac{y_m/2}{|R| (0 + \beta \frac{t}{|R|})} = c + d \left(\frac{y_m/2}{R} \right) + e \left(\frac{y_m/2}{R} \right)^2 \quad (6.13)$$

is utilized in order to find the effects of curvature. Constants β , c , d and e are obtained by using the method of least squares.

The value of $\beta = 5.86$, obtained in Ref. 19 for the combination of one convex and one concave surface, is tried for the present experimental points. The results are shown in Fig. 19. The agreement between the equation and experimental points is found to be poor.

Since the values of $y_m/2/t$ are affected by the curvature as shown in Figs. 20 and 21, the jet growth for different radii of curvature may be expressed by polynomials with different coefficients. By using the suggested values of $\beta = 6.25$ for convex surfaces (Ref. 19) and $\beta = 16.86$ for concave surfaces (Ref. 19), different polynomials (also see Fig. 22) are obtained. The values c , d and e of the polynomials are given in the table below.

TABLE III

COEFFICIENTS OF EQUATION (6.13)

<u>Surface</u>	<u>c</u>	<u>d</u>	<u>e</u>
(9) _{+c}	+0.11	-0.26	+2.03
(6) _{+c}	+0.09	+0.08	+0.33
(3) _{+c}	+0.10	+0.06	+0.14
(9) _{-c}	+0.12	+1.12	+3.51
(6) _{-c}	+0.09	+0.50	+0.74
(3) _{-c}	+0.05	-0.14	-1.13

The values of c , d and e are plotted against curvature in Figs. 23 and 24. It is seen that these coefficients tend to remain constant with decreasing $|R|$.

The approximate jet boundary of the plane wall jet is given by the plot of Y vs x , where Y is the distance away from the wall where jet velocity is equal to 10% of the

local maximum velocity and x is the distance from the nozzle exit along the wall (Fig. 25). A relation $Y = 0.5 + 0.12 x$ is found to fit the data. Thus, the constants in Eq. (3.9) are: $A = 0.5$ and $B = 0.12$.

The maximum velocity decay is given by the variation of $\rho u_m^2 |R| \theta / (P_0 - P_\infty) \dagger$ with θ as shown in Fig. 26 for the convex and concave surfaces. The curvature effects on the maximum velocity decay are not appreciable in the convex case, but a small shift of the maximum jet velocity coefficient at some values of θ can be seen in the concave case. This dimensionless variable decreases with θ for the convex case and increases with θ for the concave case.

6.2.3 POTENTIAL CORE LENGTH

Conventionally, the potential core of a jet is defined as the region of uniform velocity which is equal to the jet velocity at the nozzle exit. Because of the static pressure gradient across a curved wall jet, the velocity distribution at the nozzle exit is no longer uniform. However, the total pressure is a constant across the jet at the nozzle exit except for its very thin boundary layers. Therefore, it is necessary to redefine the potential core as the region of constant total pressure having the same value as the nozzle exit.

In order to determine the potential core boundaries, traverses were taken to establish the loci of points having 95% of the total pressure at the nozzle exit at various

stations along the jet. Plots of these points are shown in Figs. 27 & 28.

The intersection of the two boundaries is used to obtain the length of the potential core. From the plots for convex and concave surfaces shown in Figs. 27 and 28, it is observed that the length of the potential core is practically independent of curvature and has an approximate value of $6t$. Further, for over the Reynolds number range studied ($1.55 \times 10^4 \leq Re \leq 7.52 \times 10^4$) no effect was observed on the potential core length.

6.2.4 NON-DIMENSIONAL VELOCITY PROFILE

The experimental non-dimensional velocity profiles of the curved wall jets for various radii of curvature are plotted in Figs. 29 to 34.

As expected these plots substantiate the theoretical prediction of Ref. 19 that in the case of constant radius of curvature, the non-dimensional velocity profiles are not entirely similar; especially in the outer layer. However, for the concave case, similarity of velocity profiles is a better approximation than for the convex case.

In order to determine the effect of curvature, a comparison of the mean experimental profiles obtained with different radii is carried out (Fig. 35).

It is found that for convex surfaces the mean non-dimensional velocity profile is not affected by curvature of the surface. However, as compared with the concave surfaces,

the profiles are fuller in the region $0.5 \leq u/u_m \leq 0.99$ and above $y_m/y_{m/2}$ point.

For the concave surfaces there is a slightly increasing value of $y/y_{m/2}$ in the outer layer of the jet with the decrease of radius of curvature over the range of $0.50 \leq u/u_m \leq 0.99$.

6.2.5 INNER LAYER VELOCITY POWER LAW

It has been observed previously that a portion of the inner layer velocity distribution in a plane wall jet may be approximated by:

$$\frac{u}{u_m} \propto \left(\frac{y}{y_{m/2}} \right)^{1/N} \quad (6.14)$$

One of the aims of the present investigation was to determine the effect of R on N .

The log - log plots of the variation of the velocity in the inner layer of the curved wall jets are shown in Figs. 36 to 41. It is noted that in the limited regions defined by $0.007 \leq y/y_{m/2} \leq 0.16$ for convex surface and $0.025 \leq y/y_{m/2} \leq 0.16$ for concave surface, u/u_m varies approximately as $(y/y_{m/2})^{1/N}$.

Values of N , determined from the slopes of the lines, are plotted against curvature in Fig. 42. It is seen that for the convex surfaces N increases with increasing radius of curvature and remains constant for the concave surfaces.

6.3 COMPARISON BETWEEN ANALYSIS AND EXPERIMENTS

As a starting point, the sink strengths $m_1 = 0.064u_0$ and $m_2 = (3t/45x)^{1/2}u_0$, used in the free jet analysis of Ref. 35, were tried in Eq. (3.8) which is for the plane wall jet. It was found that the calculated values of \bar{v}_{en} were overestimated to an order of 30% compared to the experimental results. However, no appreciable differences were found in the general trend of the variation of \bar{v}_{en} with \bar{x} . Thus it is believed that the introduction of the wall so alters the nature of the jet that the sink strength differs from the free jet value.

In the second trial the value of constant m_1 was changed such that the calculated value of \bar{v}_{en} at the nozzle exit agreed with the experimental value ($m_1 = 0.032u_0$).

Further m_2 is expressed as:

$$m_2 = K (1/x)^{1/2}u_0 \quad (6.15)$$

where K is an empirical sink strength coefficient determined by matching the maximum value of \bar{v}_{en} to the experimental value. For curved wall jets Eq. (3.21) instead of Eq. (3.8) is used with the condition $m_2 = m_3$. The resulting distributions of \bar{v}_{en} along the different surfaces are compared with the experimental results in Fig. 43. It is seen that there is a good agreement between the analysis and experiments in

the range of $\bar{x} \geq 6$. In the potential core region, i.e., $\bar{x} \leq 6$ the agreement is not satisfactory.

In order to improve the agreement in the potential core region, the value of m_1 is allowed to vary with x . Figure 16 shows that \bar{v}_{en} increases almost linearly with \bar{x} in the potential core region. Therefore, the following linear relation is used to express m_1 as a function of x :

$$m_1 = (a_1 + b_1 x) u_0 \quad (6.16)$$

where a_1 & b_1 are empirical coefficients determined by a trial and error fitting with the experimental data. The optimum values found for a_1 , b_1 and K for different surfaces are tabulated below:

TABLE V

EMPIRICAL COEFFICIENTS IN EQUATION (6.15) & (6.16)

<u>Surface</u>	<u>a_1</u>	<u>b_1</u>	<u>K</u>
$(\infty)_{oc}$	0.016	0.010	0.109
(9) _{tc}	0.016	0.013	0.164
(6) _{tc}	0.016	0.014	0.185
(3) _{tc}	0.005	0.040	0.250

The resulting distributions of \bar{v}_{en} based on the line sink and its image system are plotted and compared with the experimental data in Fig. 44.

From the good agreement shown in Fig. 44, it can be concluded that the line sink - image technique used to predict the entrainment velocity \bar{v}_{en} and the assumed variation of m with x [Eqs. (6.15) & (6.16)] are satisfactory.

An examination of Table V indicates that a_1 is equal to 0.016 for all cases except the $(3)_{+c}$ surface. With constant a_1 , the expression for m_1 would be simpler than with varying a_1 . Therefore, $a_1 = 0.016$ is tried for $(3)_{+c}$ surface and the optimum value of b_1 is found to be 0.030. The resulting distribution is shown as the dotted line in Fig. 44. It is seen the agreement is not satisfactory in the potential core region.

The values of a_1 , b_1 and K are plotted against $1/R$ in Fig. 45. It is of special interest to note from Fig. 45 that the sink strength coefficient K varies almost linearly with curvature, $1/R$. With the help of these plots the entrainment flow could be predicted as the distribution of \bar{v}_{en} along the surface for the other values of R in the range of R used in the experiment.

However, it should be pointed out that in the case of a_1 and b_1 there is some uncertainty about the curves joining the points for $(6)_{+c}$ and $(3)_{+c}$ surfaces. It is hoped that a future experiment will cover this range of R so that the curves can be drawn with more certainty.

6.4 SOME SUGGESTIONS FOR FUTURE WORK

The following problems are suggested as continuation of the present work.

1. The line sink analysis could be extended to other jet flow problems such as plane wall jet deflection.

2. An experimental investigation of curved wall jets with t and R (especially $R \leq 6$ in.) as simultaneous variables can be carried out to obtain better empirical coefficients.

CHAPTER VII

CONCLUSIONS

1. The entrainment velocity, \bar{v}_{en} , distribution along the wall has a flat portion at the peak occurring just after the potential core ($6 \leq \bar{x} \leq 10$).
2. For a given \bar{x} , \bar{v}_{en} increases linearly with curvature.
3. Mathematical models, formed by continuous line sink and its image system, could be used to predict the entrainment velocity. The sink strength coefficient K is found to increase linearly with curvature.
4. Because of the curvature effects on the jet growth, one polynomial equation can no longer describe the jet growth satisfactorily for all radii.
5. It is found that in the inner layer of the curved wall jets the region, where u/u_m varies approximately as $(y/y_m/2)^{1/N}$, is rather limited. The regions are $0.007 \leq y/y_m/2 \leq 0.16$ for convex surfaces and $0.025 \leq y/y_m/2 \leq 0.16$ for concave surfaces.
6. Value of N increases with R for convex surfaces and remains constant for concave surfaces.
7. There are no appreciable curvature effects on the mean non-dimensional velocity profile and the potential core length.

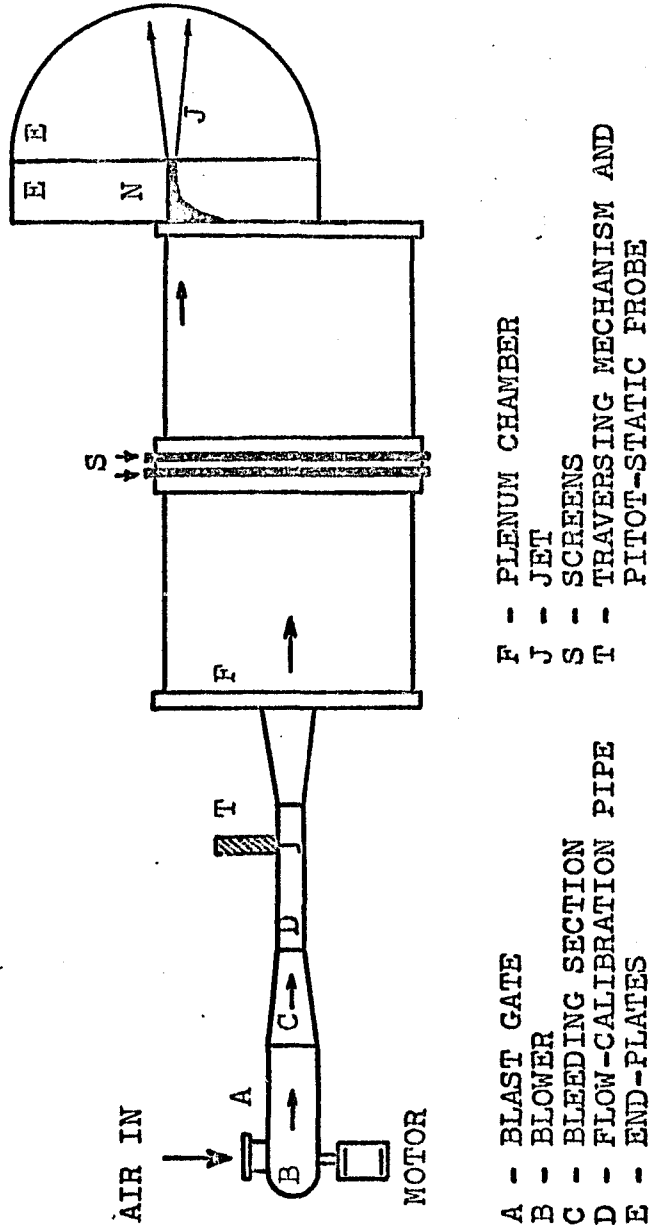
REFERENCES

1. Durand, W. F. Aerodynamic Theory, Vol. 3, Section on the Mechanics of Viscous Fluids (by L. Prandtl), P. 166 (1935)
2. Schlichting, H. Boundary Layer Theory, McGraw Hill Book Company (1960)
3. Lachmann, G. V. Boundary Layer and Flow Control Volume 1, Pergamon Press, P. 232, (1961)
4. Forthmann, E. Turbulent Jet Expansion, N.A.C.A. T.M. 789 (1936)
5. Glauert, M. B. The Wall Jet, J. Fluid Mech, Volume 1, P. 625 (1956)
6. Sigalla, A. Measurements of Skin Friction in a Plane Turbulent Wall Jet, J. Roy. Aero. Soc., 62 P. 873 (1958)
7. Schwarz, W. H. Two-Dimensional Turbulent Wall Jet, J. Fluid Mech., Volume 10, Part 4, P. 481 (1961)
Cosart, W. P.
8. Myers, G. E. Plane Turbulent Wall Jet. Part 1, Dept. of Mechanical Engineering, Stanford University, Tech. Report No. 1 (1961)
Schauer, J. J.
Eustis, R. N.
9. Gartshore, I. The Design of A Two-Dimensional Blowing Slot and its application to a Turbulent Wall Jet in Still Air. Tech. Note 64-5 McGill University (1964)
Hawaleshka, O.
10. Bradshaw, P. Turbulent Wall Jets with and without an External Stream. ARC R & M 3252 (1960)
Gee, M. T.
11. Eskinazi, S. Turbulence Measurements in A Two-Dimensional Wall Jet with Longitudinal Free Stream. Syracuse Univ. Res. Inst. Rep. ME 937-6205 P. (1962)
Kruka, V.
12. Eskinazi, S. The Wall Jet in a Moving Stream. J. Fluid Mech. 20,555 (1964)
Kruka, V.

13. Patel, R. P. Self-Preserving Two-Dimensional Turbulent Jets and Wall Jets in A Moving Stream, McGill University MEng. Thesis (1962)
14. Eyles, A. J.
Foster, D. N. An Investigation of the Curved Flow Induced by A High Pressure Jet. Univ. of Bristol, Aeronautical Laboratory, Rep. 30 (1957)
15. Newman, B. G. Deflection of Plane Jets by Adjacent Boundaries-Coanda-Effect. Article in Boundary Layer and Flow Control. Its Principles and Application. Pergamon Press. (1961)
16. Sawyer, R. A. Two-Dimensional Turbulent Jets with Adjacent Boundaries. Cambridge Univ. Ph.D. Thesis. (1962)
17. Nakaguchi, H. Jet Along A Curved Wall. Dept. of Aeronautics, University of Tokyo, Research Memo No. 4 (1961)
18. Fekete, G. J. Coanda Flow of a Two-Dimensional Wall Jet on The Outside of A Circular Cylinder. McGill Univ. Montreal, Rep. No. 63-11. (1963)
19. Gutton, D. E. Two-Dimensional Turbulent Wall Jets over Curved Surfaces. McGill Univ. Montreal. Rep. 64-7. (1964)
20. Giles, J. A.
Hays, A. P.
Sawyer, R. A. Turbulent Wall Jets on Logarithmic Spiral Surfaces. The Aeronautical Quarterly, Vol. XVII, August (1966)
21. Sridhar, K. An Experimental Investigation of the Flow in and behind Two-Dimensional Jet Sheets Bounding A Cavity, UTIA Rep. No. 94 (1963)
22. Spalding, D. B.
Chi, S. W. The Drag of A Compressible Turbulent Boundary Layer on A Smooth Flat Plate with and without Heat Transfer. J. Fluid Mech. 18, 117 (1964)
23. Ricou, F. P.
Spalding, D. B. Measurements of Entrainment By Axisymmetrical Turbulent Jets. J. Fluid Mech. Vol. 11, 21. (1961)

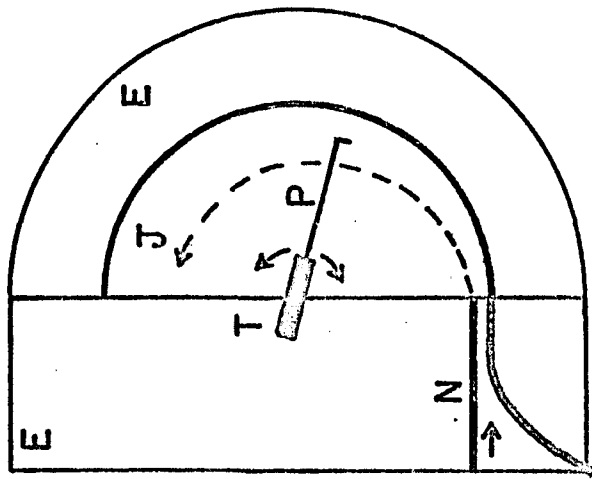
24. Sridhar, K.
Tu, P. K. C. Effects of An Initial Gap on The Flow in A Turbulent Wall Jet, J. Royal Aeronautical Society Vol. 70 (1966)
25. Paranjpe, S. C.
Sridhar, K. Effects of An Initial Gap On The Turbulent Jet Flow over A Curved Wall. J. Royal Aeronautical Society Vol. 72 (1968)
26. Arora, P. K. An Experimental Investigation of The Hysteresis Phenomenon and Effects of Gap on Curved Wall Jet Separation. M.A.Sc. Thesis, Dept. of Mech. Eng. University of Windsor. (1967)
27. Chang, P. K.
Casarella, M. J.
Kelnhofer, W. J. The Incompressible Coanda Flow Around Circular Cylinder Affected by Sound Energy. Tech. Report. Dept. of Mech. Eng. The Catholic University of America Washington. (1966)
28. Wagnanski, I.
Newman, B. G. The Effect of Jet Entrainment on Lift and Moment for a Thin Aerofoil with Blowing. The Aeronautical Quarterly May, (1964)
29. Milne-Thomson, L.M. Theoretical Hydrodynamics, The MacMillan Company (1960)
30. Schuh, H.
Person, B. Heat Transfer on Circular Cylinders Exposed to Free Jet Flow. Int. J. heat & Mass Transfer, 7, 1257 (1964)
31. Wille, R.
Fernholz, H. Report on The First European Mechanics Colloquium, on The Coanda Effect, J. Fluid Mech. Vol. 23, part 4, Pp. 801-819 (1965)
32. Stratford, B. S.
Jawor, Z. M.
Golesworthy, G.T. The Mixing with Ambient Air of A Cold Airstream in A Centrifugal Field. ARC Paper, No. 687. (1963)
33. Taylor, G. I. Flow Induced By Jets, J.A.S., Vol. 25 Pp 464-465 (1958)
34. Wagnanski, I. The Flow Induced by Two-Dimensional and Axisymmetric Turbulent Jets Issuing Normally From An Infinite Plane Surface. The Aeronautical Quarterly, Vol. (1964)

35. Wagnanski, I. The Effect of Jet Entrainment on Loss
of Thrust for A Two-Dimensional
Symmetrical Jet-Flap Aerofoil. The
Aeronautical Quarterly, Vol. (1966)
36. Tollmien, W. Calculation of Turbulent Expansion
Processes. NACA TM 1085. (1945)
37. Liepmann, H. W. Investigation of Free Turbulent Mixing.
Laufer, J. NACA TN 1257. (1947)
38. Young, A. D. The Behavior of A Pitot-Tube in a
Maas, J. N. Transverse Pressure Gradient, ARC
RANDM 1770

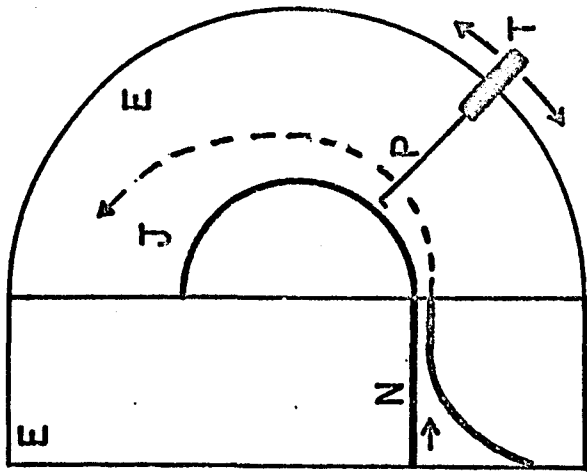


- A - BLAST GATE
- B - BLOWER
- C - BLEEDING SECTION
- D - FLOW-CALIBRATION PIPE
- E - END-PLATES
- F - PLENUM CHAMBER
- J - JET
- S - SCREENS
- T - TRaversing MECHANISM AND PITOT-STATIC PROBE

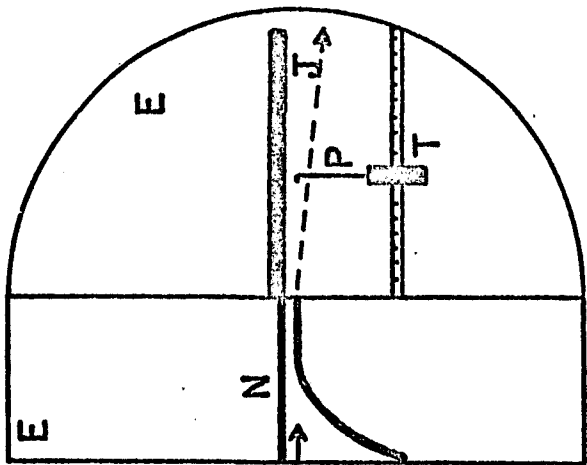
FIG. 7(a) SCHEMATIC DIAGRAM OF THE TEST FACILITIES



CONCAVE SURFACE



CONVEX SURFACE



PLANE SURFACE

(E - END-PLATES N - NOZZLE J - JET P - PROBES T - TRAVERSE)

FIG. 7(b) SCHEMATIC DIAGRAM OF THE TEST REGIONS

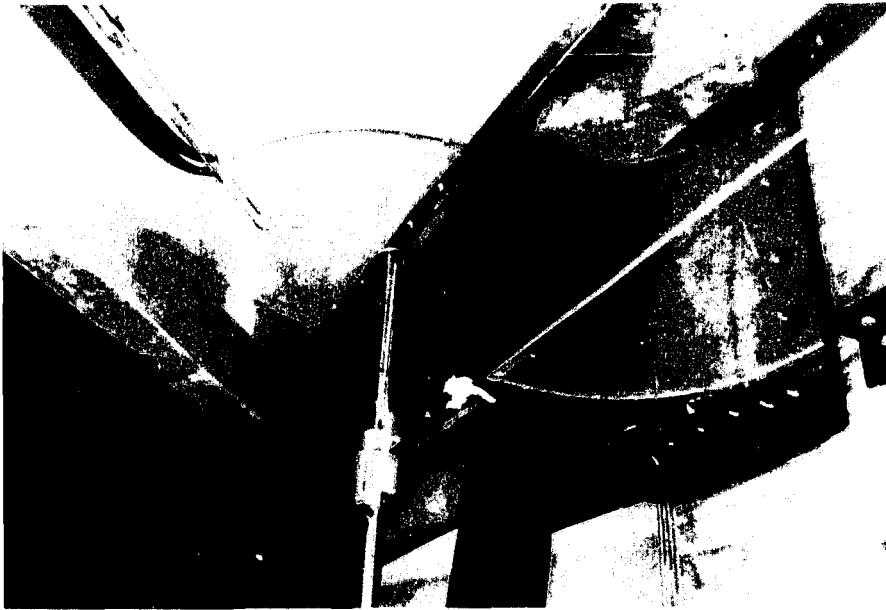


FIG. 8(a) TEST REGION AND PRESSURE PROBES
FOR CONVEX SURFACE

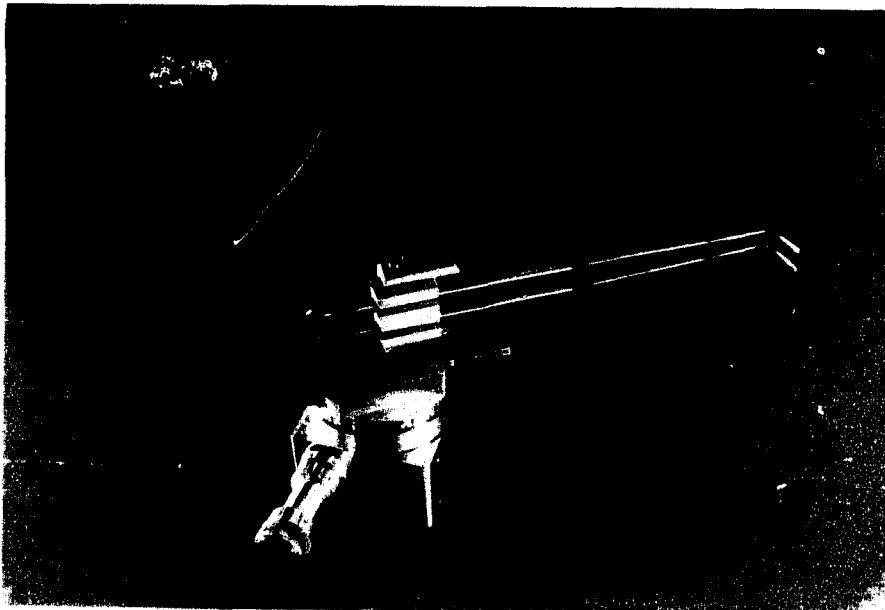
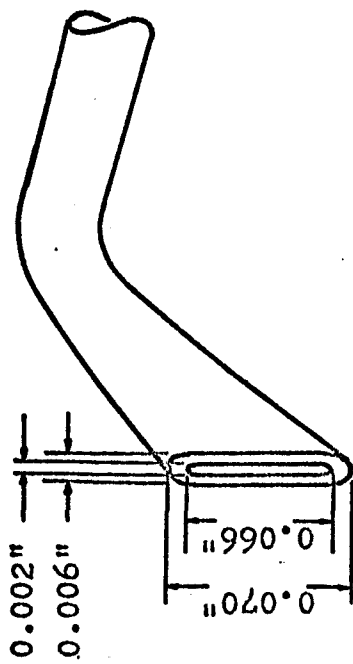
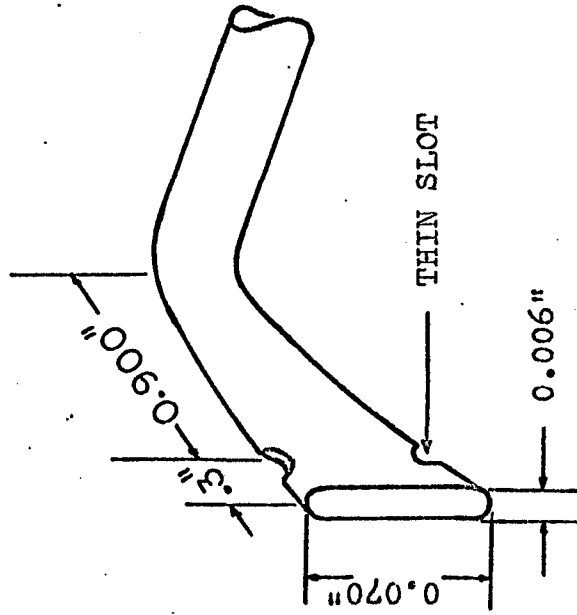


FIG. 8(b) TRAVERSING MECHANISM AND PRESSURE
PROBES FOR CONCAVE SURFACE



TOTAL PRESSURE PROBE



STATIC PRESSURE PROBE

FIG. 9 STATIC AND TOTAL PRESSURE PROBE

REGION OF STILL AIR

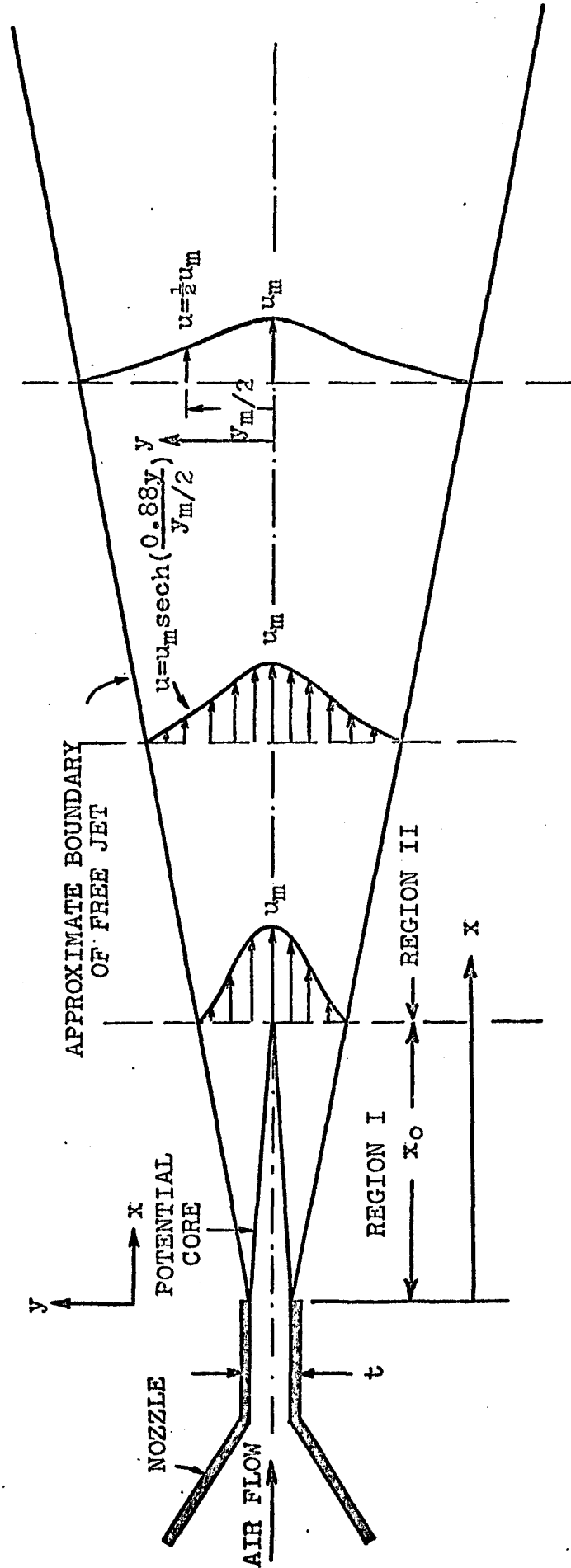


FIG. 10 . FREE JET NOMENCLATURE

REGION OF STILL AIR

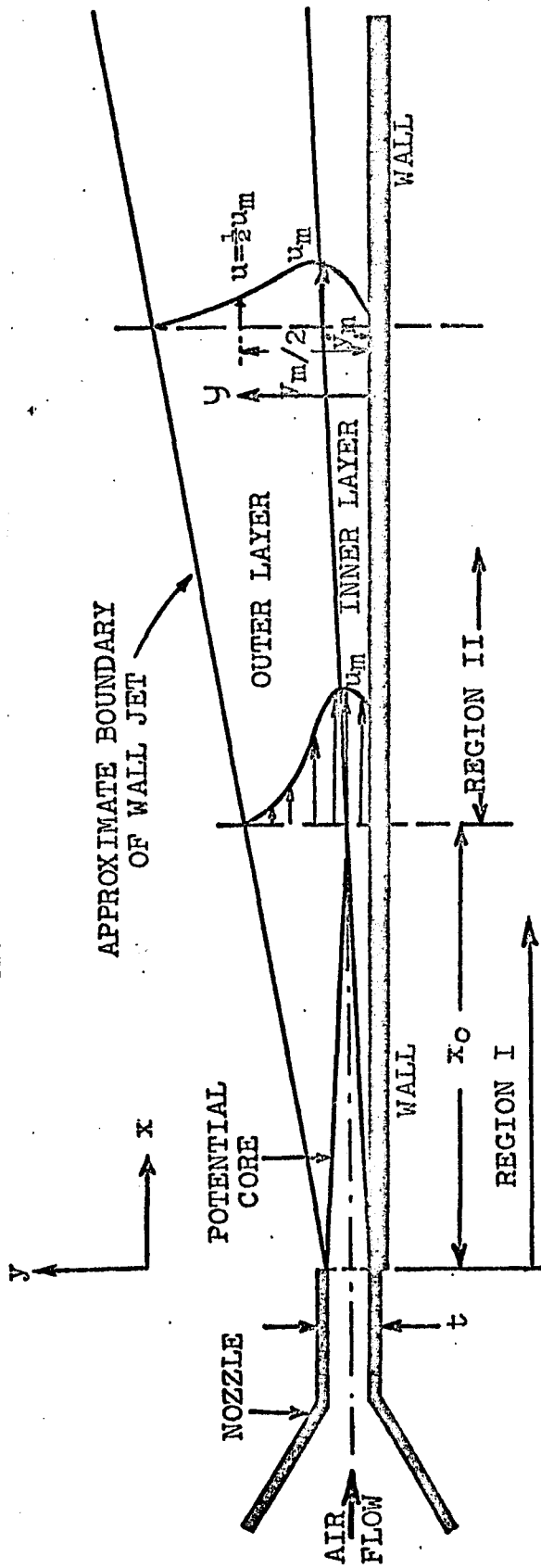


FIG. 11 WALL JET NOMENCLATURE

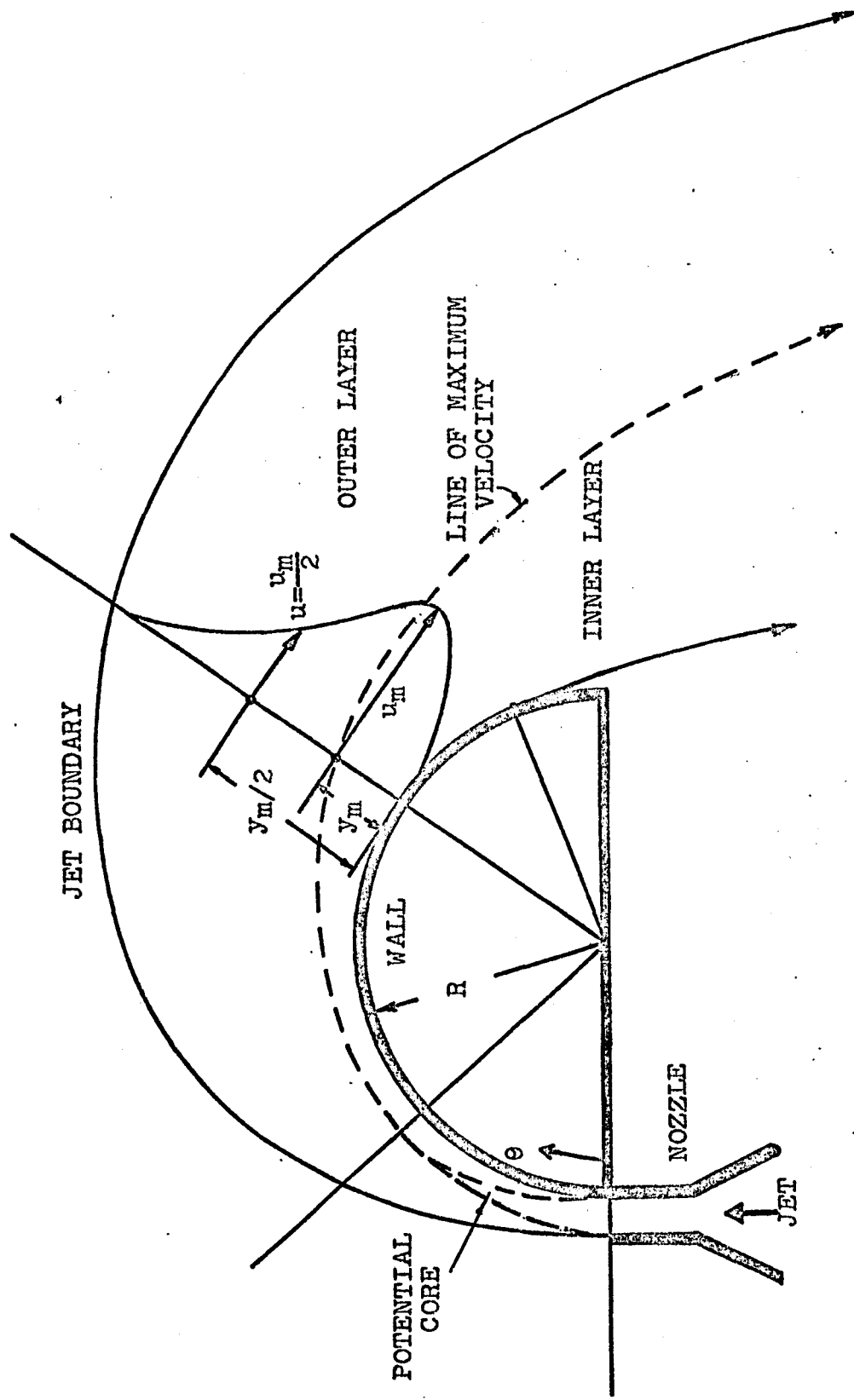


FIG. 12 NOMENCLATURE OF CURVED WALL JET WITH CONVEX CURVATURE

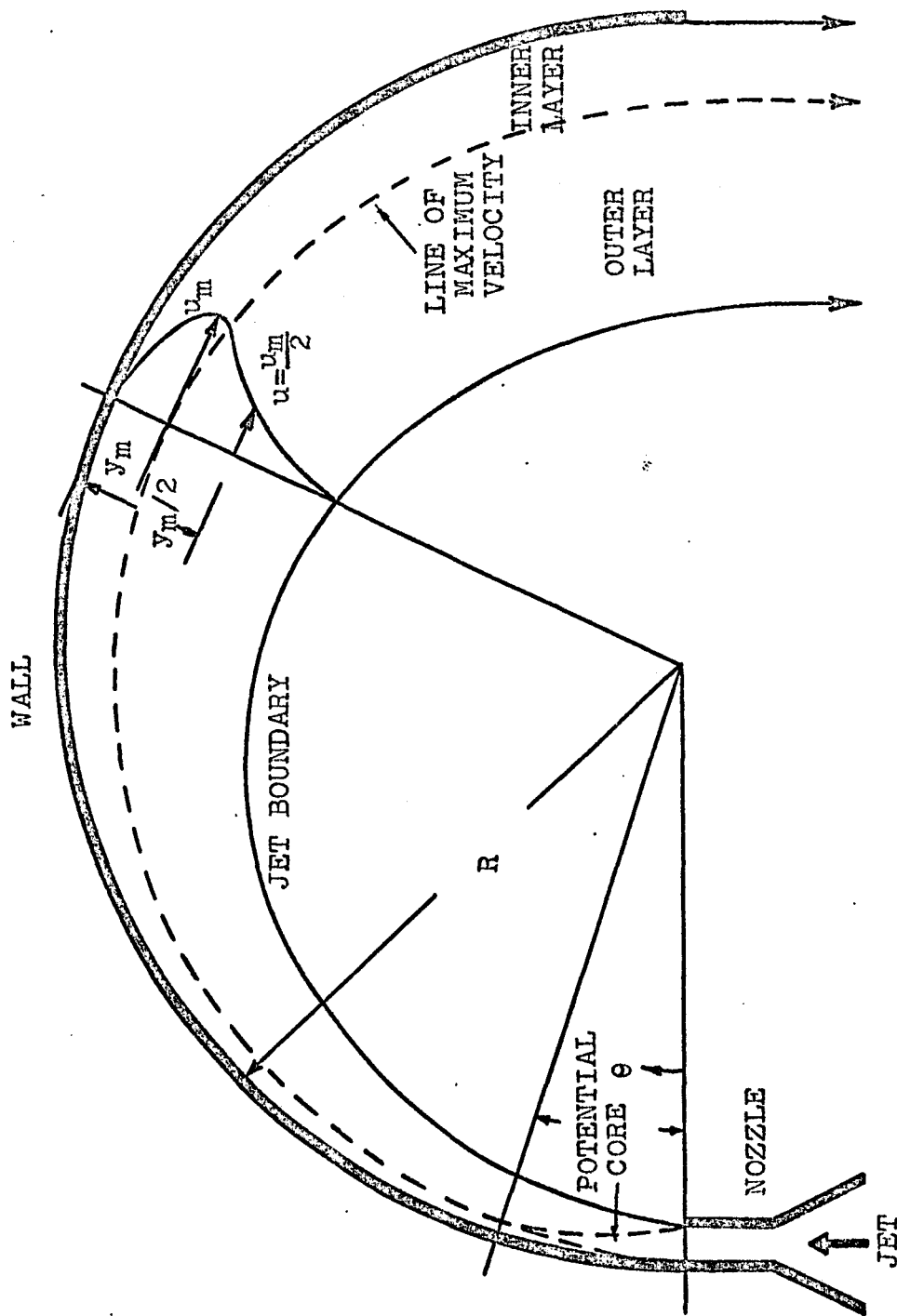


FIG. 13 NOMENCLATURE OF CURVED WALL JET WITH CONCAVE CURVATURE

SCALE 1:1 IN INCH

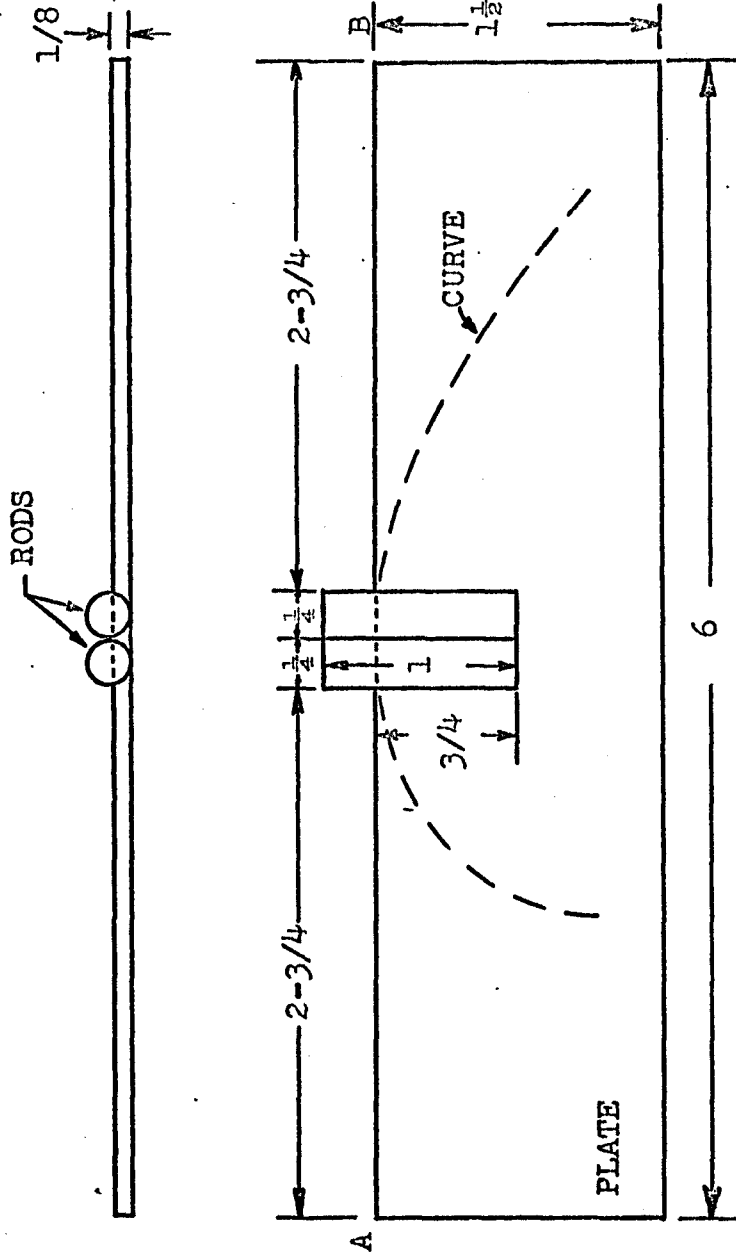


FIG. 14 SKETCH OF THE INSTRUMENT FOR DRAWING TANGENT TO A CURVE

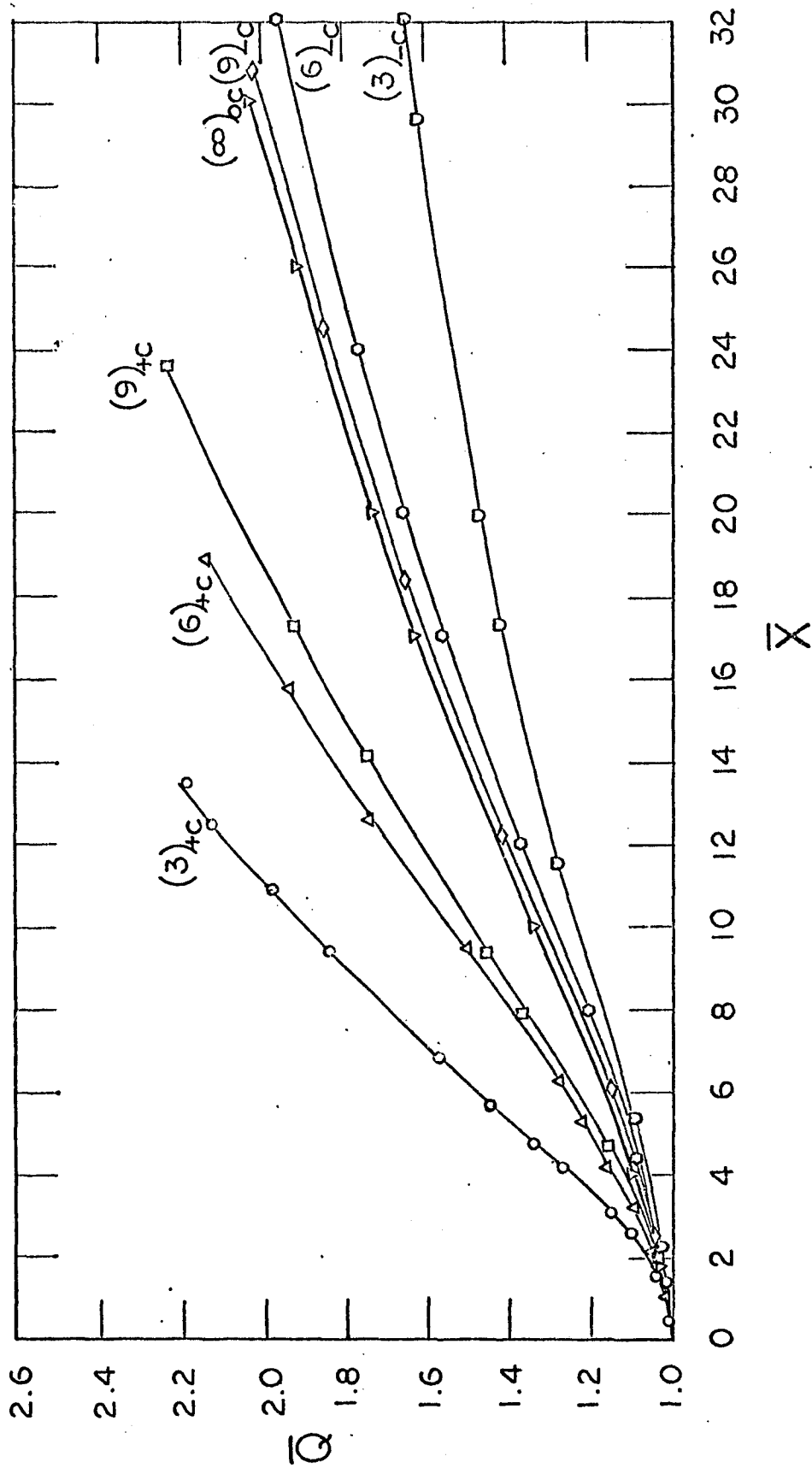


FIG. 15 VARIATION OF FLOW RATE ALONG THE JET

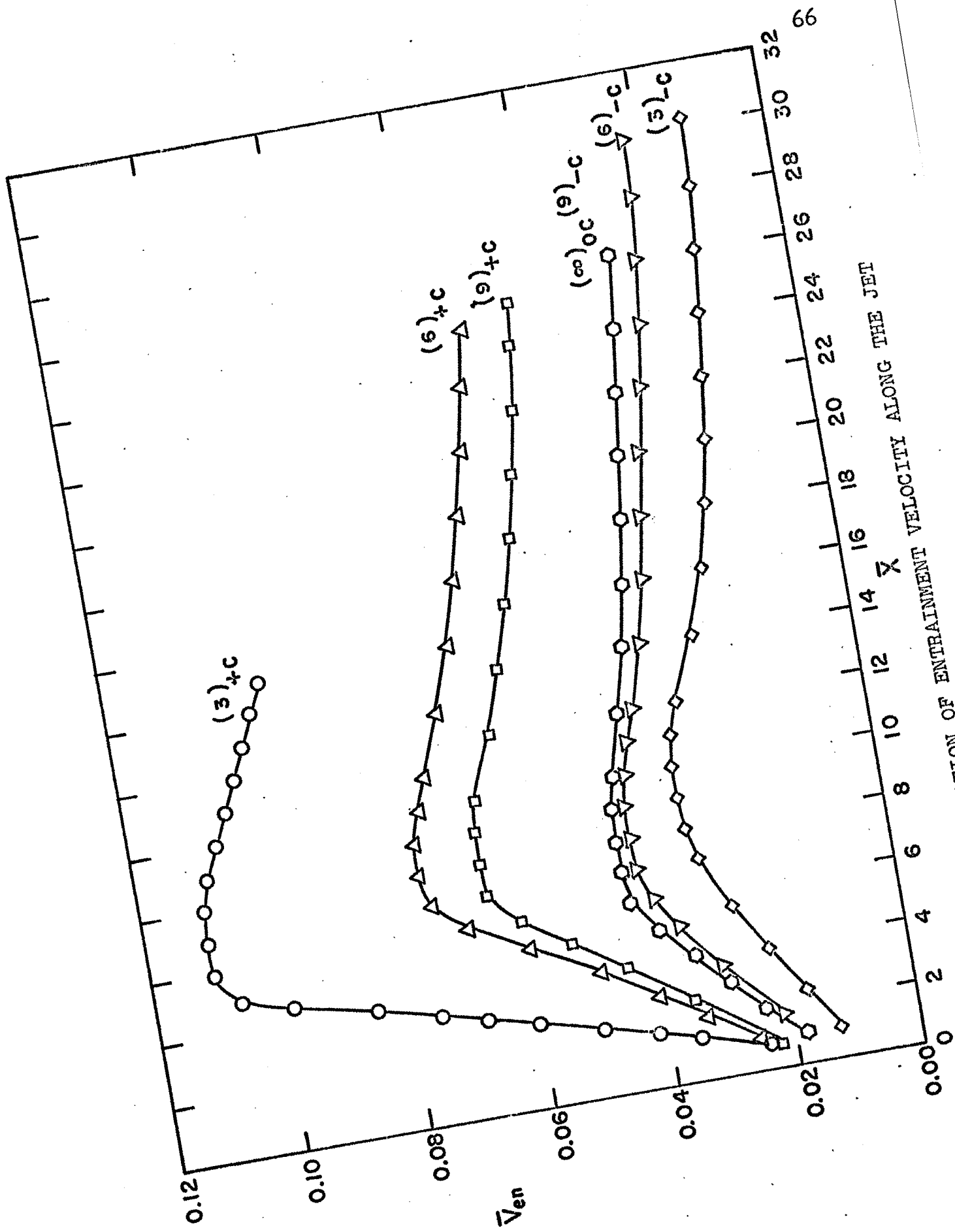


FIG. 16 VARIATION OF ENTRAINMENT VELOCITY ALONG THE JET

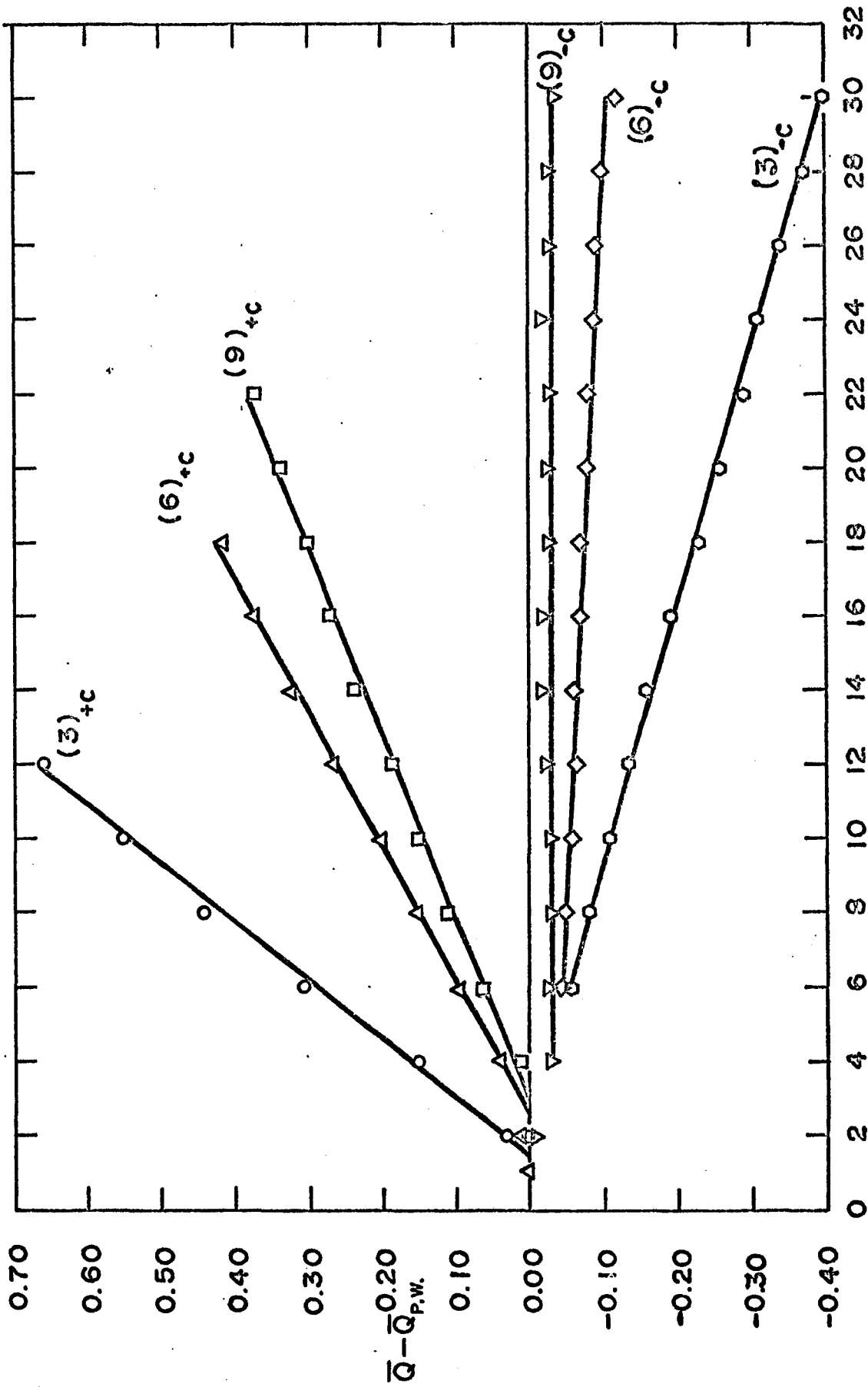


FIG. 17 VARIATION OF THE FLOW RATE DIFFERENCE BETWEEN THE CURVED WALL JETS AND PLANE WALL JET ALONG THE SURFACE

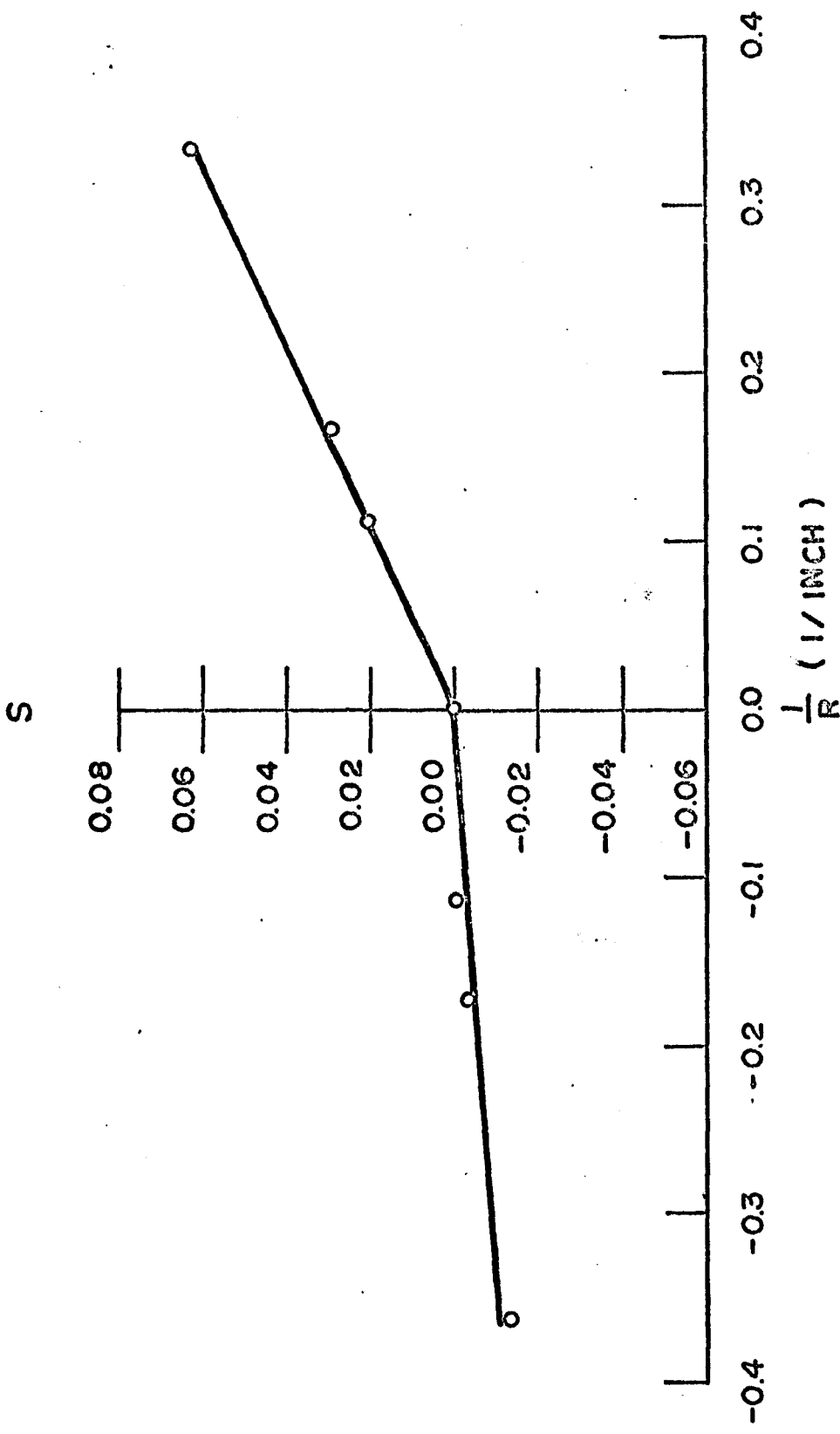


FIG. 13 PLOT OF SLOPE S VS CURVATURE

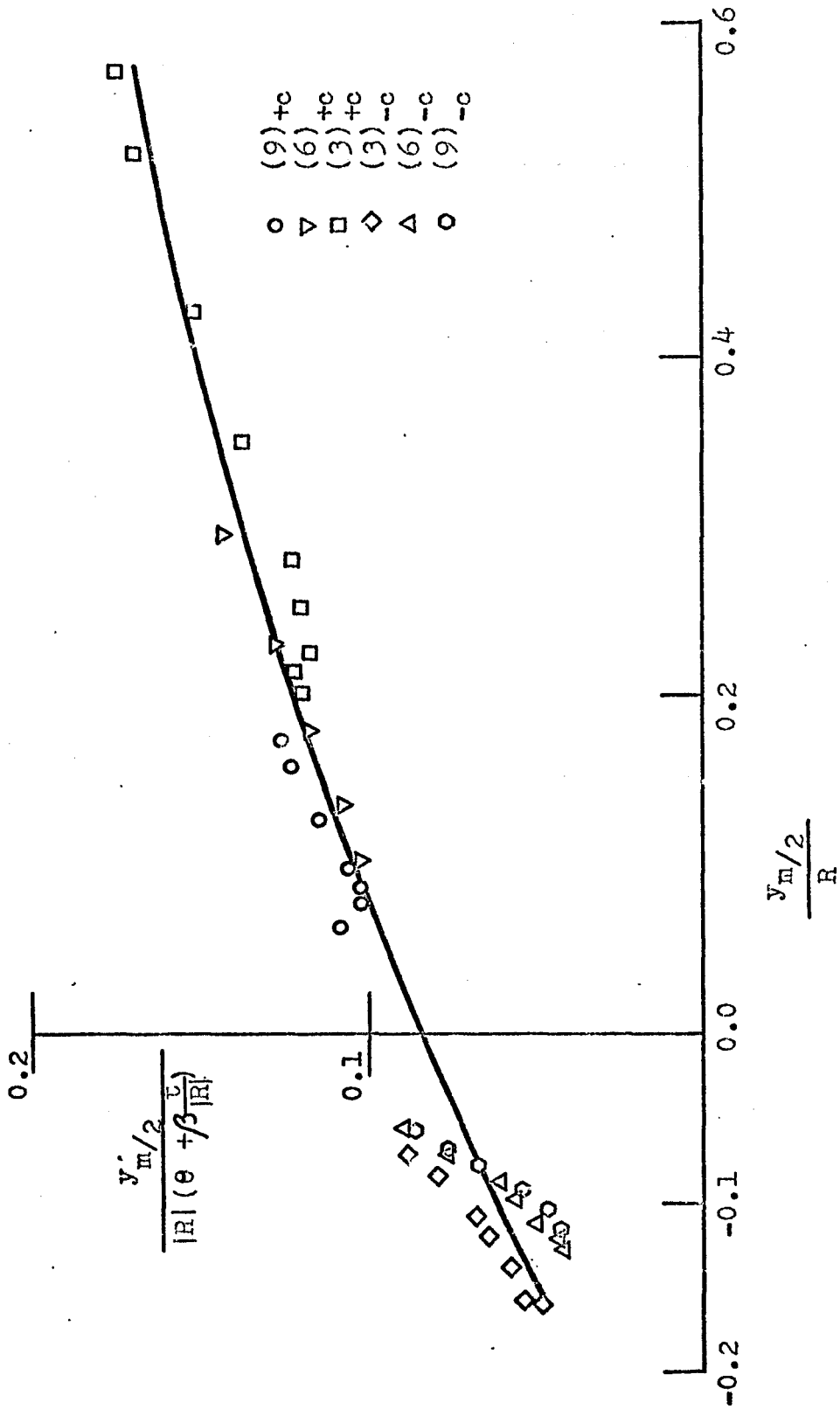


FIG. 19 PLOT FOR JET GROWTH LAW

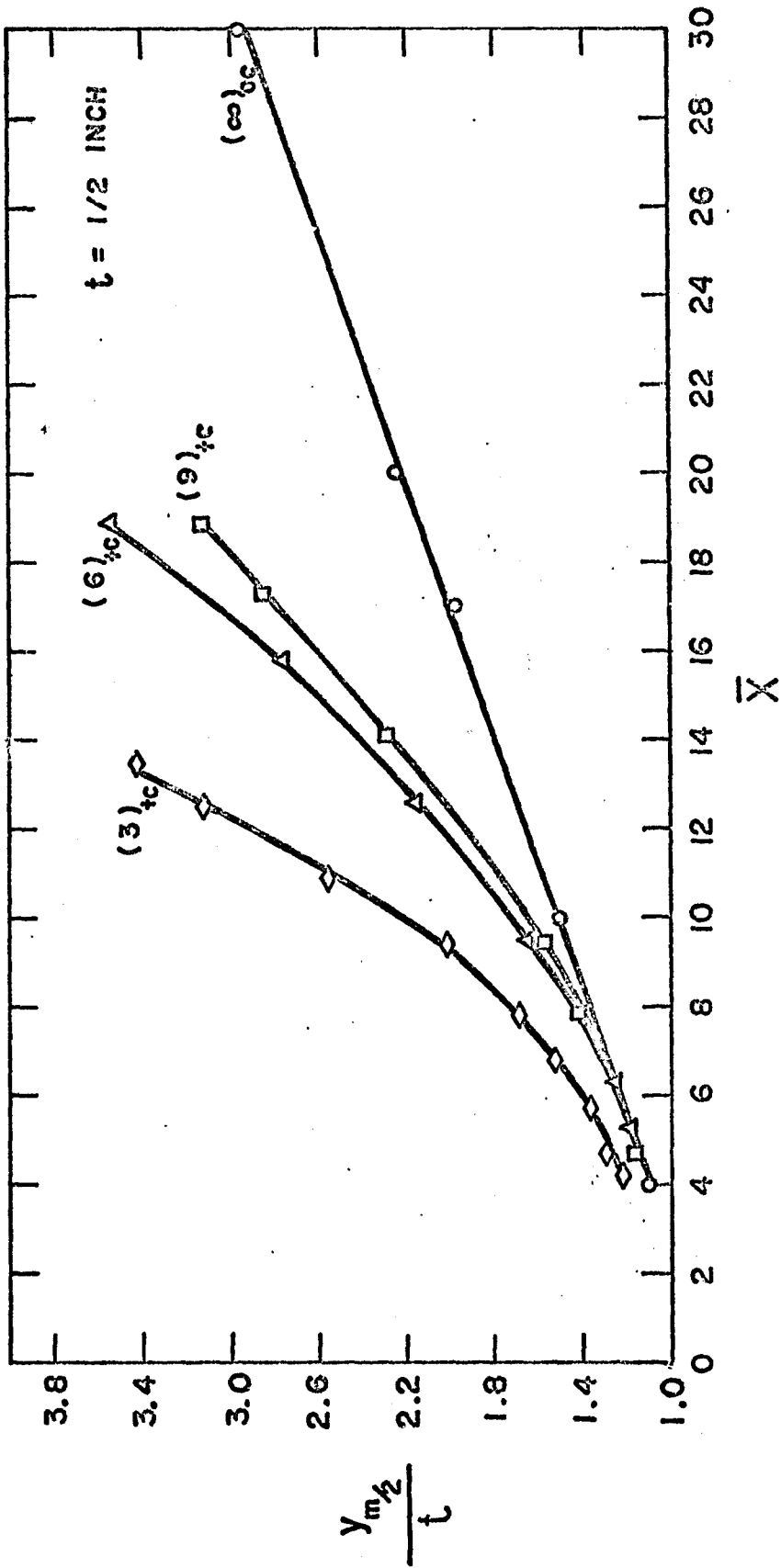


FIG. 20 JET GROWTH FOR PLANE AND CONVEX SURFACES

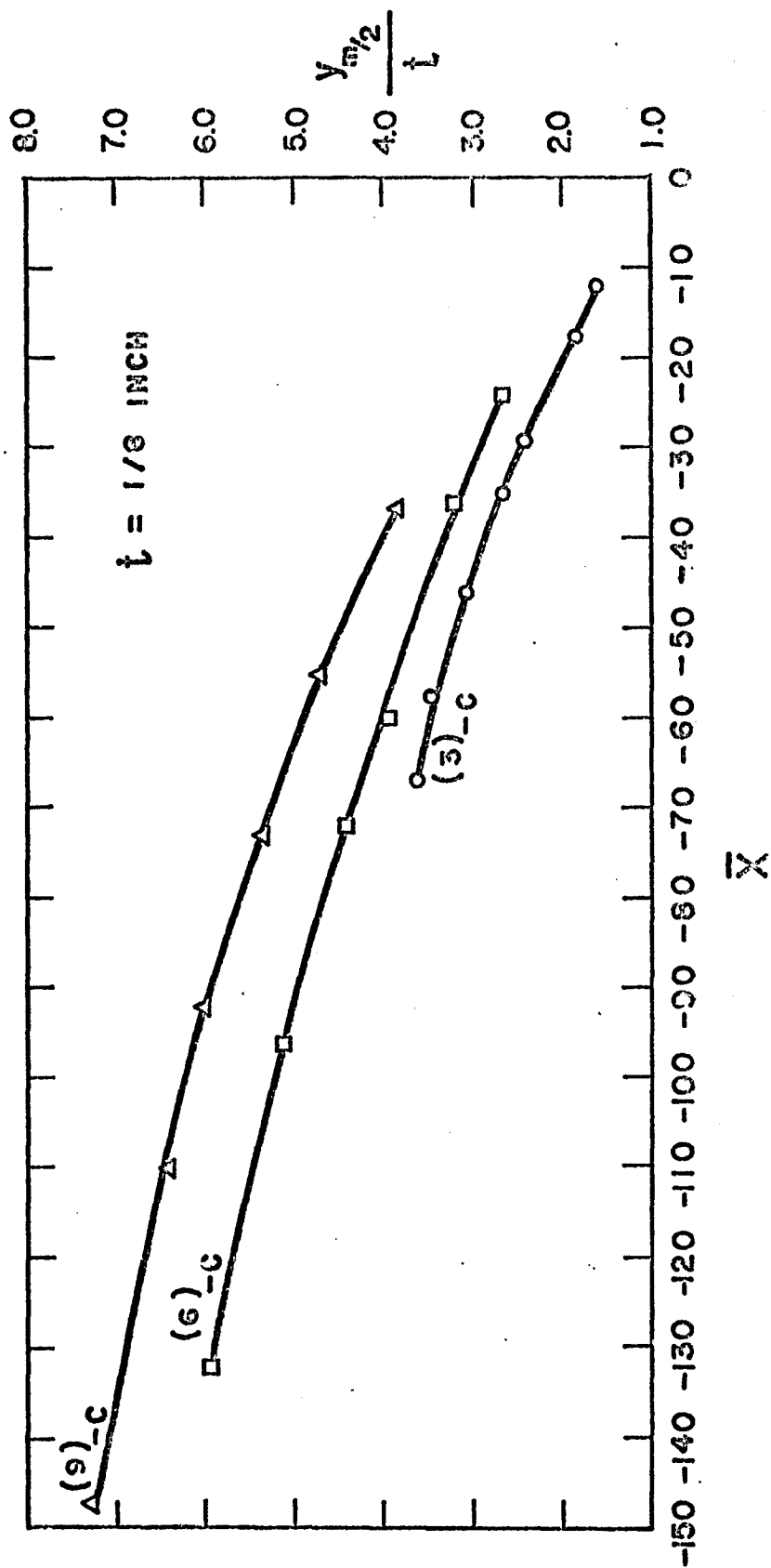


FIG. 21 JET GROWTH FOR CONCAVE SURFACE

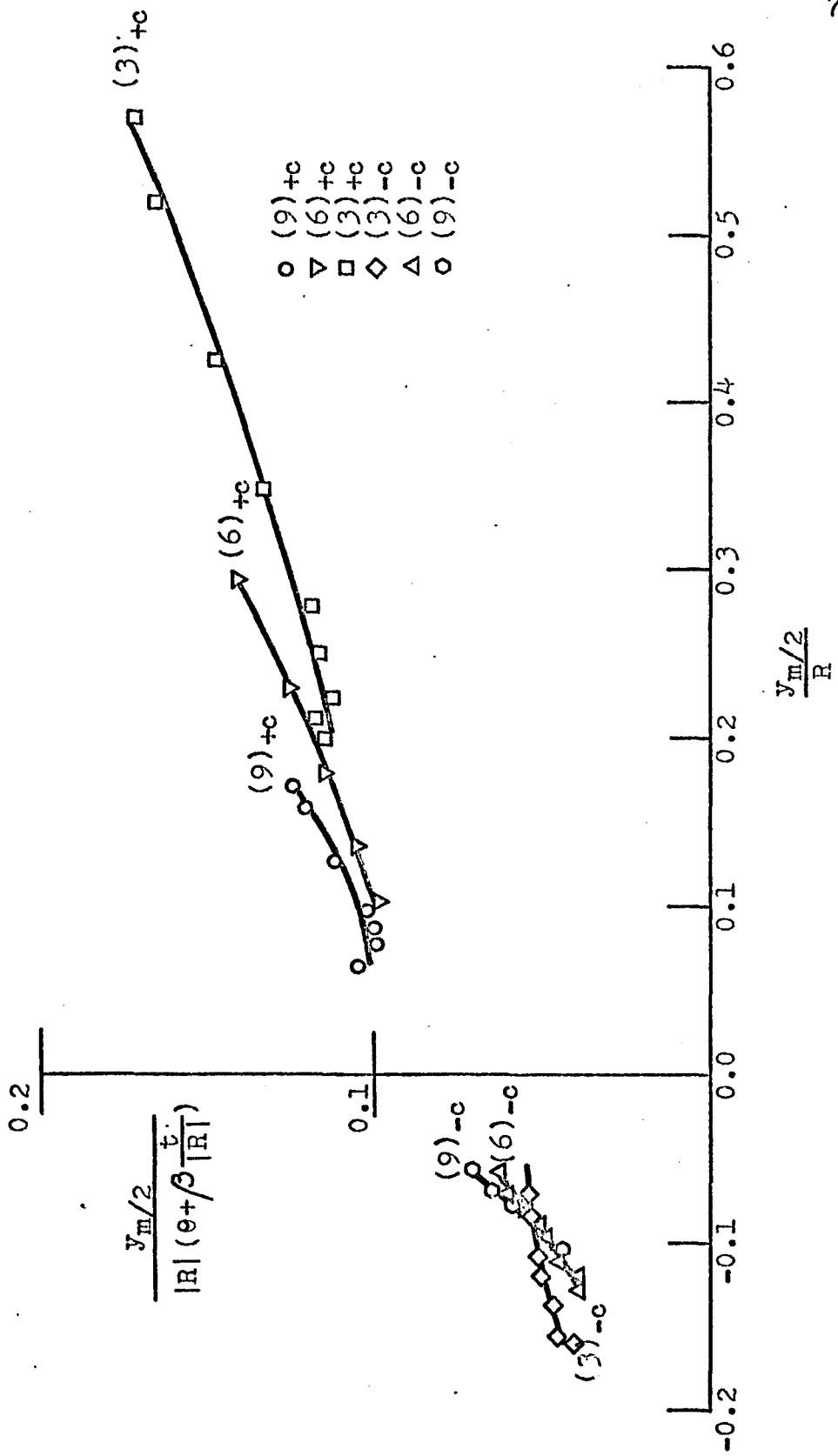


FIG. 22 PLOT FOR JET GROWTH LAW

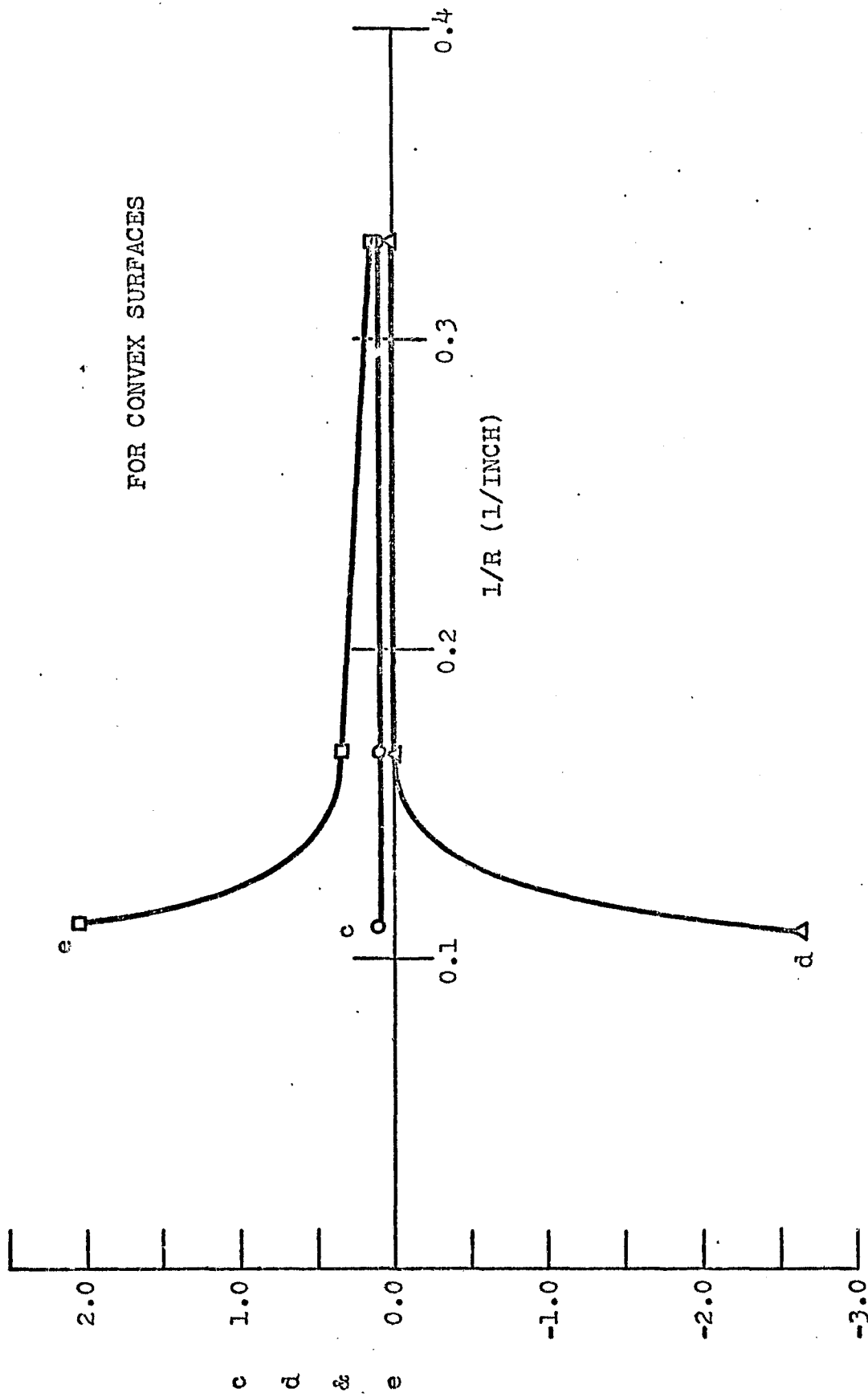


FIG. 23 VARIATION OF c, d AND e WITH CURVATURE

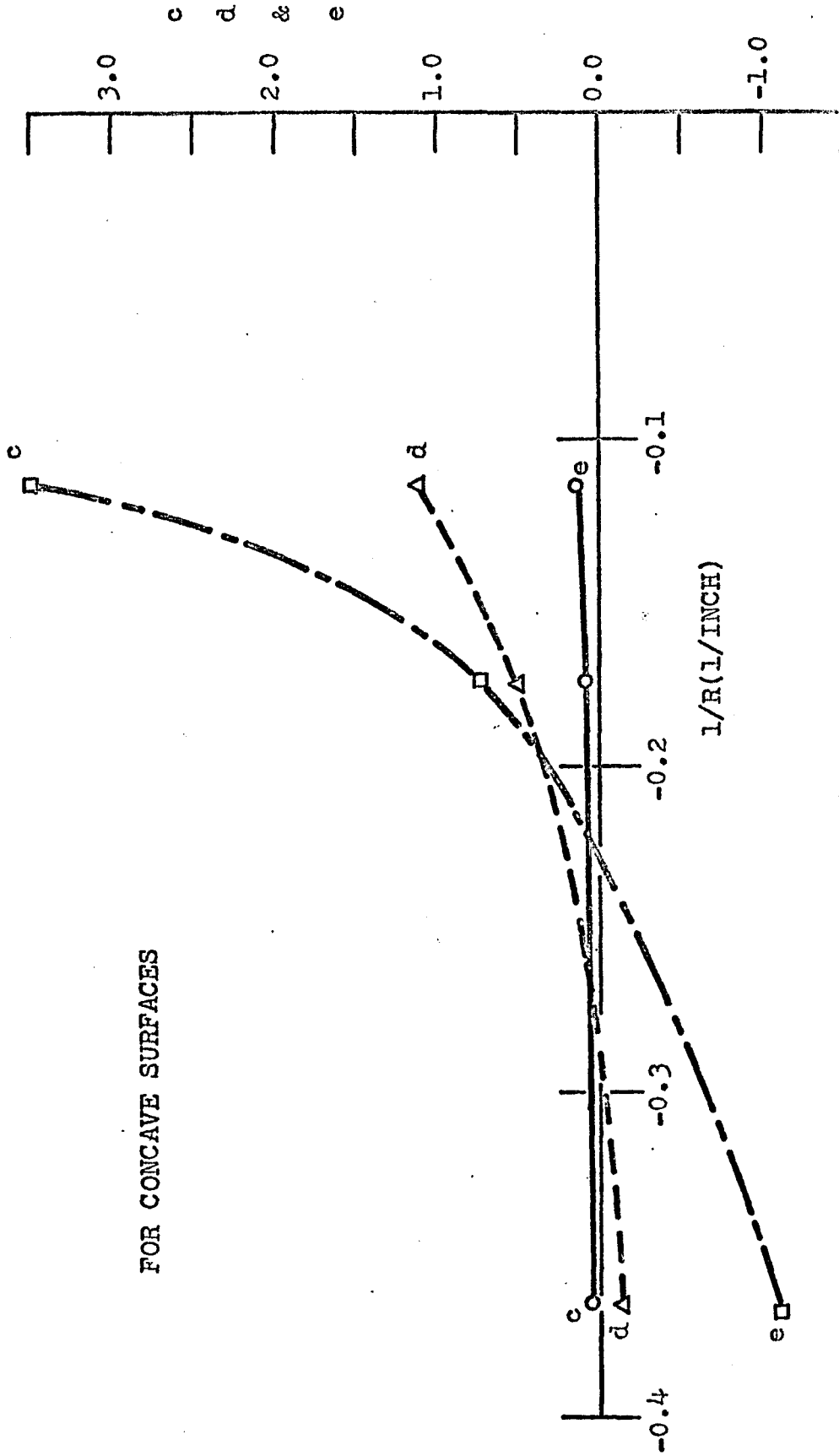


FIG. 24 VARIATION OF c, d AND e WITH CURVATURE

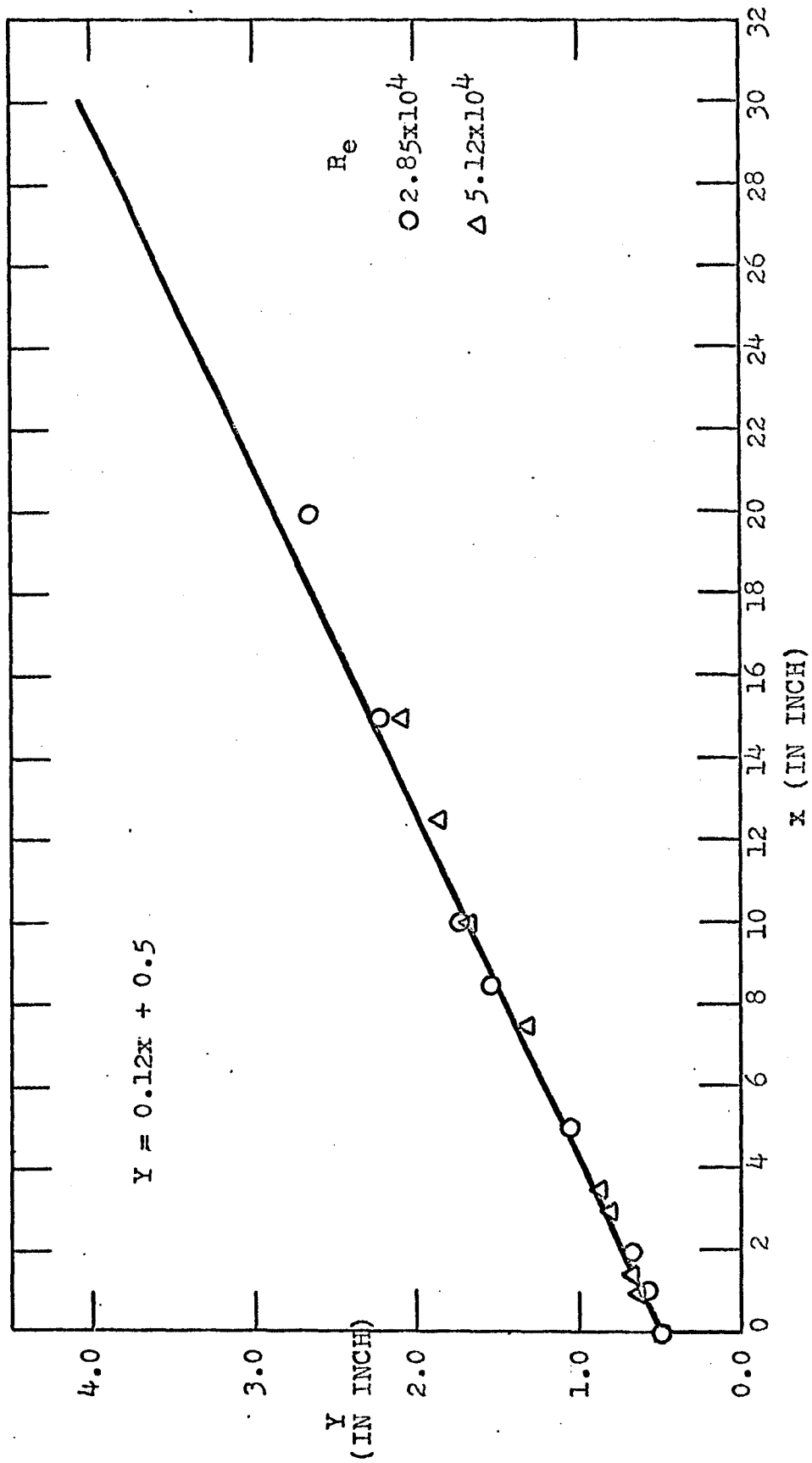


FIG. 25 APPROXIMATE JET BOUNDARY OF THE PLANE WALL JET

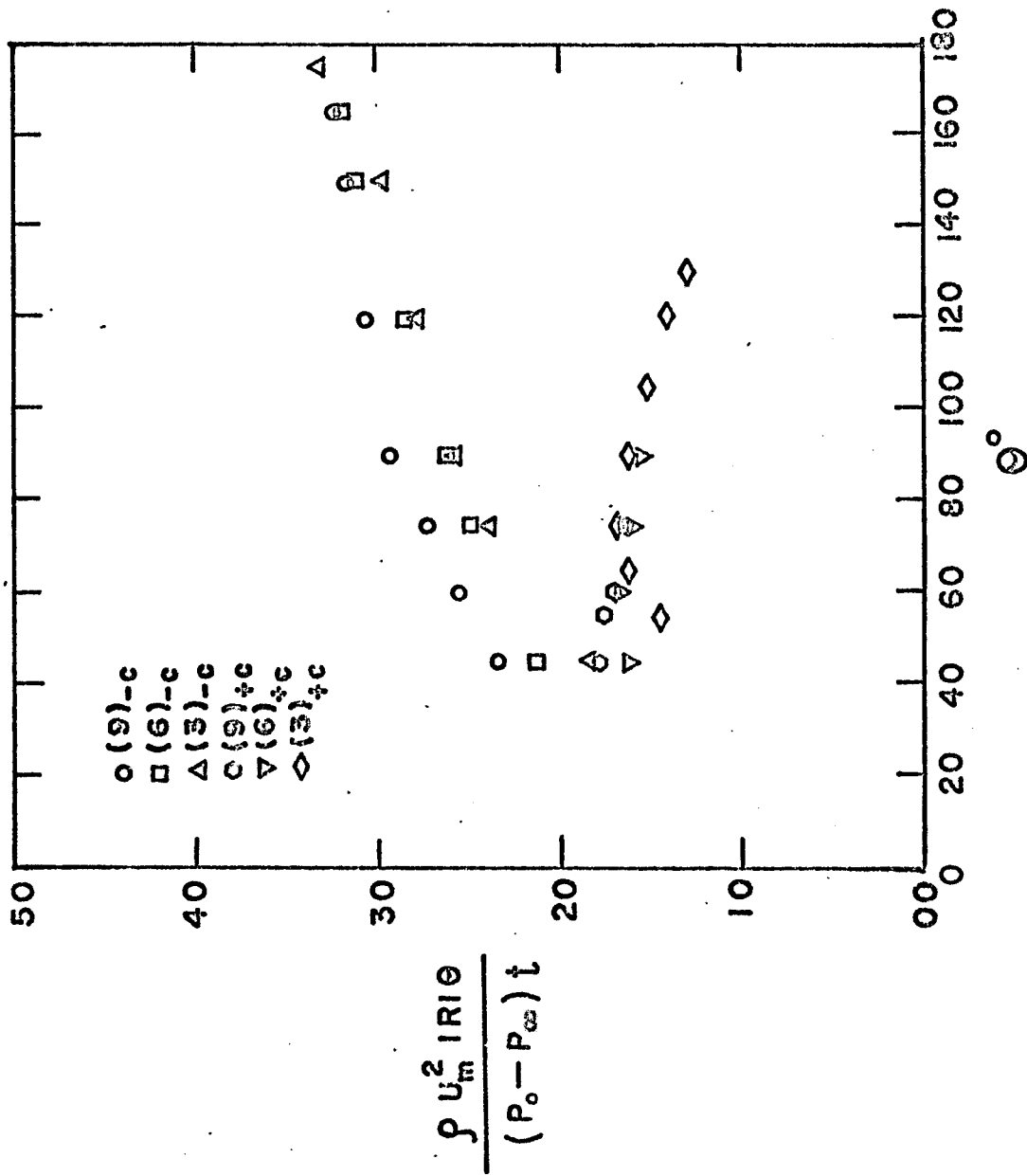


FIG. 26 MAXIMUM VELOCITY DECAY

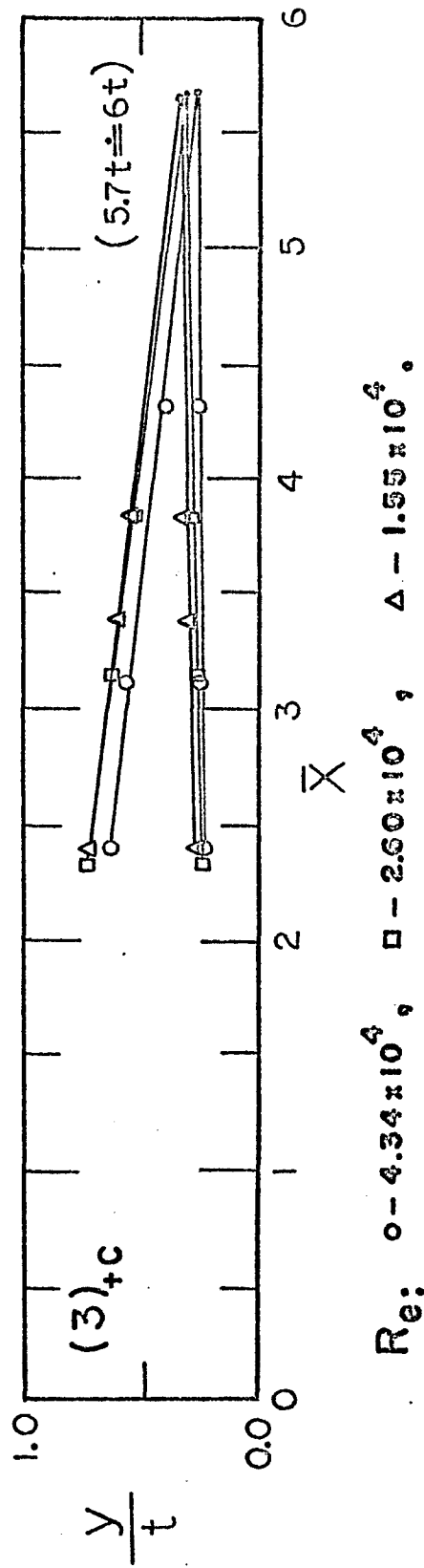
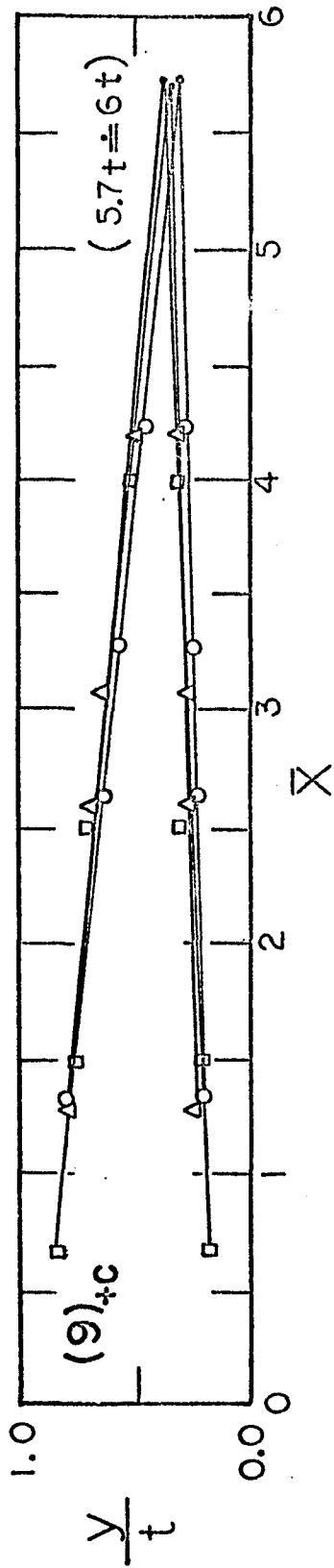
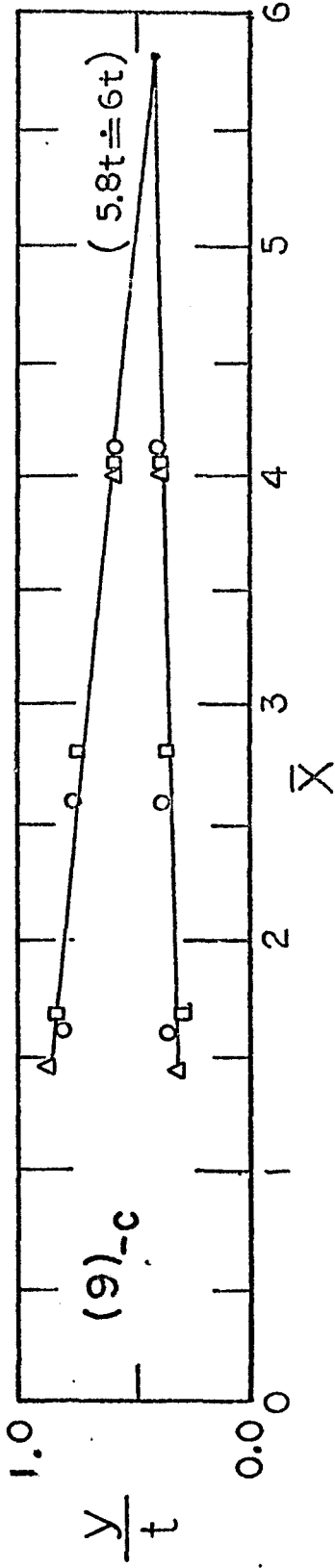
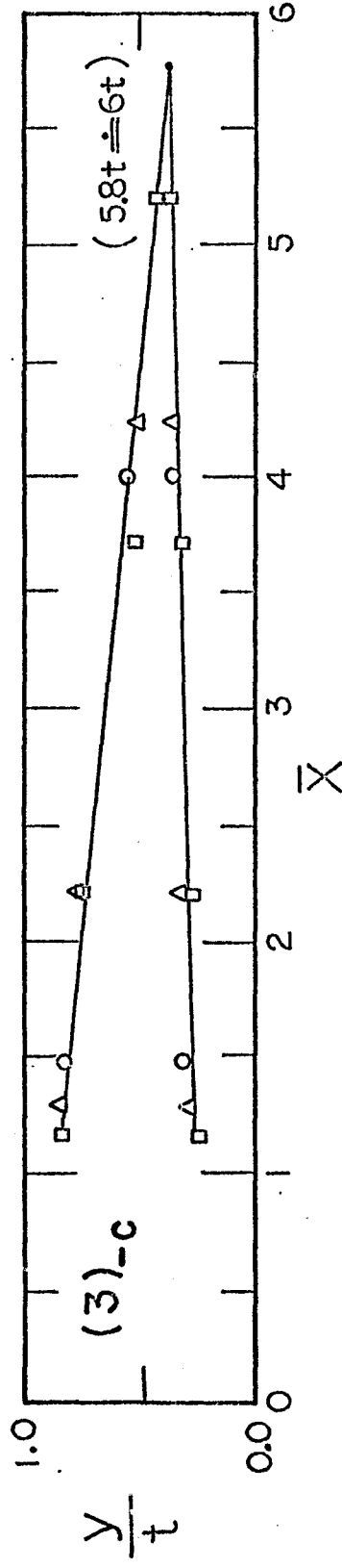


FIG. 27 POTENTIAL CORE BOUNDARIES FOR CURVED WALL JETS WITH CONVEX CURVATURE



$Re: \circ - 7.52 \times 10^4, \square - 4.50 \times 10^4, \Delta - 2.77 \times 10^4.$



$Re: \circ - 4.22 \times 10^4, \square - 2.53 \times 10^4, \Delta - 1.55 \times 10^4.$

FIG. 28 POTENTIAL CORE BOUNDARIES FOR CURVED WALL JETS WITH CONCAVE CURVATURE

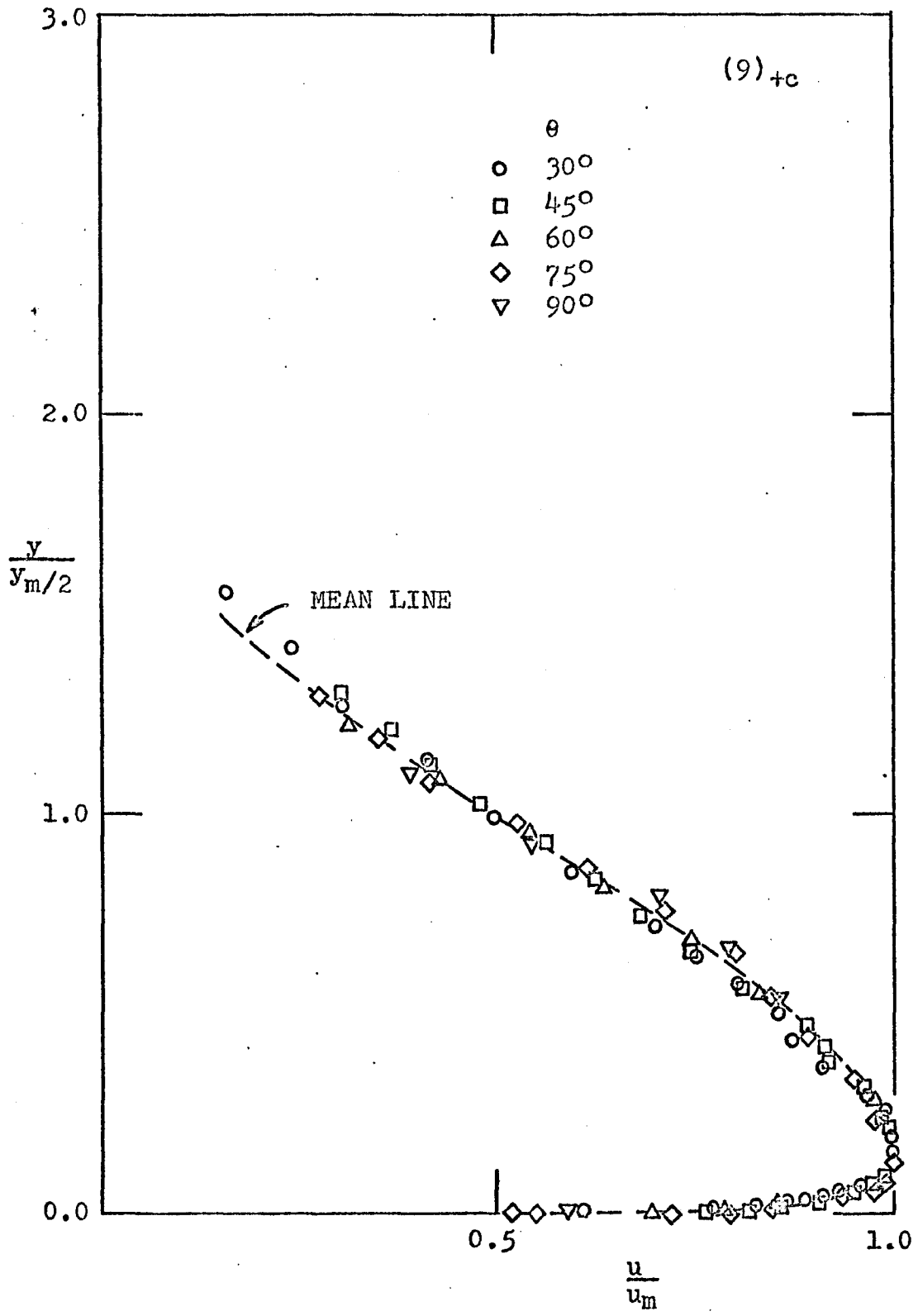


FIG. 29 NON-DIMENSIONAL VELOCITY PROFILES FOR (9)_{+c} SURFACE

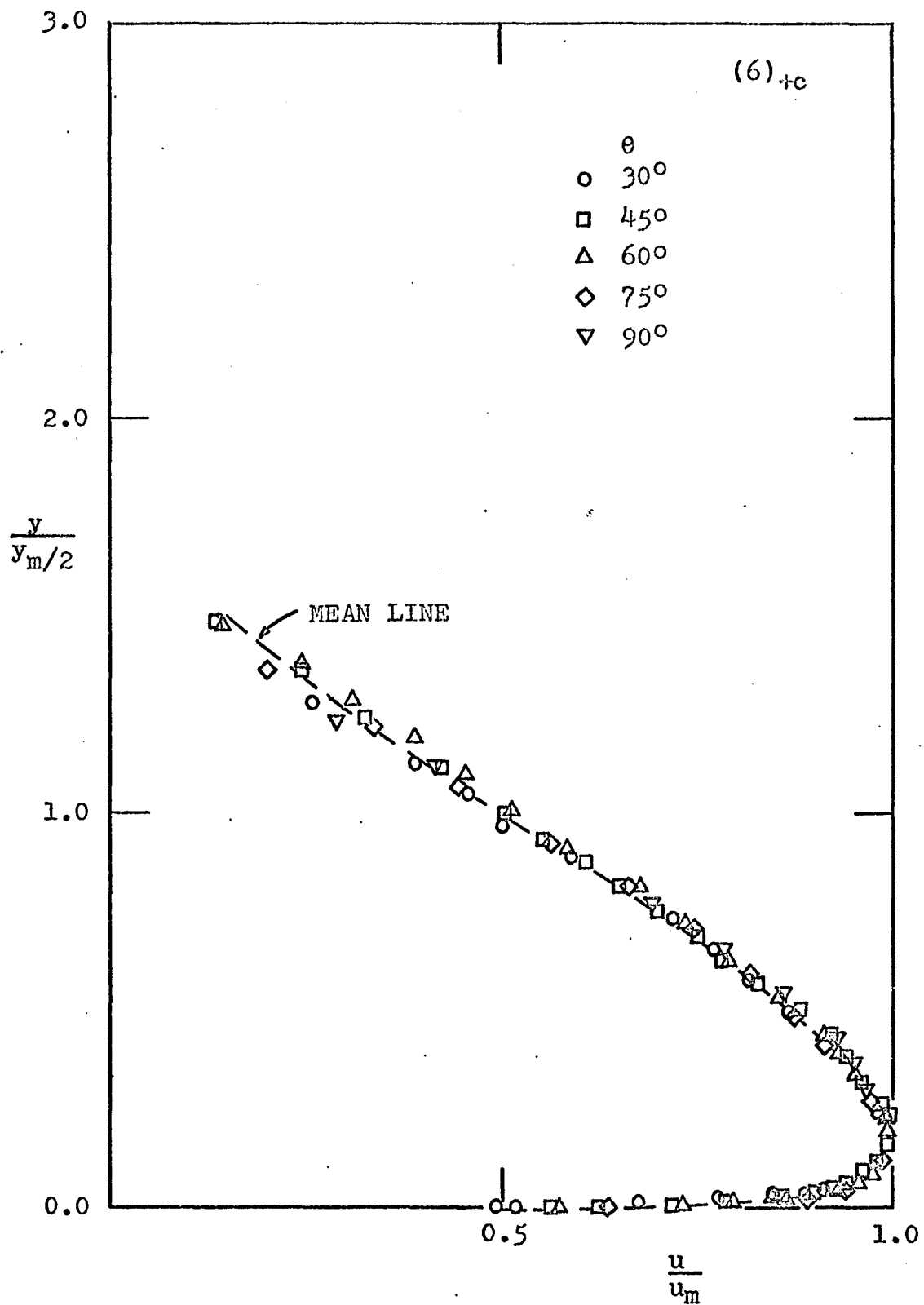


FIG. 30 NON-DIMENSIONAL VELOCITY PROFILES FOR $(6)_{+c}$ SURFACE

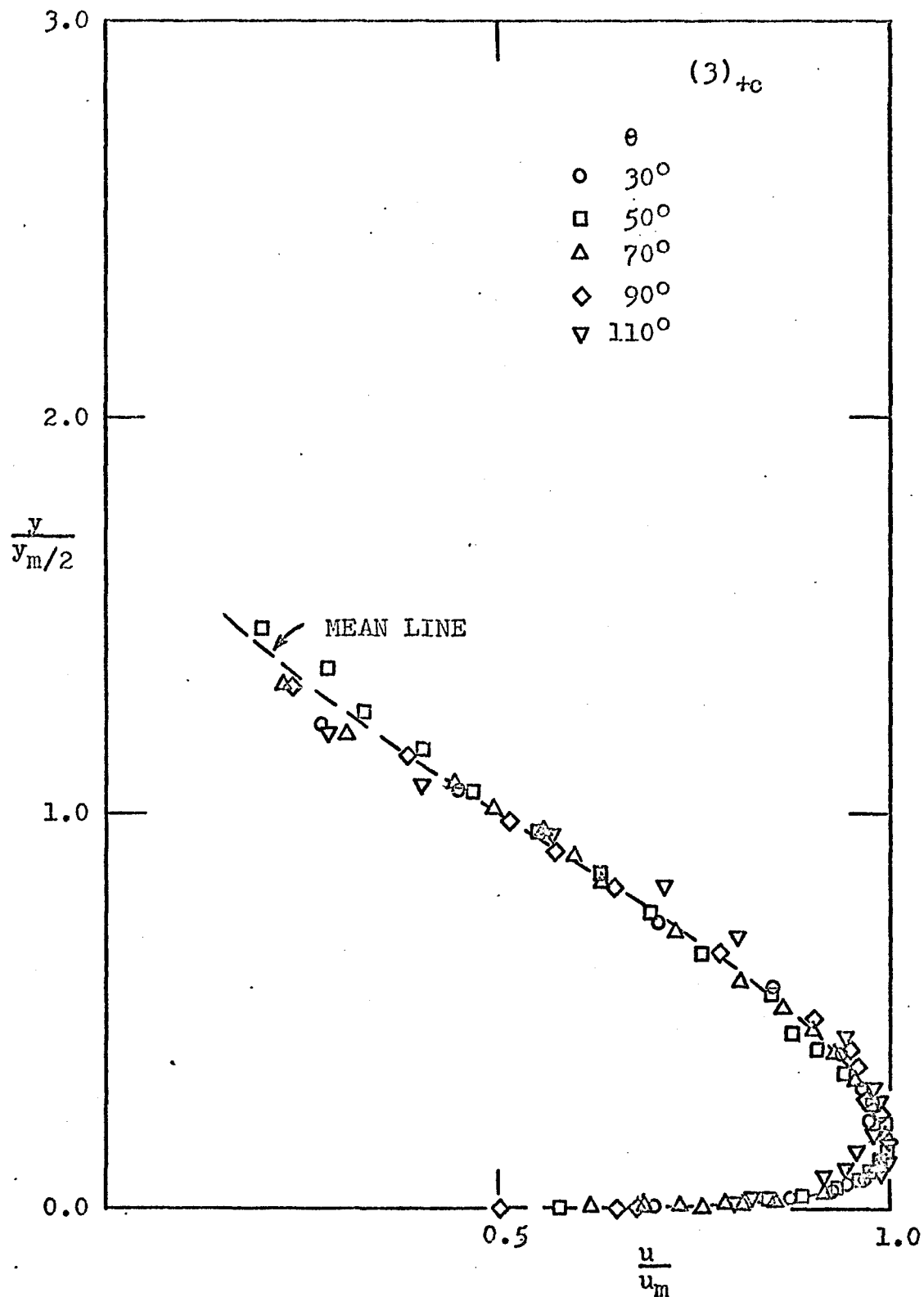


FIG. 31 NON-DIMENSIONAL VELOCITY PROFILES FOR (3)_{tc} SURFACE

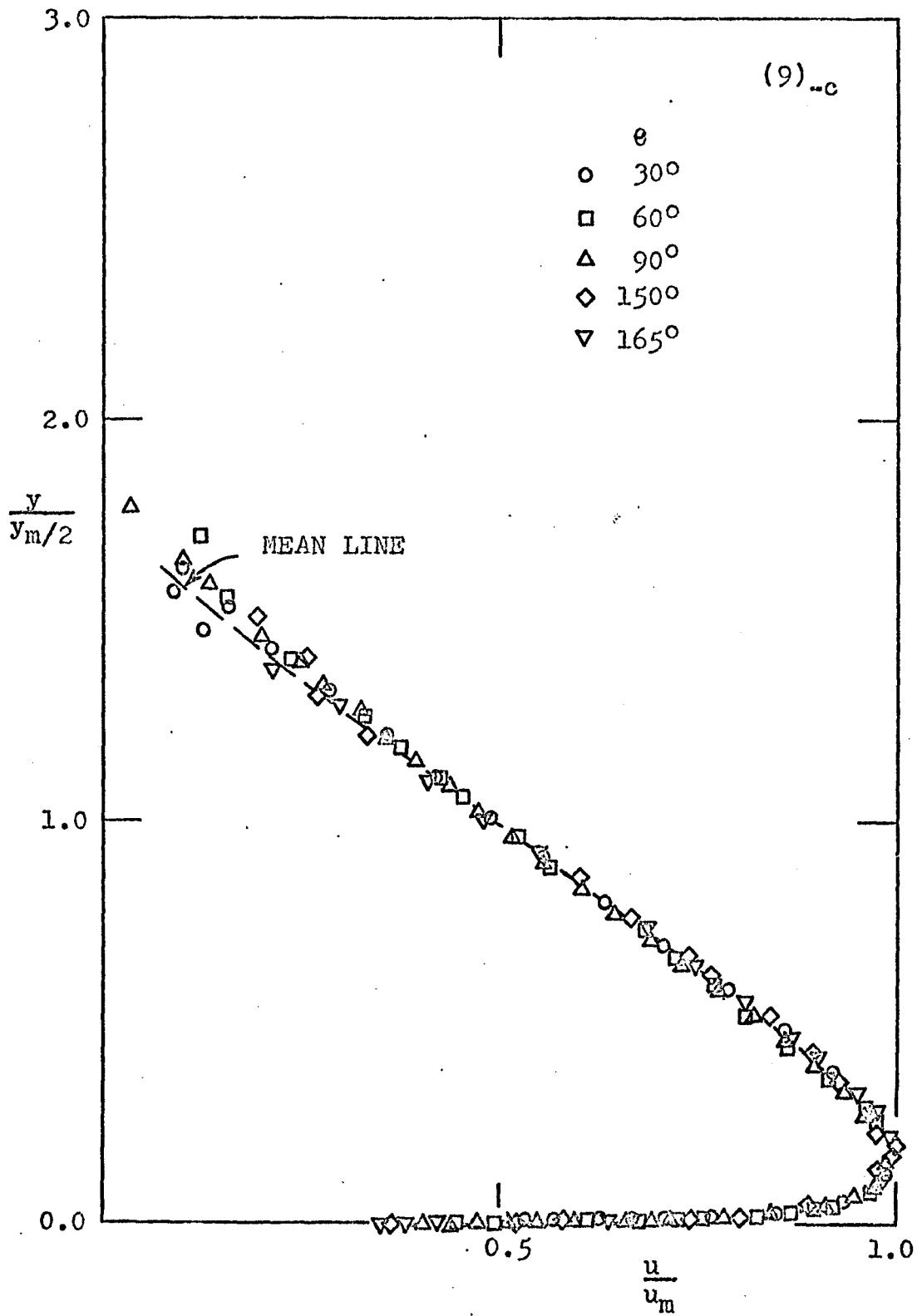


FIG. 32 NON-DIMENSIONAL VELOCITY PROFILES FOR (9)_{-c} SURFACE

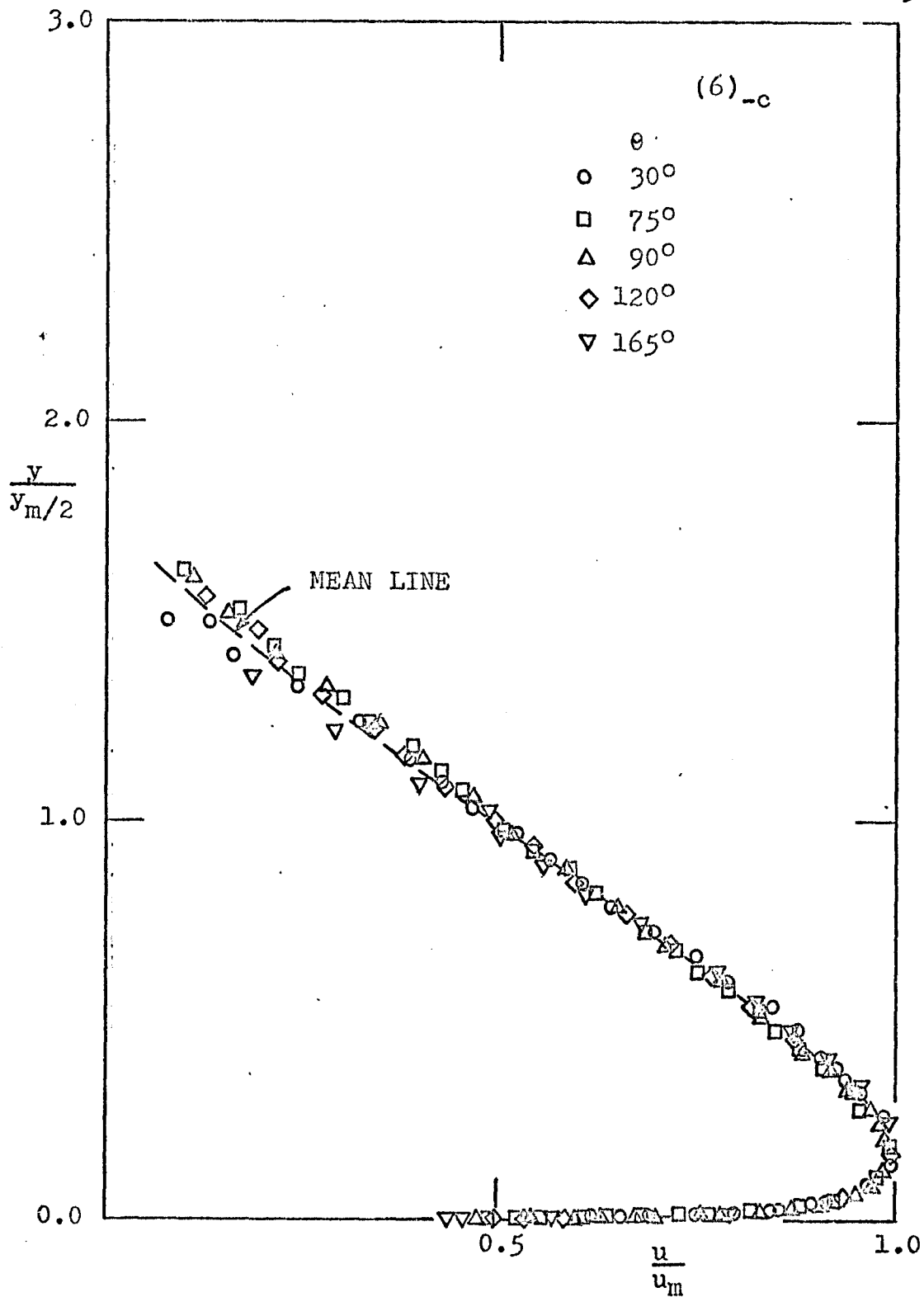


FIG. 33 NON-DIMENSIONAL VELOCITY PROFILES
FOR (6)_{-c} SURFACE

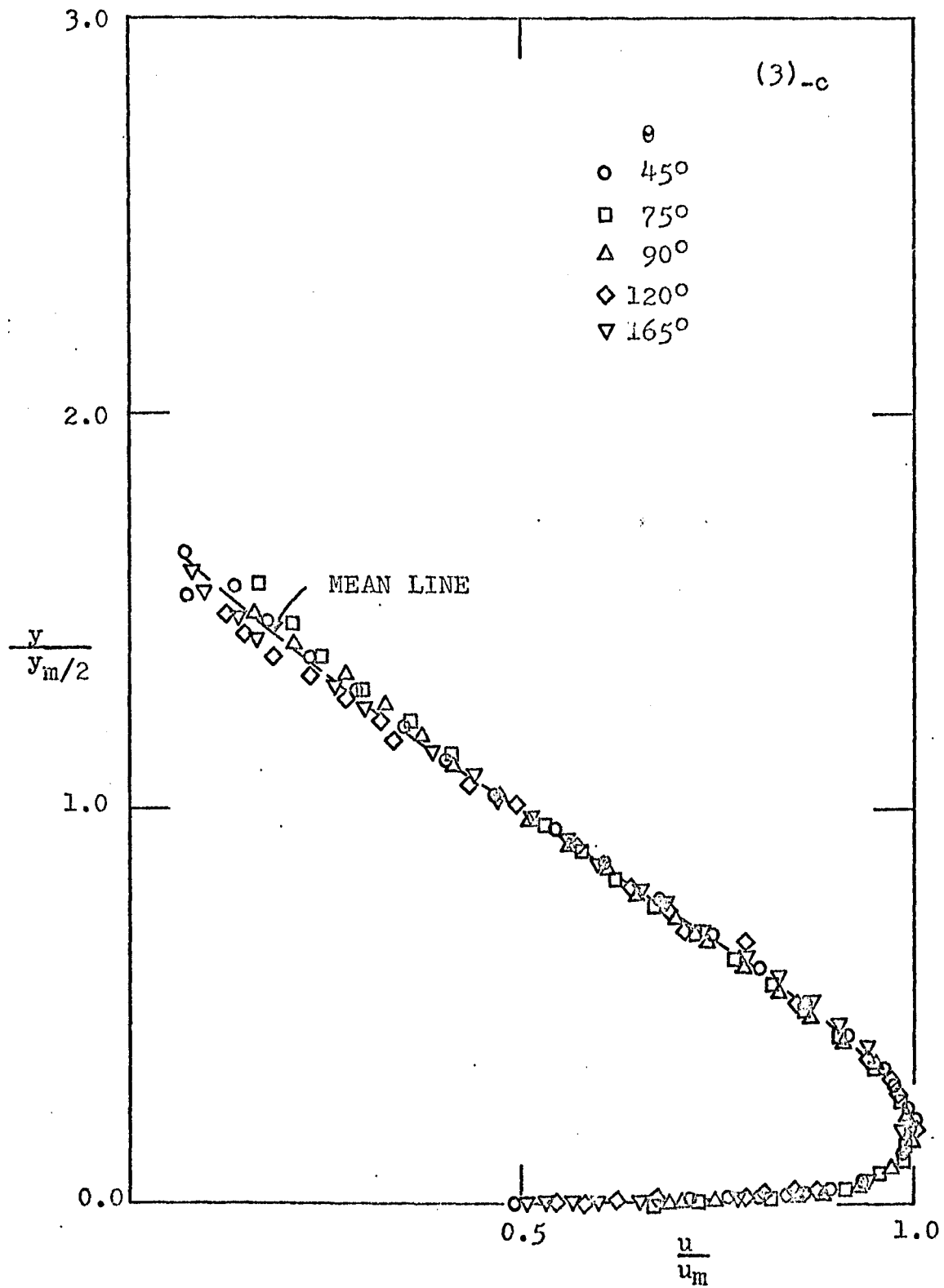


FIG. 34 NON-DIMENSIONAL VELOCITY PROFILES
FOR (3)_{-c} SURFACE

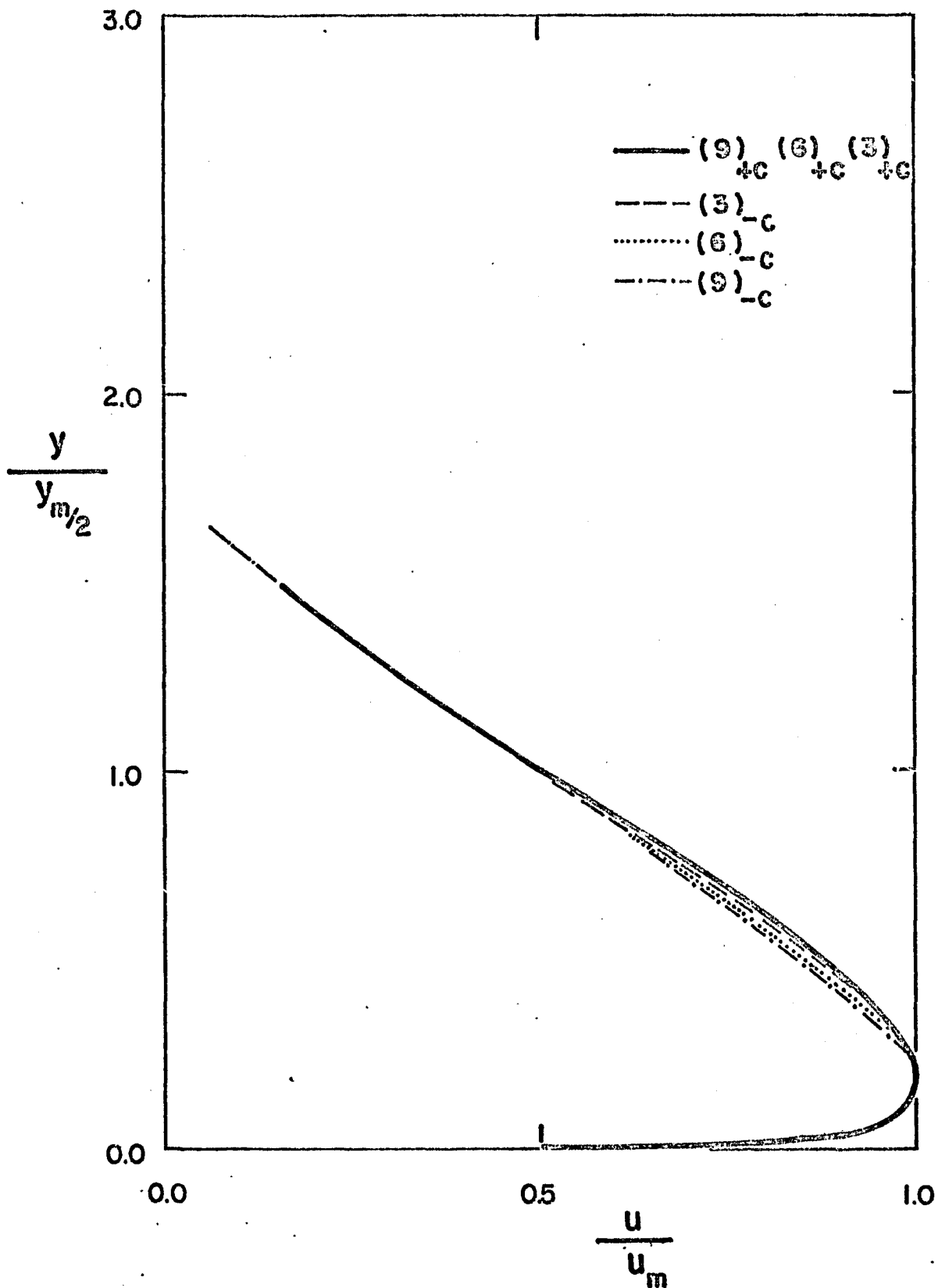


FIG. 35 MEAN NON-DIMENSIONAL VELOCITY PROFILES FOR DIFFERENT RADII OF CURVATURE

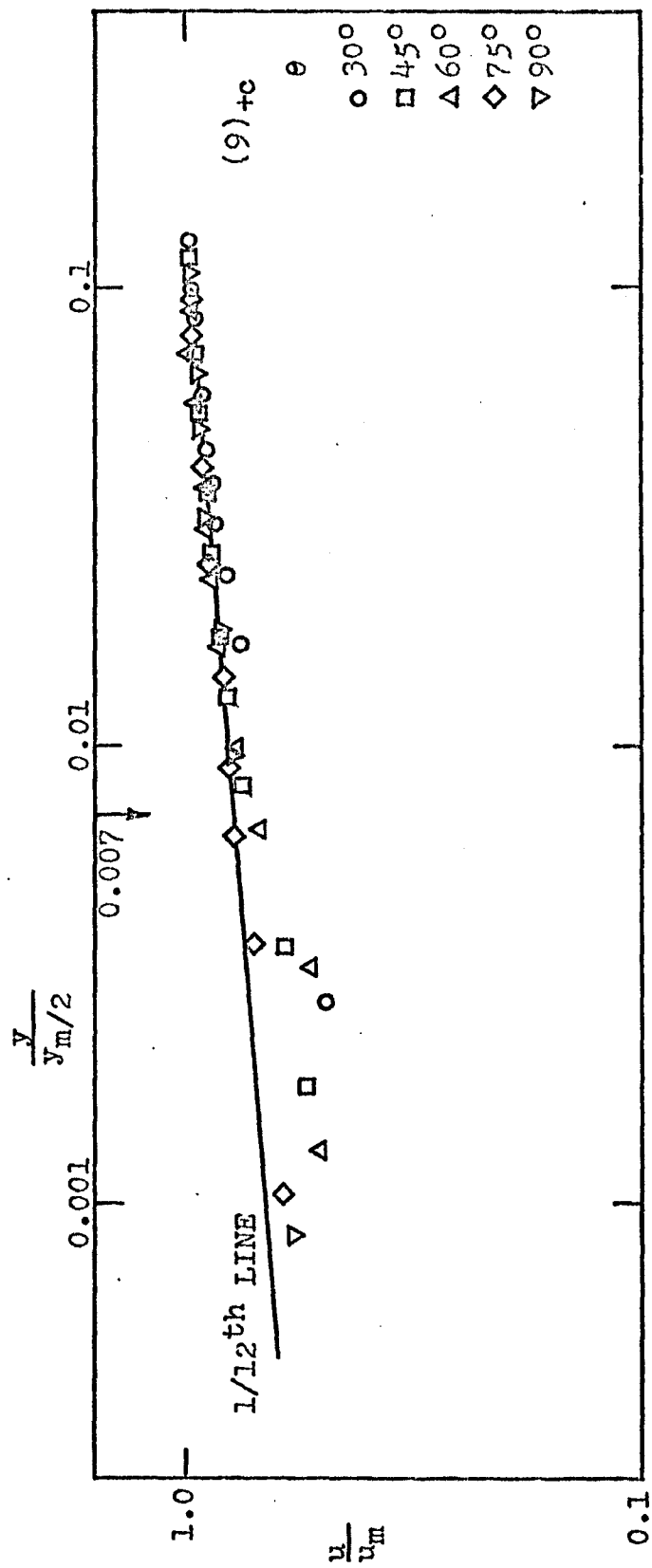


FIG. 36 NON-DIMENSIONAL INNER LAYER VELOCITY PROFILES FOR (9) +c SURFACE

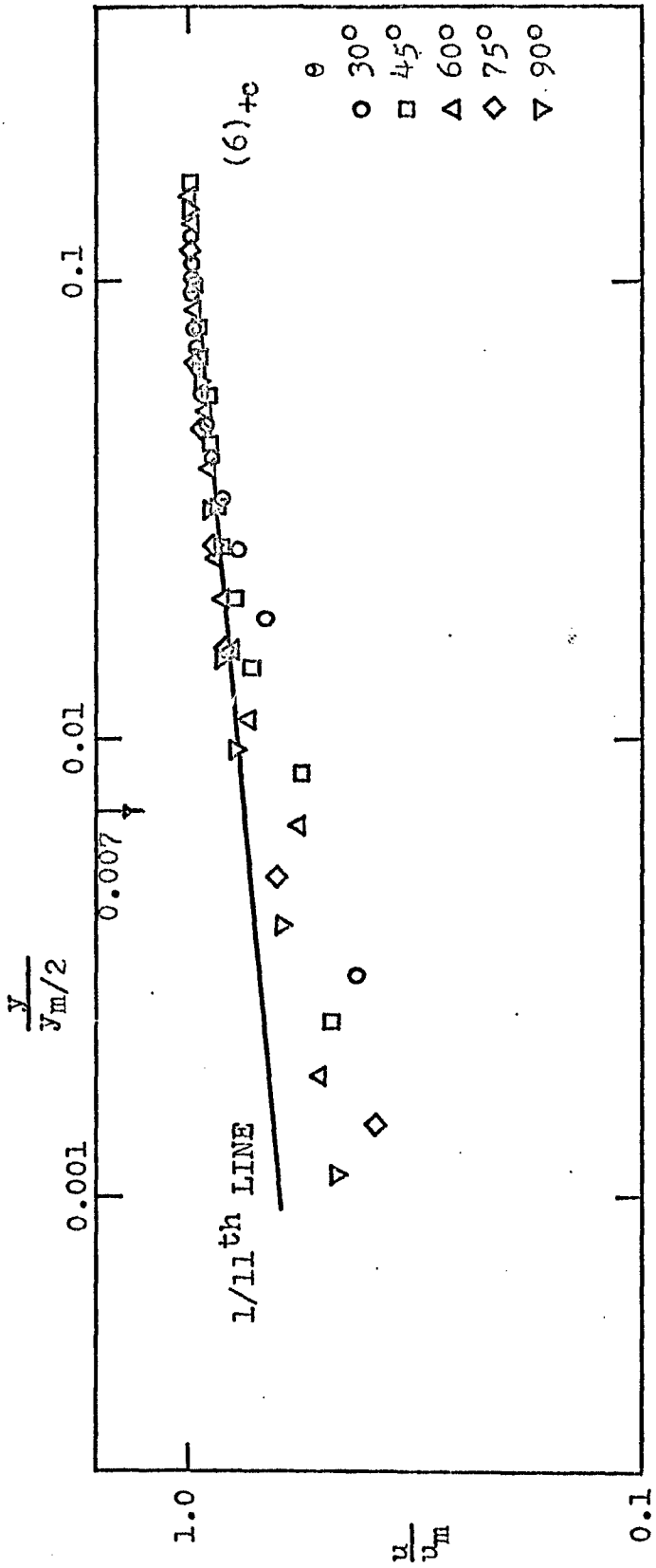


FIG. 37 NON-DIMENSIONAL INNER LAYER VELOCITY PROFILES FOR $(6)_{tc}$ SURFACE

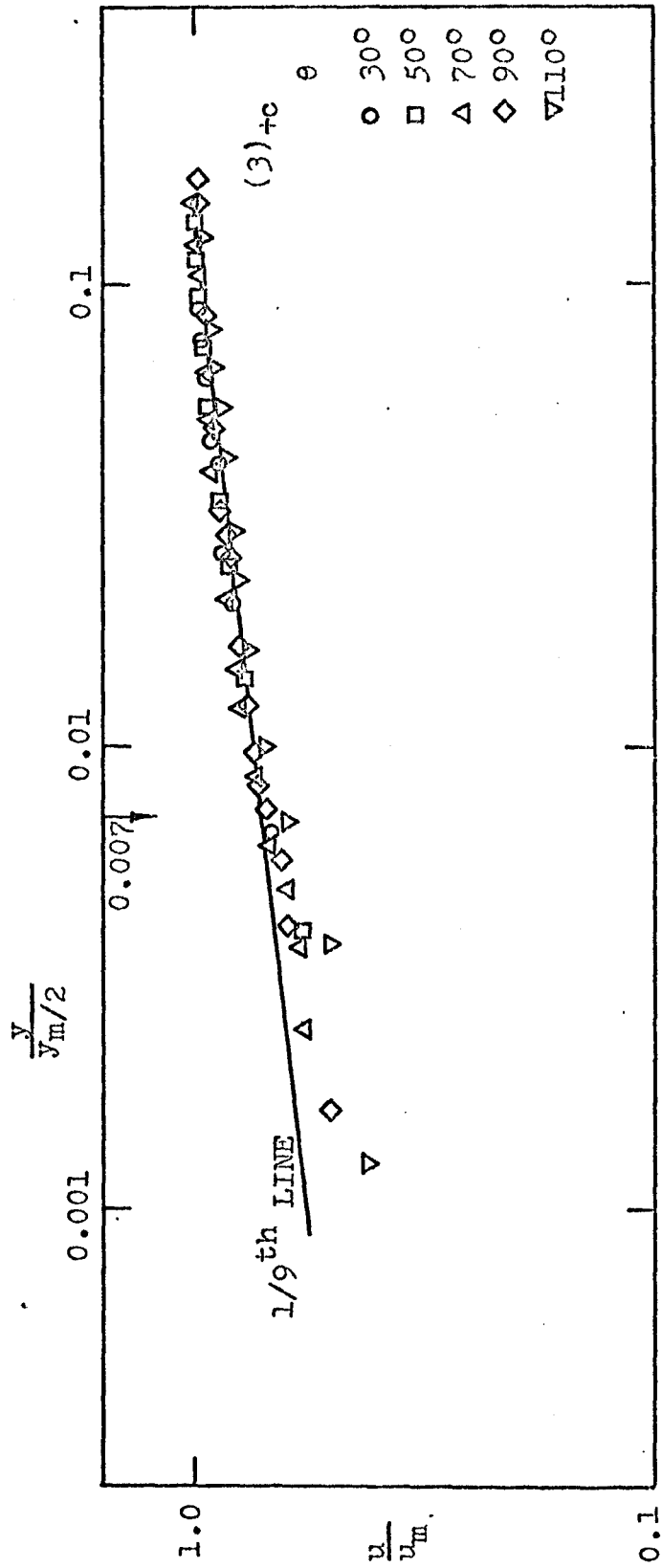


FIG. 38 NON-DIMENSIONAL INNER LAYER VELOCITY PROFILES FOR $(3)^{+c}$ SURFACE

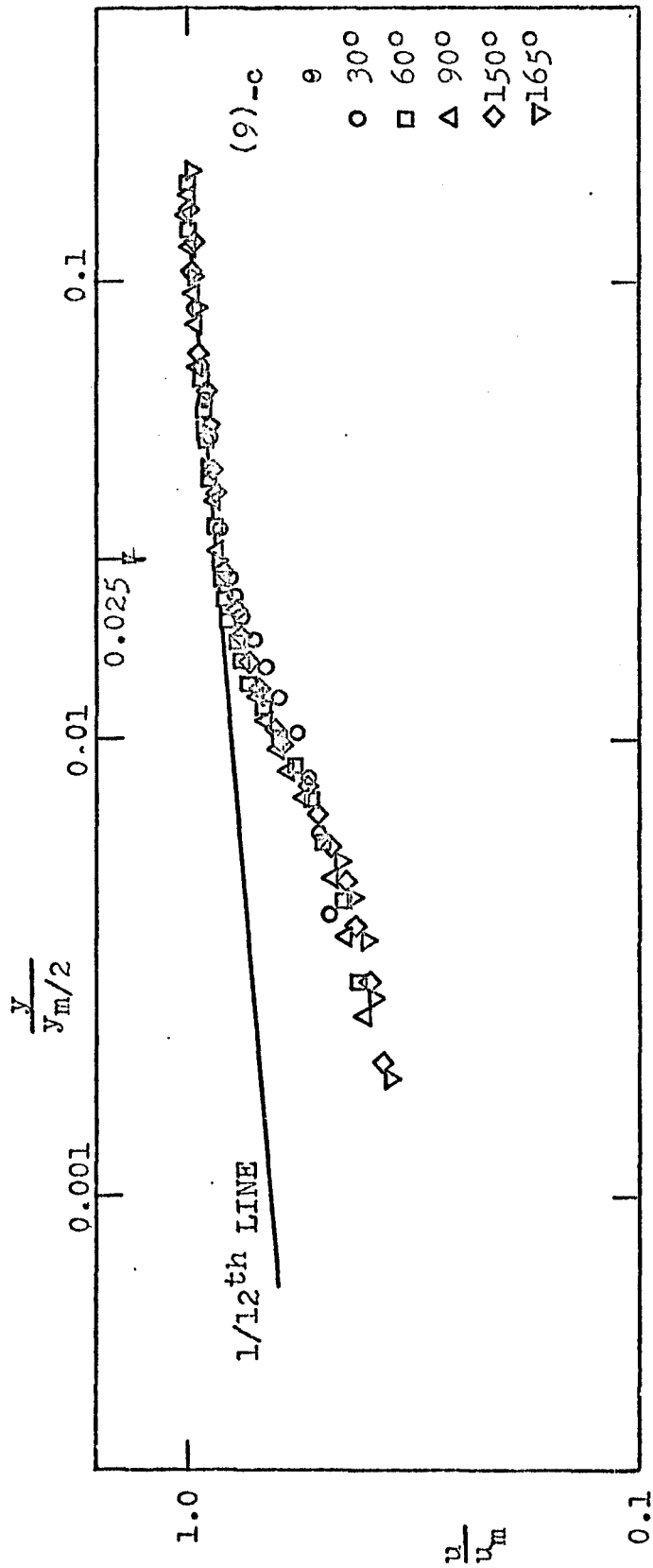


FIG. 39 NON-DIMENSIONAL INNER LAYER VELOCITY PROFILES FOR (9)-c SURFACE

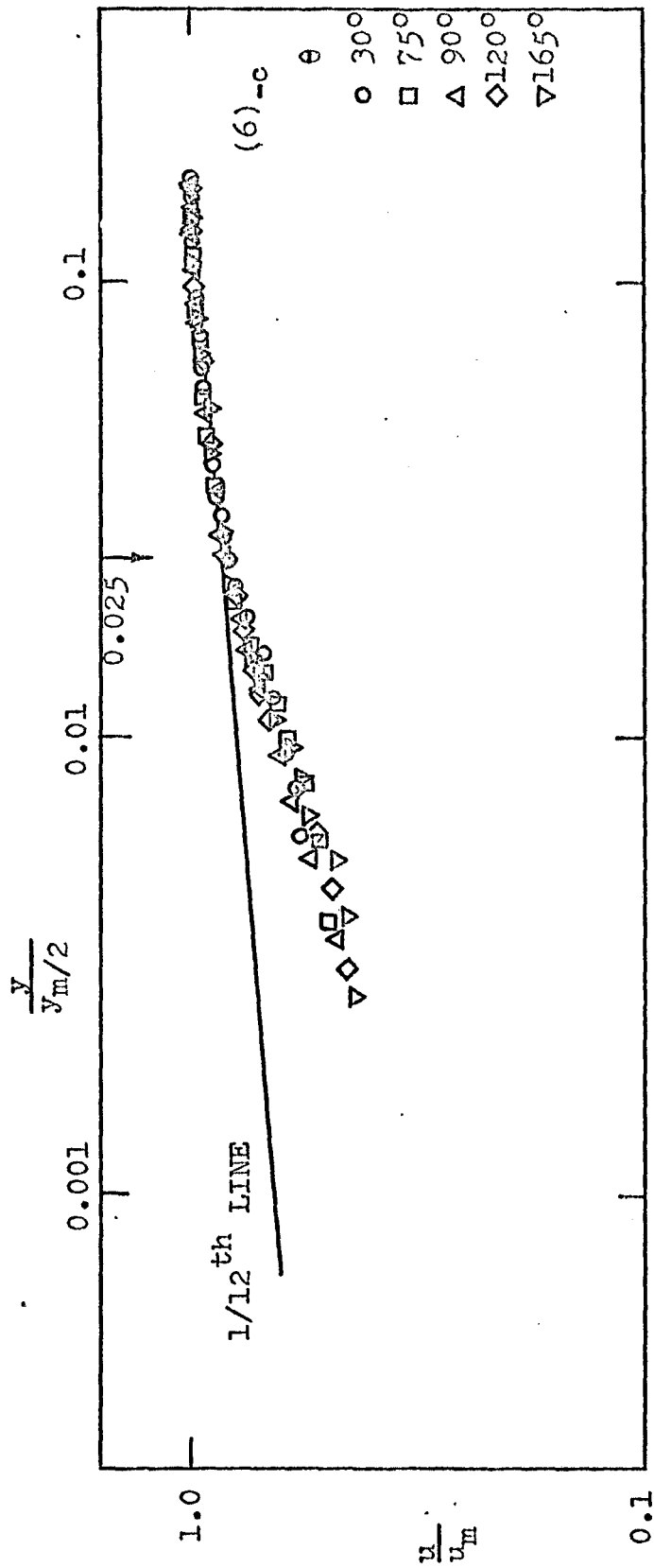


FIG. 40 NON-DIMENSIONAL INNER LAYER VELOCITY PROFILES FOR (6)_c SURFACE

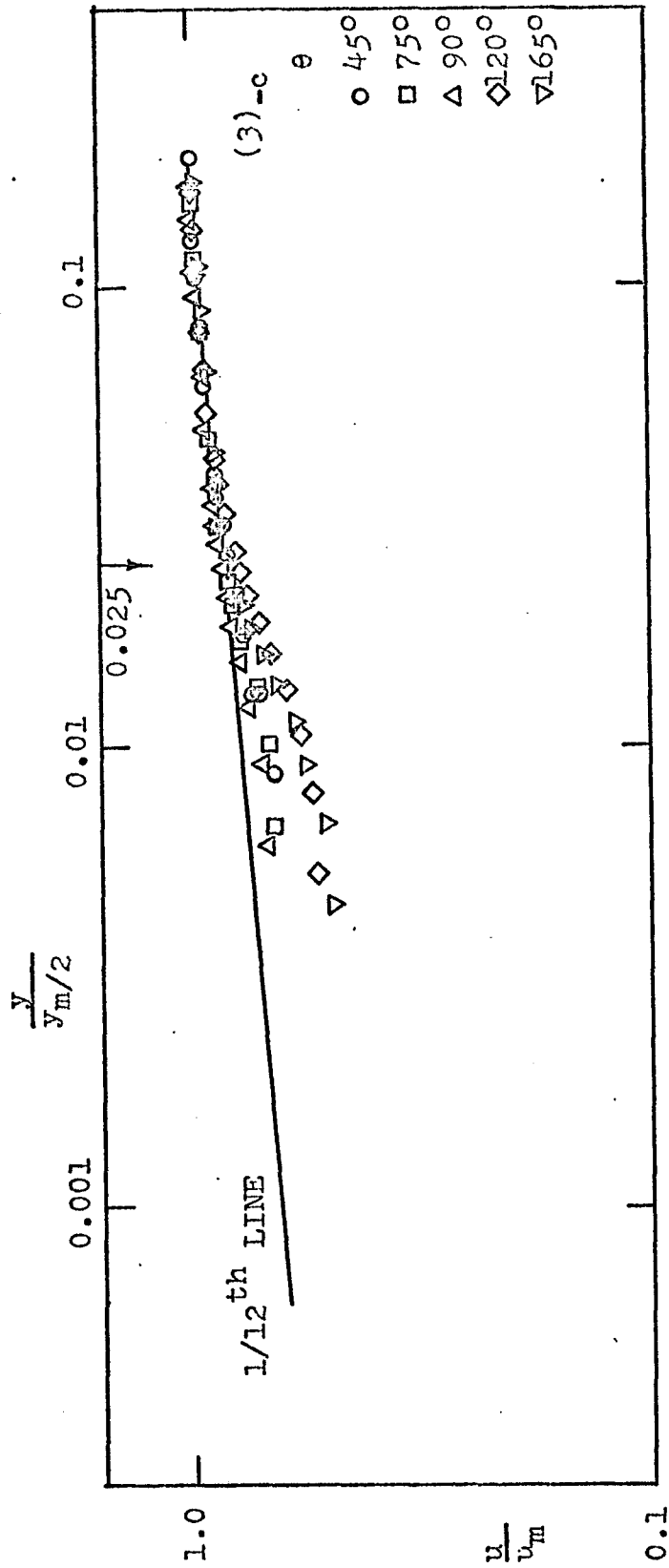


FIG. 41 NON-DIMENSIONAL INNER LAYER VELOCITY PROFILES FOR (3)-c SURFACE

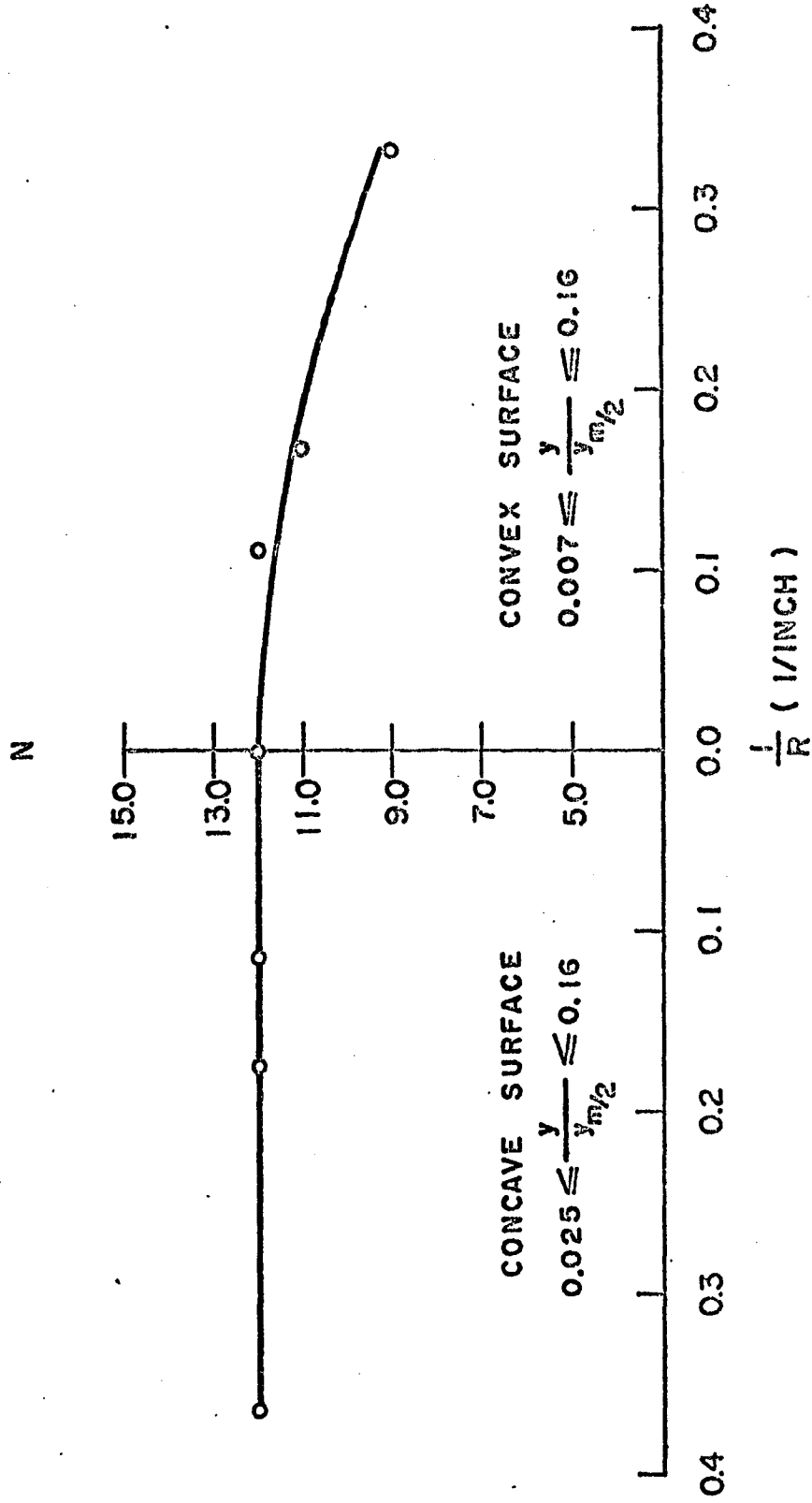


FIG. 42 VARIATION OF POWER LAW EXPONENT WITH CURVATURE

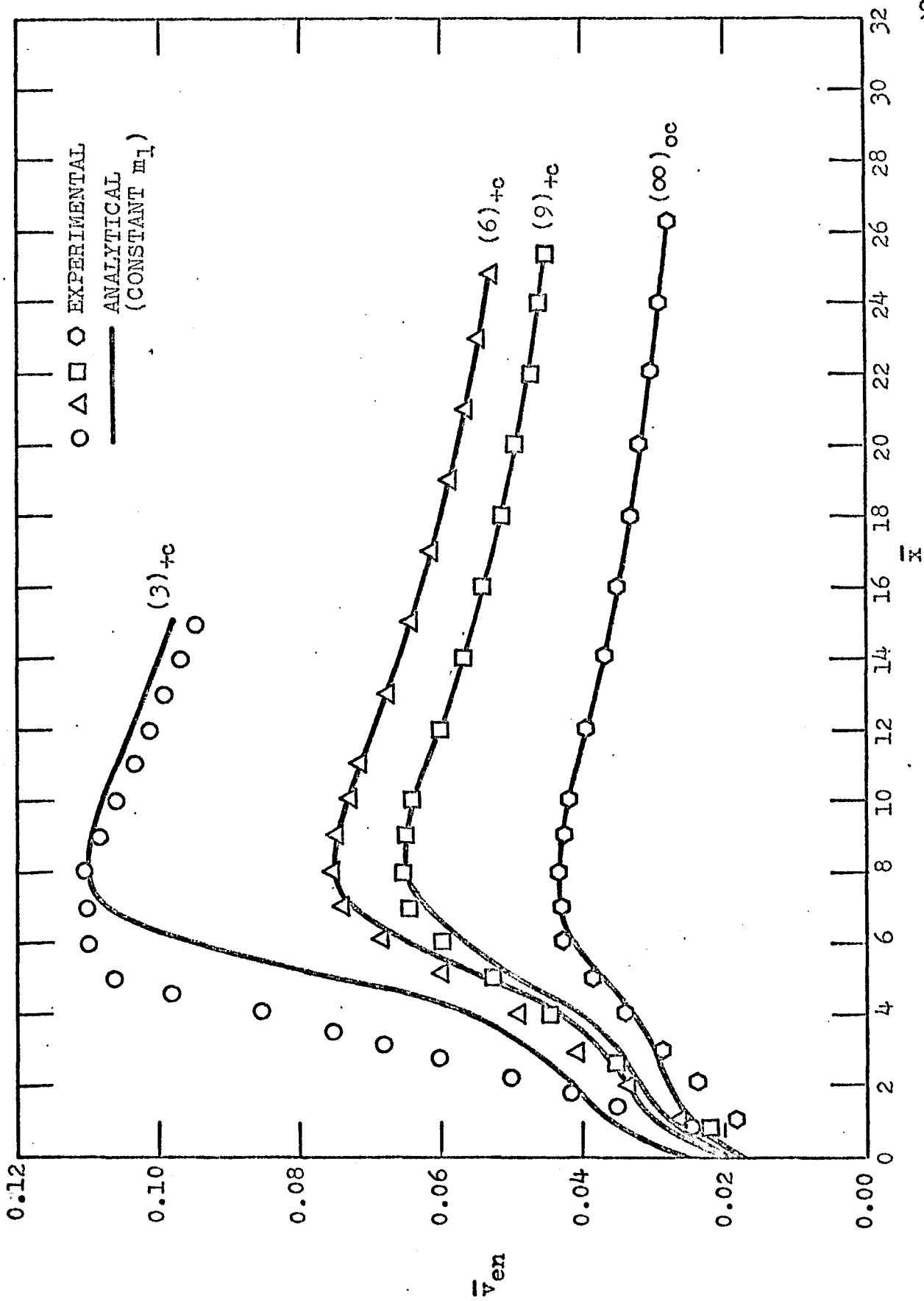


FIG. 43 ANALYTICAL (CONSTANT m_1) AND EXPERIMENTAL VARIATION OF ENTRAINMENT VELOCITY ALONG THE JET

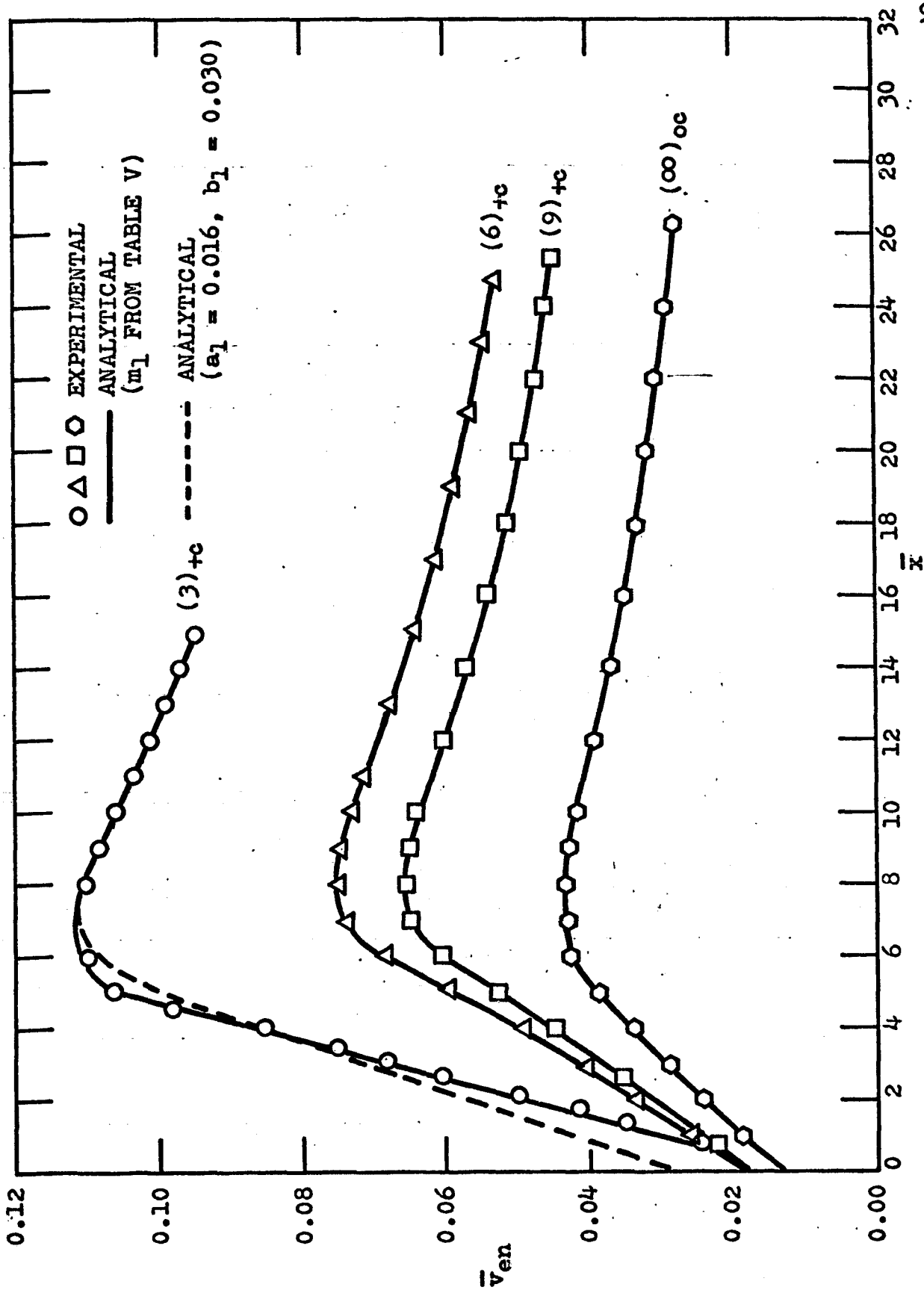


FIG. 44 ANALYTICAL (m₁ VARIED WITH x) AND EXPERIMENTAL VARIATION OF ENTRAINMENT VELOCITY ALONG THE JET

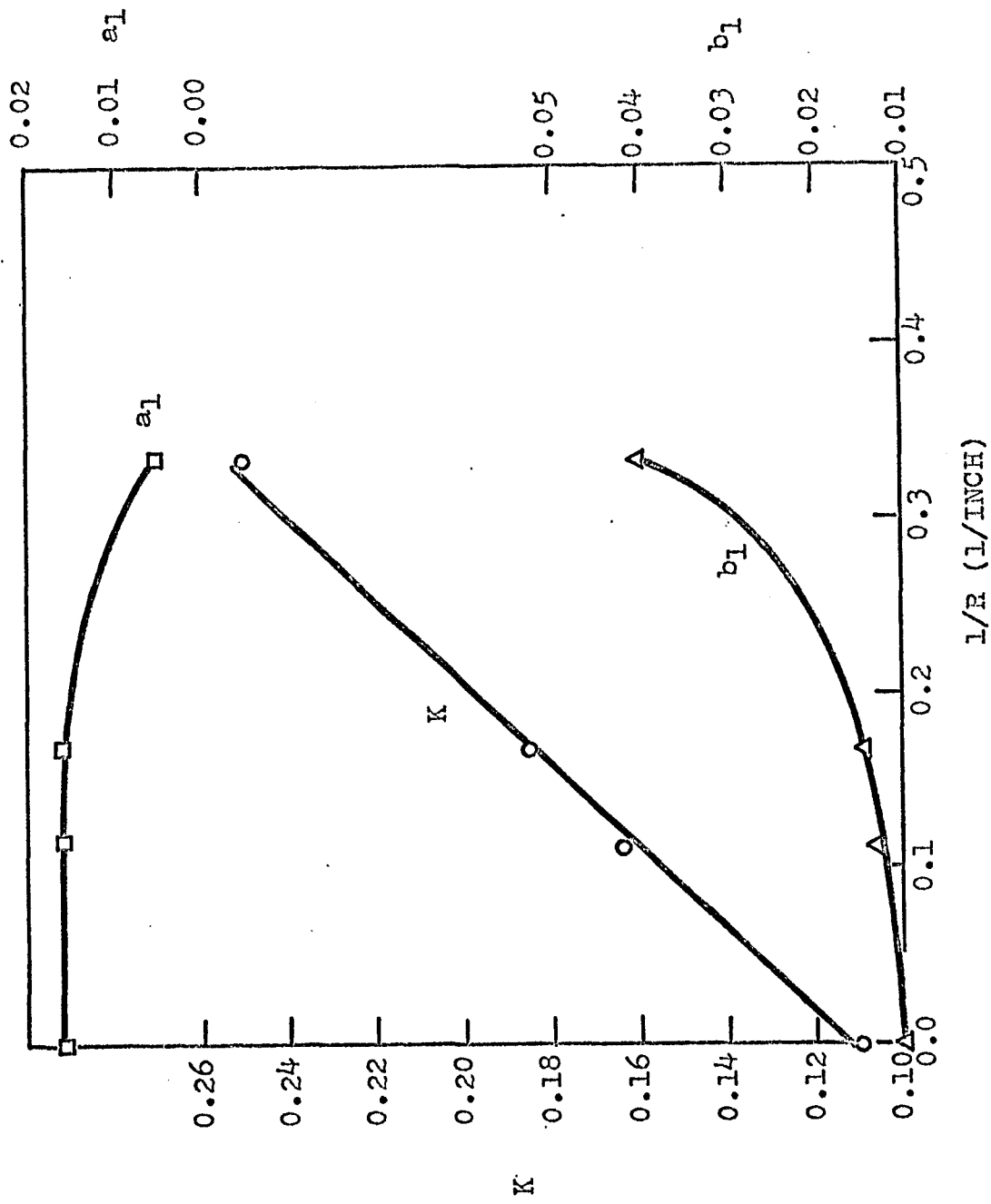


FIG. 45 VARIATION OF a_1 , b_1 & K WITH CURVATURE

TABLE I

CONSTANTS a AND b IN $u_m \propto x^a$ AND $y_m/2 \propto x^b$

Investigator	a	b
Sigalla, A. (Ref. 6)	-0.5	1.0
Schwarz, W. H. Cosart, W. P. (Ref. 7)	-0.555	1.0
Myers, G. E. Schauer, J. J. (Ref. 8) Eustis, R. N.	-0.49±0.03	0.95±0.03
Gartshore, I. Hawaleshka, O. (Ref. 9)	-0.53	1.00
Sridhar, K. Tu, P. K. C. (Ref. 24)	-0.49	1.00

TABLE II

INDEX OF THE POWER LAW MEASURED BY EXPERIMENTS

		Investigator	1/N
Plane Wall Jet		Schwarz, W. H. Cosart, W. P. (Ref. 7)	1/14
		Myers, G. E. Schauer, J. J. (Ref. 8) Eustis, R. N.	1/14
		Gartshore, I. Hawaleshka, O. (Ref. 9)	1/11.4
		Sridhar, K. Tu, P. K. C. (Ref. 24)	1/12
Curved Wall Jet	Convex Surface	Present Investigation	(9) _{tc} : 1/12 (6) _{tc} : 1/11 (3) _{tc} : 1/9
	Concave Surface	Present Investigation	1/12

TABLE IV

TEST CONDITIONS

<u>Surface</u>	<u>R</u>	<u>t</u>	$\frac{R_e}{\gamma}$
	inch	inch	$\frac{u_{ot}}{\gamma}$ or $\left(\frac{P_o - P_\infty}{\rho}\right)^{\frac{1}{2}} \frac{(Rt)^{\frac{1}{2}}}{\gamma}$
			$\times 10^4$
(3) _{+c}	3.00	1/2	5.18
(6) _{+c}	6.00	1/2	7.33
(9) _{+c}	9.00	1/2	8.97
(∞) _{oc}	∞	1/2	2.85
(9) _{-c}	8.75	1/8	4.50
(6) _{-c}	5.75	1/8	3.65
(3) _{-c}	2.75	1/8	2.53

VITA AUCTORIS

- 1937 Born in Nanking, China, on April 11.
- 1955 Completed high school from the Chie -Kuo High School, Taipei, Taiwan, China, in July.
- 1959 Received the Degree of Bachelor of Science in Mechanical Engineering from the National Taiwan University, Taipei, Taiwan, China, in July and entered the R.O.T.C. in Chinese Navy in September.
- 1960 Served in Chinese Navy as an Ensign in April.
- 1962 Employed as a design engineer in the National Taiwan Science Education Centre, Taipei, Taiwan, China, in January.
- 1965 Received the Degree of Master of Applied Science in Mechanical Engineering from the University of Windsor, Windsor, Ontario, Canada, in October.
- 1968 Currently a candidate for the Degree of Doctor of Philosophy in Mechanical Engineering at the University of Windsor.